



Graz University of Technology
Institute for Paper, Pulp and Fiber Technology

PhD Thesis

AUTOMATED SERIAL SECTIONING
APPLIED TO THE ANALYSIS OF
COATING LAYER STRUCTURES AND
FIBER CROSS SECTION PROPERTIES

by

Johannes Kritzinger

Graz, October 2010.

Thesis Supervisor
Prof. Dr. Wolfgang Bauer

STATUTORY DECLARATION

I declare that I have authored this thesis independently, that I have not used other than the declared sources / resources, and that I have explicitly marked all material which has been quoted either literally or by content from the used sources.

date

(signature)

Automated Serial Sectioning Applied to the Analysis of Coating Layer Structures and Fiber Cross Section Properties

by

Johannes Kritzinger

The demand for detailed knowledge regarding the physical dimensions and the spatial arrangement of the raw materials in a paper sheet necessitates the development of novel 3D digitization techniques and further analysis steps. This thesis presents two applications using data obtained with automated serial sectioning in three dimensional paper structure analysis; spatial coating layer analysis and the evaluation of fiber cross section properties.

A fully automated serial sectioning process provides a three dimensional digital representation of a paper sample as a sequence of paper cross sections. Image analysis is used to extract the features of interest like coating layers or fiber cross sections for further analysis. Paper samples of an area of up to 1 cm^2 are digitized at a resolution in the micro-meter scale, making automated serial sectioning a unique 3D digitization system.

A representative analysis of coating layer properties is the most important application of the data obtained by the use of serial sectioning and subsequent image analysis. A novel method to quantify the interaction between coating thickness and base sheet topography is presented. The results showed that predominantly large structures like fiber flocs affect the characteristic formation of a coating layer; a contour type coat in curtain coating or a leveling type coat in blade coating. Other approaches to evaluate coating holdout and coating coverage are presented and influencing parameters are discussed. Both approaches reveal further research potential.

The determination of fiber cross section properties in the dry state is a further application of the three dimensional data obtained in serial sectioning. The image analysis methods required to evaluate fiber cross section properties like fiber wall area, fiber wall thickness or a measure for fiber collapse are presented. The applicability of the new approach is demonstrated by analyzing the effect of beating on fiber cross section properties and by estimating the influence of these properties on dewatering properties of pulp and on the final sheet properties.

Keywords:

Serial sectioning, three dimensional, paper structure, paper physics, coating layer formation, leveling coat, contour coat, coating holdout, coating coverage, fiber cross section analysis, fiber collapse, fiber wall area, fiber wall thickness, fiber width.

Anwendung automatisierter Mikrotomie zur Untersuchung von Strichstruktur und Faserquerschnittsmorphologie

von

Johannes Kritzinger

3D Digitalisierungsverfahren sowie deren Anwendungsmöglichkeiten werden getrieben durch den steigenden Bedarf an Informationen über physikalische Dimensionen und die räumliche Anordnung von Rohstoffen in einem Papierblatt ständig weiterentwickelt. In dieser Arbeit werden zwei Beispiele für die Anwendung von Daten aus automatisierter Mikrotomie detailliert vorgestellt; die Analyse von Strichstrukturen sowie die Ermittlung von Faserquerschnittseigenschaften.

Vollautomatisierte Mikrotomie ermöglicht eine digitale dreidimensionale Darstellung einer Papierprobe in Form einer Sequenz aus Papierquerschnitten. Bildanalysealgorithmen werden eingesetzt, um bestimmte Strukturmerkmale für weitere Auswertungen zu detektieren, wie beispielsweise die Strichschichten oder Faserquerschnitte. Mit dieser Methode können bis zu 1 cm^2 große Papierproben bei einer Auflösung im Mikrometerbereich digitalisiert werden.

Eine repräsentative Untersuchung von Strichstrukturen ist die wichtigste Anwendung der Serienschnitttechnik mit zugehöriger Bildanalyse. Ein neuer Weg zur Beschreibung der Interaktion zwischen Strich und Rohpapiertopographie wird vorgestellt. Im Wesentlichen sind Strukturen in der Größenordnung von Faserflocken für die charakteristische Strichstruktur verantwortlich, z.B. ein Konturstrich bei Strichauftrag im Curtain Coater oder ein Glättstrich bei Auftrag mit dem Blade. Weitere Anwendungen zur Beurteilung der Streichfarbenpenetration sowie der Strichabdeckung werden vorgestellt und dienen als Grundlage für weiterführende Arbeiten.

Die Untersuchung von Faserquerschnittseigenschaften im trockenen Zustand, wie Faserwandfläche, Faserwanddicke oder Faserkollaps, stellt eine weitere Anwendungsmöglichkeit der Mikrotomiedaten dar. Die einzelnen Prozessschritte zur Messung von Eigenschaften des Faserquerschnittes werden detailliert erklärt. Die Anwendbarkeit der Methode wird anhand verschiedener Studien gezeigt, wie beispielsweise die Veränderung von Eigenschaften des Faserquerschnittes durch die Mahlung, oder der Effekt von Faserquerschnittseigenschaften auf Entwässerungs- und Blatteigenschaften.

Schlagwörter:

Serienschnitte, dreidimensional, Papierstruktur, Papierphysik, Strichstruktur, Glättstrich, Konturstrich, Streichfarbenpenetration, Strichabdeckung, Faserquerschnitt, Faserkollaps, Faserwandfläche, Faserwanddicke, Faserbreite.

Acknowledgements

During the course of this thesis I was supported by a lot of people who have earned my gratitude.

First I would like to thank my supervisor, Professor Wolfgang Bauer, for spending hours in discussing new findings or alternative ways to apply data obtained in serial sectioning. His ideas were very important for the development of the different approaches presented in this thesis.

I am grateful to Mario Wiltsche, who started research activities on three dimensional paper structure analysis with automated serial sectioning at the Institute for Paper, Pulp and Fiber Technology and thus laid the basis for my work. I want to thank Michael Donoser, who developed most of the image analytical algorithms to extract either coating layer or fiber cross section data.

Special thanks to Ulrich Hirn - during the years of working on this thesis I shared the office with him. We spent a lot of time discussing ideas and cooperated on various topics which resulted in several publications.

Also thanks to the laboratory staff and the administrative staff of the IPZ-team. Heidi Bakhshi, Barbara Hummer, Harald Streicher and the others performed most of the laboratory work - always faster than agreed. Claudia Bäuml and Ingrid Reininger protected me from administrative work as far as it was possible.

Last but not least I want to thank my parents and my sisters. It is really important to mention that they supported my education for almost a quarter of a century!

Johannes Kritzinger
Graz, October 31, 2010.

Contents

1	Introduction	1
1.1	3D analysis of paper structures	2
1.2	Contributions and background	3
1.3	Thesis outline	5
2	Methods Capable to Analyze 3D Paper Structure	6
2.1	Introduction	7
2.2	Common 3D digitization methods used in paper structure analysis . . .	7
2.3	Automated serial sectioning technique	9
2.3.1	Hardware components in use	9
2.3.2	Sample preparation	11
2.3.3	Digitization routine and processing of image data	12
2.3.4	Fields of applications	14
2.4	Conclusions	15
3	Advances in Coating Layer Analysis	16
3.1	Introduction	17
3.2	Exploring the spatial coating layer structure	18
3.2.1	The different methods applied in coating layer analysis	18
3.2.2	Analysis steps to extract coating thickness data	20
3.2.3	Validation	24
3.3	Sampling procedure for coating layer analysis	29
3.3.1	Influential parameters on sampling and digitization.	32
3.3.2	Expected confidence intervals	38
3.3.3	Summary	40
3.4	Description of spatial coating layer formation	40
3.4.1	Approach	42
3.4.2	Example I: Pilot coating trial with different application systems .	48
3.4.3	Example II: Pilot calendering trial on curtain coated samples. . .	54
3.4.4	Summary	58
3.5	Relevance and evaluation of coating holdout	59

3.5.1	Measuring principle	60
3.5.2	Relevance of coating holdout and influencing parameters	64
3.5.3	Summary	69
3.6	New ways to analyze coating coverage	69
3.6.1	Determination of uncoated areas	70
3.6.2	Discussion of influencing parameters	72
3.6.3	Analysis of individual uncoated spots	76
3.6.4	Summary	77
3.7	Conclusions	78
4	Analysis of Fiber Cross Section Properties	79
4.1	Introduction	80
4.2	Analysis of fiber cross section properties in the dry state	81
4.2.1	Considerations regarding analysis in the dry state	81
4.2.2	Digitization techniques used for analysis in the dry state	84
4.3	Quantification of fiber cross section properties in serial sectioning	88
4.3.1	Analysis steps to obtain fiber cross section properties	88
4.3.2	Representative number of fiber cross sections	97
4.3.3	Weaknesses and limitations of the approach	99
4.4	First results obtained with the presented approach	101
4.4.1	Effect of laboratory beating on cross section properties	101
4.4.2	Effect of cross section properties on paper properties	105
4.4.3	Comparison to flow cell measurements	108
4.5	Conclusions	110
5	Conclusions and Outlook	112
A	Burnout Test	117
B	Samples Analyzed with Coating Layer Analysis Tools	119
C	Publications	121
	Bibliography	124

List of Figures

2.1	Layout of the prototype built.	10
2.2	Embedding technique for preparation of large sample areas.	11
2.3	Coating thickness map obtained with new embedding technique.	12
2.4	3D image data set obtained from serial sectioning.	13
3.1	Definition of measuring points in the paper plane.	22
3.2	Definition of thickness and topography data.	23
3.3	Coating uniformity obtained with serial sectioning and burnout test.	25
3.4	Cross section image obtained with LM and SEM.	27
3.5	Correlation of coating thickness data obtained with LM and SEM.	27
3.6	Cross section image obtained with LM and tomography.	28
3.7	Correlation of c.t. data obtained with LM and micro tomography.	28
3.8	Similarity of coating thickness distributions at different sample sizes.	29
3.9	Definition of a similarity measure to compare distributions.	31
3.10	Effect of measuring grid size on coating thickness maps.	33
3.11	Coating thickness maps - sample size and geometry.	34
3.12	Similarity measure at different sample sizes and geometries.	34
3.13	Sampling on three different sheets.	36
3.14	Influence of sample position on mean coating thickness.	37
3.15	Quantifying the influences of different sampling procedures.	37
3.16	Expected confidence intervals for important coating properties.	39
3.17	Correlation of coating thickness and base sheet topography data.	41
3.18	Cross section images of differently coated sheets.	42
3.19	Basic operations in frequency domain filtering.	44
3.20	Cutoff wavelength applied in frequency filtering.	45
3.21	Highpass- and lowpass-filtered base sheet topography data.	46
3.22	Highpass- and lowpass-filtered coating thickness data.	46
3.23	Correlation of filtered coating thickness and topography data.	47
3.24	Coating thickness maps obtained from different application systems.	49
3.25	Effect of coating application systems on R^2	50
3.26	Effect of coating application systems on slope.	51

3.27	Base sheet surface uniformity at different application systems.	52
3.28	Coating thickness uniformity at different application systems.	53
3.29	Effect of pre- and post-calendering on R^2	55
3.30	Effect of pre and post calendering on slope.	56
3.31	Base sheet uniformity influenced by calendering.	57
3.32	Coating thickness uniformity influenced by calendering.	58
3.33	Segmentation of coating regions from cross section images.	61
3.34	Coating thicknesses used to define holdout.	61
3.35	Removal of separated regions detected as coating in the base paper. . .	62
3.36	Cross sections of papers with different porosity.	65
3.37	Coating holdout influenced by paper porosity.	66
3.38	Cross sections of papers coated with different coating colors.	68
3.39	Coating holdout influenced by different coating colors.	69
3.40	Thresholds to quantify coating coverage.	71
3.41	Indication of uncoated areas and areas with low coat weight.	71
3.42	Application system affecting uncoated areas.	73
3.43	Coverage influenced by coating thickness.	73
3.44	Coverage influenced by base sheet roughness.	74
3.45	Coverage influenced by variance of coating thickness.	75
3.46	Coverage determined by the use of the burnout test.	75
3.47	Evaluating topography at and around uncoated spots.	76
3.48	Elevated topography regions as a reason for uncoated areas.	77
4.1	Fiber tilt causes overestimation of fiber cross section properties.	82
4.2	Analysis steps for measuring fiber cross section properties.	83
4.3	Cross section images obtained with different digitization techniques. . .	85
4.4	Reconstruction of detected fibers.	87
4.5	Definition of measures to transform cross sections.	91
4.6	Paper cross section of a kraft paper sample.	92
4.7	Collapsed or visible lumen.	92
4.8	Collapsed lumen or broken fiber wall: Part I.	93
4.9	Collapsed lumen or broken fiber wall: Part II.	93
4.10	Collapsed lumen or broken fiber wall: Part III.	94
4.11	Fiber wall thickness for fibers with a broken fiber wall.	95
4.12	Threshold defining a reasonable number of fiber cross sections.	98
4.13	Sample dimensions giving a reasonable number of fibers.	99
4.14	Limited number of fiber cross sections in mechanical pulp hand sheets. .	100
4.15	Difficulties in classification.	100
4.16	Effect of beating on fiber cross sections.	102
4.17	Effect of beating on fiber wall thickness distribution.	104
4.18	Correlation of fiber thickness and width affected by beating.	104

4.19	Fiber wall area versus coarseness (Kajaani FS200).	104
4.20	Influence of beating on dewatering properties.	106
4.21	Cross section properties influencing dewatering properties.	106
4.22	Tensile strength influenced by shape factor.	107
4.23	Tear strength affected by fiber wall thickness.	108
4.24	Distributions of fiber cross section properties in dry and wet state. . . .	109
4.25	Dry and wet measurement of fiber cross section properties.	110
A.1	Burnout images of blade and film coated samples.	118

List of Tables

2.1	Selected parameters of the optical microscope.	11
3.1	Thickness and topography data measured in coating layer analysis. . .	23
3.2	Changes in statistical parameters alter the similarity measure.	31
3.3	Effect of resolution in the paper plane on statistical measures.	32
3.4	Measures defining coating layer structures.	47
3.5	Coating formulation to study influence of application systems.	50
3.6	Parameters and results of calendering study.	55
3.7	Coating formulations to study effects on holdout.	64
4.1	Definition of basic fiber cross section properties.	91
4.2	Changes of cross section properties caused by beating.	103

Introduction

In this chapter the motivation to analyze the three dimensional structure of paper as well as the main contributions, the background and the outline of this thesis are presented.

1.1 3D analysis of paper structures

The analysis of the highly complex 3D structure of paper in the micro-meter scale became an important research topic in pulp and paper science during the last decade.

A detailed knowledge about the physical dimensions and the spatial arrangement of the raw materials used in paper production is required to explain their influence on the final paper properties. For example, print non-uniformities of coated papers were attributed to a poor coating layer uniformity resulting from variations in local coating layer thickness [ENGSTRÖM AND LAFAYE, 1992] or spatial variations in surface porosity [PRESTON ET AL., 2008]. The spatial arrangement and shape of the individual fibers were found to play a decisive role in the development of paper strength e.g. [DINWOODIE, 1965]. The porosity of a sheet of paper was reported to be influenced by the presence and distributions of fiber fines and fillers [BLOCH AND ROLLAND DU ROSCOAT, 2009]. A reliable estimation of physical dimensions as well as the spatial arrangement of raw materials used are prerequisites for a deeper insight into important paper properties.

Recent advances in numerical simulation techniques allow the investigation of the properties and structures of paper as an engineering material. As an example, the permeability of a sheet of paper was explained with fiber width and fiber thickness, e.g. [SHALLHORN AND GURNAGUL, 2009]. For the development and verification of these models, an adequate representation of 3D paper structures in the micro-meter scale is essential. This is the same for the physical dimensions of individual raw materials used in paper production.

Physical dimensions of raw materials as well as their arrangement in a sheet of paper are detected from digital representations of a paper sample obtained with high resolution imaging techniques. Paper samples having a size of several square millimeters are digitized at a resolution in the micro-meter range. The property of interest, e.g. coating layers, individual fibers or the pore structure of paper can be extracted and analyzed in detail [BLOCH AND ROLLAND DU ROSCOAT, 2009; CHINGA-CARRASCO, 2009; WILTSCHKE ET AL., 2010].

A rapid development of different imaging techniques, a remarkable gain in computational power and the availability of novel image analysis routines enable new insights on the structures to be analyzed. At the same time this is triggering further extensive research work, as applications to extract the properties of interest have to be developed and applied.

The work presented in this thesis uses data obtained with automated serial sectioning for a detailed analysis of coating layer structures and fiber cross section properties.

1.2 Contributions and background

Analysis of three dimensional paper structure with automated serial sectioning is one of the major fields of research at the Institute for Paper, Pulp and Fiber Technology at Graz University of Technology. The following list summarizes the main contributions of this thesis in the development and applications of the automated serial sectioning technique:

- **Enhancements of digitization process**

A newly developed curing form enables embedding and digitization of $>20\text{ mm}$ long paper cross sections. The obtained blocks allow an analysis of sample areas covering up to 1 cm^2 .

The final process added to the automated serial sectioning technique was the automated removal of slices from the diamond knife. Now, a triggered blowing device allows a fully unsupervised digitization of samples.

- **Definition of a sampling procedure in coating layer analysis**

A reasonable sampling procedure for a reliable analysis of coating layer structures was defined. The effects of several sampling variables on the results obtained were analyzed: resolution in the paper plane, sample size and sample geometry as well as the number of samples considered. The results do not only apply to serial sectioning, but are also valid for other analysis techniques of coating layer structure.

- **Analysis of fundamental coating layer properties**

Several properties of coating layers were estimated from the 3D data sets obtained with automated serial sectioning.

The spatial formation of coating layer was analyzed at different length scale to differ between the void filling effect at small structures (individual fibers) and the coating layer formation at large structures (fiber aggregates).

The relevance of coating holdout was evaluated with a novel measuring tool. Base paper porosity as well as coating formulation were discussed as possible influencing parameters on coating holdout.

First approaches to determine coating coverage were presented and influencing parameters were discussed. These include the estimation of an uncovered fraction of the base sheet as well as the analysis of neighboring regions of uncovered spots.

- **Estimation of fiber cross section properties**

A fundamental concept to estimate fiber cross section properties in the dry state from a sequence of paper cross sections obtained with automated serial sectioning was developed. The proposed way to analyze fiber cross section properties

starts with the segmentation results of individual fibers which have to be re-sized. This is followed by an estimation of basic properties, classification of fiber cross sections and the calculation of several specific fiber parameters.

A first approach to determine the size of a sample for a representative analysis of fiber cross section properties was introduced.

The applicability of the introduced concept was demonstrated by the analysis of various examples like the effect of PFI-mill treatment on fiber cross section properties or the influence of fiber cross section properties on dewatering properties of pulp and on final sheet properties.

This work formed the basis of a research proposal titled "**FiberMorph - Cross Sectional Pulp Fiber Morphology**" submitted to the Austrian Science Fund. The project was approved and will be started in November 2010. The goal is to tackle the limitations of the current approach to analyze fiber cross section properties.

The work presented in this thesis resulted from various research projects, dealing with development as well as application of automated serial sectioning to the analysis of three dimensional paper structure:

- **Digitized Paper Structure**

This project was funded by the Austrian Research Promotion Agency Ltd. (FFG) and by the Austrian paper industry during the period from October 2003 to September 2008. In order to analyze 3D paper structure a basic concept of the automated serial sectioning technique as well as some first applications were designed and developed. DONOSER [2007]; WILTSCHKE [2006] conducted their PhD-theses within this research project.

- **Research Studio Austria μ STRUCSCOP**

The program line "Research Studio Austria" is funded by the BMWFJ - Federal Ministry of Economy, Family and Youth of the Republic of Austria. The project μ STRUCSCOP runs from February 2009 - January 2012. The goal of this project is a construction of a second generation prototype of the automated serial sectioning technique. The concept for a second generation automated serial sectioning prototype is based on WILTSCHKE ET AL. [2010].

- **Analysis of Coating Holdout and Coating Coverage Using the μ STRUCSCOP Automated Serial Sectioning Method**

The main goal of this industrially funded research project during the period from July 2009 to June 2011 is to use data obtained from automated serial sectioning in the description of coating layer properties. The major topics of interest are a definition of a sampling procedure for detailed coating layer analysis as well as detailed analysis of spatial coating layer formation, coating holdout and coating coverage.

1.3 Thesis outline

This thesis is structured as follows:

Automated serial sectioning is the central theme of this thesis. Chapter 2 is closely related to an already accepted publication in the Journal of Microscopy written by Mario Wiltsche and myself, see WILTSCHÉ ET AL. [2010]. A basic concept of the digitization technique including hardware components and operating sequences is summarized. This section includes also a short review about its competing digitization methods in three dimensional paper structure analysis. The different applications of image data obtained are briefly outlined. Since these topics were already treated by WILTSCHÉ [2006] only a short overview is given.

Chapter 3, advances in coating layer analysis, as well as chapter 4, analysis of fiber cross section properties, are the main contributions of this thesis.

In Chapter 3 the application of automated serial sectioning in coating layer analysis is compared to the burnout test, scanning electron microscopy and X-ray microtomography. A focus is given to sampling strategies in order to get reliable and statistically meaningful results. Coating layer properties like the spatial formation of a coating layer, coating holdout and coating coverage are discussed in more detail.

A general concept to estimate fiber cross section properties in the dry state from data obtained with serial sectioning is introduced in chapter 4. Possibilities and current limitations of this approach are discussed in detail.

Finally, chapter 5 summarizes the presented work and gives an outlook pointing out further developments in the presented fields of research as well as other applications of data obtained with automated serial sectioning.

Appendix A explains the burnout test which is commonly used to quantify coating layer uniformity. Here, the burnout test is applied to validate results obtained with automated serial sectioning. Coating layer analysis was performed on several different samples, the sample parameters are summarized in Appendix B. Publications during my research work are compiled in Appendix C.

Methods Capable to Analyze 3D Paper Structure

This section is closely related to a recent publication, WILTSCHKE ET AL. [2010]. After a short introduction various important techniques used for three dimensional imaging of paper structures are discussed in section 2.2. Automated serial sectioning, the technique applied in the presented work to evaluate 3D paper properties, is explained in more detail. Section 2.3 gives a summary of the major hardware components and a basic working principle. Recent modifications and improvements allowing a fully unsupervised digitization of paper samples are presented. This section also gives a brief overview of the different applications in 3D paper structure analysis, see also the following chapters 3 and 4.

2.1 Introduction

Due to the complex nature of paper, the techniques applied to the analysis of 3D paper structures in the micron-range have to fulfil two conflicting requirements [WILTSCHE, 2006].

1. A high spatial resolution is required to detect important structural details. The diameter of papermaking fibers is usually in a range of 10 to 30 μm ; therefore a resolution at least in the micron-range is required.
2. Because of the highly inhomogeneous nature of paper, a sufficient sample size is needed to obtain reliable and statistically meaningful results. A sample size of several square millimeter is necessary to cover irregularities caused by e.g. fiber flocs.

This chapter summarizes the most important high resolution methods used in three dimensional paper structure analysis. The automated serial sectioning technique is explained in more detail since this is the method applied for different purposes in this thesis.

2.2 Common 3D digitization methods used in paper structure analysis

Different techniques are applied for the analysis of three-dimensional paper structures [BLOCH AND ROLLAND DU ROSCOAT, 2009; CHINGA-CARRASCO, 2009].

X-ray microtomography

SAMUELSEN ET AL. [2001] demonstrated the applicability of synchrotron radiation based X-ray microtomography as a non destructive method for 3D paper structure analysis at high resolution. First digital reconstructions of paper samples obtained with this technique were published by ANTOINE ET AL. [2002]. This technique is capable of analyzing paper samples in dry and wet state [HOLMSTAD ET AL., 2006]. High resolution X-ray microtomography was used to identify and characterize individual fibers [HAGEN ET AL., 2004] and to evaluate 3D fiber orientation [AXELSSON, 2008]. Also porosity and permeability as well as thermal conductivity of fibrous materials were evaluated based on data obtained with this technique [AXELSSON AND SVENSSON, 2009; GOEL ET AL., 2006; LUX ET AL., 2006; ROLLAND DU ROSCOAT ET AL., 2005, 2008]. Synchrotron radiation based X-ray microtomography is only possible at a small number of research facilities around the world.

The applicability of low resolution X-ray microtomography was discussed by HOLMSTAD ET AL. [2005]. Compared to the synchrotron radiation based technique

with a maximum achievable resolution of about $0.35 \mu m$ per voxel, a lower resolution in the range of 1 to $5 \mu m$ per voxel is possible. Applications of this technique were focused on the analysis and visualization of coating structures [CHINGA ET AL., 2007A; TURPEINEN ET AL., 2005] and surfaces of coated papers [CHINGA-CARRASCO ET AL., 2008]. A limiting factor of this technique is its inverse relation between resolution and sample size. For example, in coating layer analysis samples of about $2 \times 2 mm^2$ are analyzed at the highest resolution possible.

Confocal laser scanning microscopy

Three dimensional analysis of paper structure can be carried out using confocal laser scanning microscopy (CLSM), another non destructive method providing a three-dimensional resolution in the sub-micron range. This technique was frequently used to analyze transverse morphology of individual fibers [HE ET AL., 2003B; JANG ET AL., 1992]. Pioneering work with CLSM in paper structure analysis was presented by MOSS ET AL. [1993]. They determined the location of fibers in a sheet of paper and characterized the internal sheet structure as well as the surface profile of paper. CLSM was also used to analyze the distribution of fibers in paper thickness direction [XU ET AL., 1997] or to estimate the macro pore structure in a sheet of paper [DICKSON, 2000B]. OZAKI ET AL. [2006] applied this method for the analysis of coating layers by detecting binders which were stained with a fluorescent dye. They reported also the possibility to detect air bubbles in a coating layer with this method. The limiting factor of confocal laser scanning microscopy in paper structure analysis is the rapid reduction of signal intensity with an increasing depth of the focal plane. This leads to difficulties in e.g. the detection of individual fibers.

Scanning electron microscopy

Three-dimensional analysis of paper structures can also be performed with scanning electron microscopy, e.g. by serial thin sectioning [ARONSSON ET AL., 2002] or serial grinding [CHINGA ET AL., 2004]. Both approaches give several subsequent single cross sections of paper with a high degree of detail. Such data sets were used for the reconstruction of a fiber network and the analysis of individual fiber properties [SVENSSON AND ARONSSON, 2003], for the analysis of pore structures in a sheet of paper [SINTORN ET AL., 2005] and for a detailed characterization of pore structures in coating layers [CHINGA AND HELLE, 2003]. These techniques require extensive manual user interaction and are time consuming. The obtained 3D digital representations of paper are limited to small sample sizes.

Serial sectioning

A combination of serial sectioning and light microscopy is - like SEM imaging - a destructive way to digitize the three dimensional structure of paper. Such a technique was first used for the explanation of the internal sheet structure by HASUIKE ET AL. [1992]. In general, serial sectioning allows a true three-dimensional analysis of structures with usually sufficient resolution (light optical microscopy). Images are acquired at the block surface or from the thin cut slices. The handling of individual slices is time consuming and often a source of failures. Geometrical distortions, caused by compressive forces during cutting, or even loss of slices due to cutting and manipulation are unavoidable. Imaging the block surface does not give this magnitude of distortions, but manual user interaction is required. The most common approach is based on unclamping and reclamping the sample during cutting and image acquisition. A first concept of an automated system, acquiring a single image of the block surface after each cut, was introduced by KERSCHMANN [2000].

2.3 Automated serial sectioning technique

A technique for automated three-dimensional digitization of paper based on block surface imaging with an increased field of view was presented by WILTSCHE [2006]. A schematic drawing of the developed prototype is shown in Figure 2.1 (a), illustrating all major hardware components. A standard microtome is used to cut off thin slices from a resin embedded paper sample. The microscope is mounted on a moveable stage in front of the microtome which enables the acquisition of an image sequence of the block surface after each cut. All components can be accessed and controlled by a digital interface using a standard personal computer. A photograph of the prototype built is shown in Figure 2.1 (b). The following subsections summarize the basic hardware components and the working principle as developed by WILTSCHE [2006]. Also the modifications to the methods, which were implemented during the course of this thesis work, are presented.

2.3.1 Hardware components in use

A fully automated imaging process requires a motorized microtome. In this case, a LEICA RM 2155¹ is used. The microtome is equipped with a stationary knife holder and a forward-moving block holder to yield an almost constant position of the block surface for straight forward focussing with the microscope after each cut. The microtome has a retraction device to avoid scratches at the block surface and to prevent the knife from damage induced by a moving block.

¹Leica Microsystems, Wetzlar (Germany). www.leica-microsystems.com

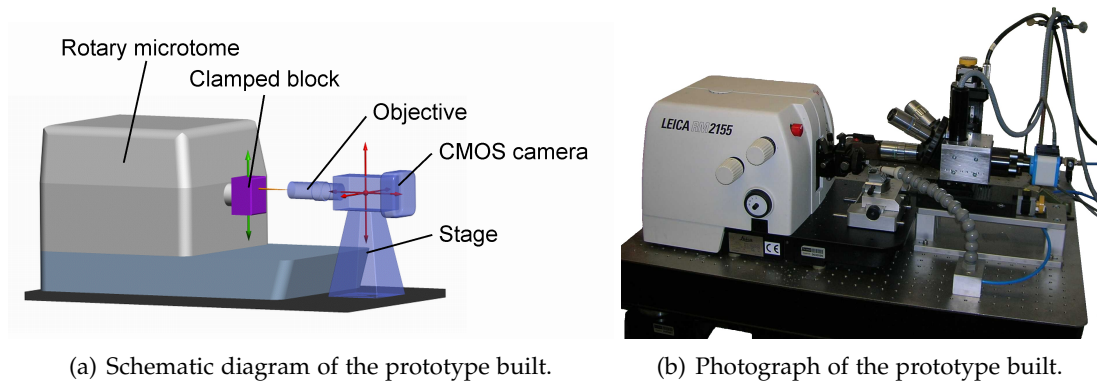


Figure 2.1 Layout of the prototype built. A schematic drawing giving the major hardware components and motions is shown in (a), [WILTSCHE, 2006]. Red arrows indicate the ability to move the microscope (light blue) in all three dimensions. The green arrows indicate the cutting movement of the rotary microtome. Images can be acquired directly at the cut surface without unclamping the embedded sample (magenta). A photograph of the prototype is shown in (b).

The image quality obtained should not change over a long time period. A critical parameter to influence the image quality is the knife material. Even soft blocks obtained with methacrylate based resins require diamond knives to obtain a smooth and scratch free surface of the cut block. A histo cryo 45° from DIATOME² with an edge length of 4 mm is in use. The cut off slices are removed by pressurized air in order to prevent the knife from damage during the sectioning sequence.

The total weight of the microscope has to be as low as possible, since it has to be moved in all three directions of space and positioned with high precision. A custom built microscope was developed; the components were supplied by ALICONA³. The microscope objectives are MITUTOYO M Plan Apro objectives⁴ with infinity correction providing a long working distance. These are optimized for bright field illumination and suitable for in-line co-axial illumination. The camera used is the ALICONA ALC13 with a CMOS chip. The chip has a size of $6.66 \times 5.32\text{ mm}^2$ with $1280 \times 1024\text{ pixel}$. The optical performance of the microscope is summarized in Table 2.1. White light for co-axial, bright field illumination is provided by a halogen cold light source supplied by VOLPI⁵ (INTRALUX DC-1100). A flexible fiber optic light guide delivers the light to the body tube of the microscope.

The microscope is fixed on a moveable stage. Three linear stages manufactured by OWIS⁶ ($2 \times$ LM 60 and $1 \times$ LIMES 90) are mounted orthogonally to each other. The linear stage with the highest precision (LIMES 90) is needed in the direction of

²Diatome Ltd., Biel (Switzerland). www.diatome.ch

³Alicona Imaging, Grambach (Austria). www.alicon.com

⁴Edmund optics, Karlsruhe (Germany). www.edmundoptics.de

⁵Volpi, Schlieren (Switzerland). www.volpi.ch

⁶OWIS, Staufen (Germany). www.owis-staufen.de

Magnification	Pixel size [μm]	Field-of-view [μm^2]	Resolution [μm]	Depth of focus [μm]
10	0.804	1028.8×823.0	1.12	3.5
20	0.402	514.4×411.5	0.84	1.6
50	0.161	205.8×164.5	0.61	0.9

Table 2.1 Selected parameters of the optical microscope depending on the magnification used. These data were summarized by WILTSCHKE [2006].

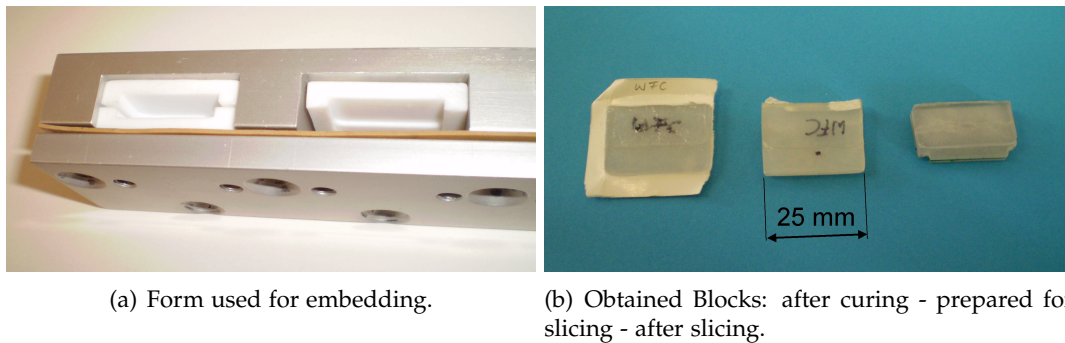


Figure 2.2 Newly developed embedding technique for the preparation of sample areas larger than 1 cm^2 (a) and the obtained blocks for serial sectioning (b).

the optical axis to be able to focus accurately. This is of particular importance when an objective with a high magnification and a low depth-of-focus is used. The three-dimensional movability of the microscope is necessary to acquire a set of adjacent images of the cut block surface.

The microtome and the stage with the microscope are placed on a vibration isolation table to avoid vibration induced disturbances during imaging. A commercially available table from TMC⁷ (63-500 Series Lab) is in use.

All operations necessary for automatic imaging are controlled with a conventional desktop PC; triggering the microtome and the pressurized air slice removal, positioning the microscope, focusing the image plane, imaging the block surface in a sequence of images and saving the images.

2.3.2 Sample preparation

Serial sectioning requires the embedding of the sample in a supporting medium to protect its structure during sectioning. A diversity of embedding materials like methacrylate, polyester and epoxy resins are available today. Slice thicknesses in a range of 1 to $5\ \mu\text{m}$ require stable and soft blocks at the same time. Sectioning tests

⁷Technical Manufacturing Company (TMC), Peabody (USA). www.techmfg.com

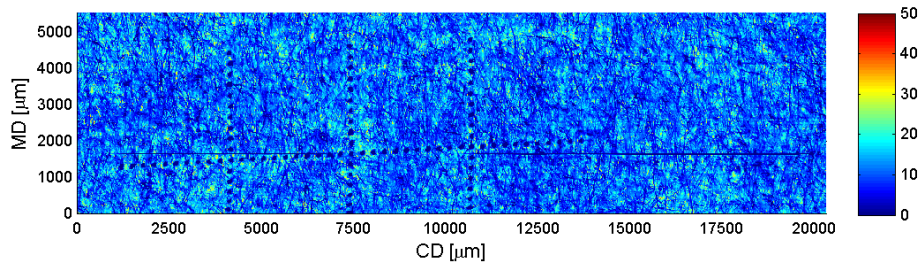


Figure 2.3 Coating thickness map obtained with new embedding technique. More than 600 cross sections each having a length of more than 20 mm were digitized and analyzed. The color bar indicates the coating thickness in μm .

revealed methacrylate based resins like Technovit®7100⁸ as suited for digitization of paper cross sections covering a sample area of up to 1 cm^2 with automated serial sectioning.

The samples are usually embedded in gelatine capsules with a diameter of 5 to 9.5 mm, which defines the maximum cross section length. A new embedding technique was developed which allows digitization of up to 25 mm long paper cross sections, see Figure 2.2. A paper sample is placed between two milled teflon plates. These plates provide the negative form of the final block, Figure 2.2 (a). After curing and adjusting the block geometry, the obtained blocks can be clamped at the microtome for slicing and imaging, Figure 2.2 (b). A 3D data set obtained with this technique after image processing is illustrated in Figure 2.3, showing a coating thickness map covering a sample area of $5.5 \times 20\text{ mm}^2$. The hole pattern in this visualization are landmarks which are used for registering this map with other 2D property maps of a paper sample like e.g. local brightness, see HIRN ET AL. [2009] for more details.

2.3.3 Digitization routine and processing of image data

Paper as a planar material is placed vertically in the microtome so that the paper thickness can be imaged. Repeatedly, thin slices are cut off the clamped block with the diamond knife and the cut surface is scanned without any need of unclamping the sample. Since the field-of-view covered by a single image does not reach the required sample size, it is necessary to acquire a sequence of adjacent images covering the entire region of interest. Therefore the microscope is moved step by step until the entire region of interest is imaged. Slicing, focusing and imaging are fully automated processes without the need of any user interaction after once adjusting the microscope before the first cut is performed. Slicing and imaging of a single paper cross section having a length of about 5 mm (15 images with the $20\times$ magnifying objective) will take about one minute.

⁸Heraeus Kulzer GmbH&Co.KG, Wehrheim (Germany). www.Kulzer-Technik.de

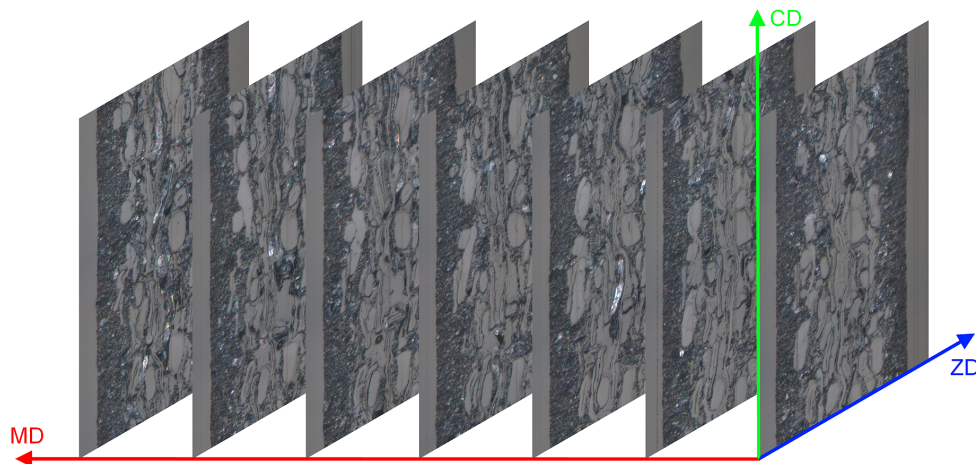


Figure 2.4 3D image data set obtained from serial sectioning. This example shows a small cut-out of a woodfree coated paper (WFC). Each cross section has a length of $240\ \mu\text{m}$.

The voxel size in the 3D image data obtained with the prototype is determined by the cut thickness ($1\text{-}12\ \mu\text{m}$) between the image planes and the magnification of the objective used in the image plane ($0.8\text{-}0.16\ \mu\text{m}/\text{pixel}$, see Table 2.1 for more details). The voxels are usually anisotropic since the pixel size is more than one order of magnitude lower than the slice thickness in the paper plane.

Two different processing steps - stitching and aligning - have to be applied to the set of acquired images. Stitching is used to convert the overlapping sequence of acquired images per slice into a single composite image. Aligning is necessary to eliminate vertical displacements between the individual slices. A commercial software, ImagePro® Plus⁹, is used for both steps leading to a final digital 3D representation of the embedded paper sample.

A small cut out of an image sequence is depicted in Figure 2.4, showing a woodfree coated paper sample. MD, CD and ZD denote a coordinate system in paper, where MD is the main direction of paper production, CD is the papers cross direction and ZD the paper thickness direction. Several three dimensional structural features of paper can be seen in this cut out. First the dark regions at the paper surfaces represent the coating layers which show considerable thickness variations already in this small cut out. Second, some fibers show remarkable changes in their position in the paper web and in their cross sectional shape along the image sequence. By the use of appropriate image analysis routines, structural features like those mentioned above are evaluated.

⁹ImagePro® Plus, Version 6.0. MediaCybernetics, Bethesda, MD (USA). www.mediacy.com

2.3.4 Fields of applications

This section gives a short overview of the different applications of the automated serial sectioning technique. Compared to other techniques, serial sectioning allows the analysis of very different properties without the need for massive changes in the digitization setup.

Coating layer analysis

The analysis of coating layer structures is currently the most important application of automated serial sectioning in paper structure analysis, see chapter 3 for more details:

A 3D color segmentation algorithm is used to extract the coating layer from the paper cross section images obtained in serial sectioning, giving a sequence of binary images where the coating layer is highlighted [DONOSER ET AL., 2006]. From these binary images, a set of distance values is extracted, representing coating and base sheet thickness as well as base sheet and coated sheet topography data [WILTSCHKE ET AL., 2005]. These data can further be used to create coating thickness maps, see Figure 2.3 or for a more detailed analysis of three dimensional coating structures like formation of a coating layer, coating holdout or coating coverage. The vast amount of data and the comparatively large sample areas accessible in a short period of time are the major benefits of automated serial sectioning in this field of research.

Evaluation of fiber cross section properties

The images obtained with serial sectioning are also often used in the in-situ analysis of fiber cross section properties in a sheet of paper, see chapter 4 for more details.

Individual fiber cross sections are detected in a first image and then followed through the entire image stack [DONOSER AND BISCHOF, 2006]. Because the fibers are usually not oriented perpendicular to the image plane, the cross sectional dimensions are generally overrated. In order to obtain true representations of the fiber cross section properties, the measurements are performed on resized cross sections. Although there are still numerous limitations in the currently used approach, first promising results were obtained like the measurement of differences between various wood specimens or changes of fiber cross section properties caused by beating in a PFI-mill.

Other approaches

The evaluation of paper surface topography respectively the measurement of paper thickness of uncoated papers is another possible application of data sets obtained with serial sectioning. For this purpose the surface contour of the paper is extracted from the images with a standard edge detection algorithm. This approach is also important

for the coating layer analysis of one side coated papers and is used to create a virtual coating layer at the uncoated side.

Also the three dimensional orientation of individual fibers in a sheet of paper can be extracted from the sequence of paper cross sections obtained with serial sectioning. An image analysis algorithm to track the fiber cross sections center of mass along the acquired image sequence was developed. In an ideal case this would result in a set of locations of the fiber's center of mass for all fibers in every image. In the current status, a user has to identify the fibers to be tracked, which is a limitation because just a fraction of the fibers in a sheet of paper can be considered.

Both approaches, the evaluation of surface topography and thickness of uncoated papers as well as the three dimensional fiber orientation, will not be discussed in more detail since only first experiments to demonstrate these utilizations of the images obtained with the serial sectioning technique were performed.

Another research group at the Institute for Paper, Pulp and Fiber Technology applied automated serial sectioning to measure the bonded area of individual fiber to fiber bonds [KAPPEL ET AL., 2009].

2.4 Conclusions

A prerequisite for a better understanding of the complex three dimensional structure of paper are imaging techniques that provide a sufficiently high resolution and are able to cover a large sample area at the same time. This chapter briefly summarized the different approaches used to digitize the three dimensional structure of paper and gave a closer description of the automated serial sectioning technique developed at the Institute for Paper, Pulp and Fiber Technology at Graz University of Technology.

The automated serial sectioning technique presented in this chapter combines a rotary microtome and a light optical microscope. Sample areas covering more than 1 cm^2 in size can be digitized; a spatial resolution below $1\text{ }\mu\text{m}$ can be achieved. The obtained digital three dimensional representation of paper is a set of paper cross sections, which are used in the analysis of several three dimensional paper properties. The coating layers on the surfaces of a paper web are analyzed in terms of uniformity or other characteristic structural measures. A true estimation of fiber cross section properties can be performed for individual fibers in a sheet of paper. Further applications are the detection and analysis of the paper surfaces and a first approach to determine the three dimensional fiber orientation.

The following chapters will focus on the two major applications, the coating layer analysis in chapter 3 and the analysis of fiber cross section properties in chapter 4.

Advances in Coating Layer Analysis

Novel coating layer analysis methods based on data obtained with serial sectioning are presented. Following a brief introduction, the first section 3.2 discusses the most important techniques used in coating layer analysis and presents comparisons of results obtained with different techniques and the serial sectioning technique showing the validity of the results. This section is followed by recommendations regarding the sampling strategy in high resolved spatial coating layer analysis, see section 3.3. The coating layer formation is analyzed at different length scales, section 3.4. The effect of different application systems as well as calendaring on the spatial coating layer formation are discussed. Two new approaches to classify coating layer properties, coating holdout in section 3.5 and coating coverage in section 3.6 are presented and reveal further research potential. Measures to define coating holdout as well as coating coverage are discussed and different influencing parameters are analyzed.

3.1 Introduction

A detailed knowledge about the coating layer on the paper surface is necessary to understand how and to what extent final sheet properties are influenced. The analysis of coating layers can be divided into two large fields of research, the chemical characterization and the structural characterization of coating layers [VYÖRYKKÄ ET AL., 2006]. The application of automated serial sectioning leads to a focus on the structural characterization of coating layers, which again has to be divided into two groups:

On the one hand, there are approaches for a detailed analysis of structures in the sub-micron range e.g. the pore structure of the coating layers or the way individual pigments are oriented. This is generally achieved with highly sophisticated measuring equipment like FIB (focused ion beam e.g. [HEARD ET AL., 2004; PRESTON ET AL., 2009]) or AFM (atomic force microscopy, scanning probe microscopy e.g. [DI RISIO AND YAN, 2006; JÄRNSTRÖM ET AL., 2007]). But also integral measuring techniques like mercury porosimetry are used, see for instance [RESCH ET AL., 2010]. A summary of these and other methods used to analyze the surface of (coated) papers was given by PRESTON [2009].

On the other hand, research focuses on the spatial coating layer structure in the micro-meter scale, the scale accessible with the automated serial sectioning technique. The term "spatial coating layer structure" can be seen as a summary for more specific terms like coating coverage, coating holdout or spatial coating layer formation. These structures are interrelated with each other and the used terms are not clearly defined in literature. In this thesis, the following definitions are used:

- **Coating layer formation / coating layer uniformity**
Variations of the spatial formation of a coating layer are caused by e.g. base sheet topography, application system type or calendering, see for instance [HUANG AND LEPOUTRE, 1995; ZOU ET AL., 2001]. A measure to quantify coating layer formation is the interrelation between coating thickness and base sheet topography. A uniform coating layer is thought to give better coverage with a uniform pore structure and a uniform chemical composition which both are prerequisites for good printability, e.g. [ENGSTRÖM AND LAFAYE, 1992; KENT ET AL., 1986].
- **Coating holdout**
Coating holdout is defined as the base paper's resistance to coating penetration [GRÖN AND AHLROOS, 2001; HUANG AND LEPOUTRE, 1998]. This property can be measured as a fraction of penetrated coating. Coating holdout is important because a loss of coating color due to penetration into the base paper can only be compensated with additional coating color to achieve the desired final paper qualities [ADAMS, 1983; TREFZ, 1996].

- Coating coverage

This property represents the fraction of a paper surface that is well covered by a coating layer [AZIMI ET AL., 2009]. The application of a uniform coating layer and the prevention of extensive coating penetration contribute to the overall goal of a perfect coverage even at the lowest coat weights [ENGSTRÖM, 1999; WIKSTRÖM AND GRÖN, 2003].

This chapter presents the different novel approaches developed to determine these coating layer properties from three dimensional data sets obtained with the automated serial sectioning technique. A comparison with other techniques used in this field of research as well as a discussion of the influence of sampling strategies is given.

3.2 Exploring the spatial coating layer structure

3.2.1 The different methods applied in coating layer analysis

WILTSCHKE [2006] summarized the methods used for analysis of the coating layer structures in the micro-meter scale. This section gives a brief overview of techniques which were repeatedly used or newly introduced in this field of research.

In general, the analysis of coating layer structures can be subdivided into two groups. The first group, including serial sectioning, enables the measurement of coating thickness and topography data directly in paper cross sections or other digital representation of a paper sample to be analyzed. Both, 3D digitization techniques as well as the analysis of single cross sections are used. The second group includes indirect measurements which result in a two dimensional coating thickness map usually covering a larger sample area of several square centimeter, e.g. the burnout test. This group is important since these methods are typically easier to handle in day to day research. The major fraction of published works dealing with coating layer structures are based on this second group.

Direct measurement of thickness and topography data

A frequently used technique to analyze coating layer structure is scanning electron microscopy (SEM). Single cross sections having a length of several millimeters are prepared and digitized at a high resolution [PETERSON AND WILLIAMS, 1992]. Imaging in the backscatter mode enables the detection of coating layers by simply setting a threshold. ALLEM [1998]; ALLEM AND UESAKA [1999] introduced a measuring concept which enables the analysis of coating and base paper thicknesses as well as base sheet and final sheet topography. This concept is employed up to now for the extraction of coating thickness data and other properties from cross section images, see for instance DAHLSTRÖM ET AL. [2008]; KLEIN AND SCHULZE [2006]; WILTSCHKE ET AL. [2005]; ZOU ET AL. [2001]. The approach presented for a 3D analysis of coating structures with

scanning electron microscopy [CHINGA ET AL., 2004] has not been applied to spatial coating layer analysis so far. Only the pore structure of coating layers in the sub micron range was analyzed with this technique so far [CHINGA AND HELLE, 2003].

The applicability of X-ray microtomography for a three dimensional analysis of coating layers was shown by TURPEINEN ET AL. [2005]. Table-top scanners (e.g. Skyscan 1172) were emerging techniques at this time, but resolution and contrast in the images obtained were still too low for the analysis of coating layers. Images obtained with synchrotron radiation based X-ray microtomography were easier to handle because of the higher degree of detail achievable with this technique (contrast and resolution). The first results presented indicate an influence of base sheet thickness on coating layer thickness whereas the base sheet porosity has no influence on coating thicknesses. Later works have also shown the applicability of table-top CT scanners for coating layer analysis because of rapid developments in imaging and image analysis [CHINGA ET AL., 2007A; CHINGA-CARRASCO ET AL., 2008].

The three dimensional formation of the coating layer on a sheet of paper was also studied with confocal laser scanning microscopy [OZAKI ET AL., 2006, 2008]. A fluorescent dye is used to stain the latex binder in the coating, the pigments as well as the cellulosic material in the base paper keep unstained. Further sample preparation is not required.

Serial sectioning combined with light microscopy and novel image analysis tools was presented as a promising method for a detailed three dimensional coating layer analysis [WILTSCHKE, 2006; WILTSCHKE ET AL., 2005, 2006], see section 2.3 for general information about the digitization concept and section 3.2.2 for process details in coating layer analysis.

Indirect mapping of coating thicknesses on large paper samples

The most common technique used to analyze the spatial formation of a coating layer on a large sample (several square centimeters) is the burnout test. This test was originally introduced by DOBSON [1975]. A coated paper sample is soaked in a dewatering agent, dried and then placed in an oven. The cellulosic material in the base paper darkens whereas the inorganic components in the coating layer keep their brightness. Non-uniformities in the coating layer become visible that way. Typical test conditions are summarized in Appendix A. Image analysis methods were introduced for a more in-depth evaluation [ENGSTRÖM AND LAFAYE, 1992]. Also local coat weights were calculated from the obtained gray scale images [ENGSTRÖM AND MORIN, 1996]. However, the test is influenced by different parameters like filler content and also the fibrous material used in paper production [DICKSON ET AL., 2002; O'NEIL AND JORDAN, 2000].

Coat weight maps can also be created with X-ray imaging [AZIMI ET AL., 2009]. Paper samples are exposed to X-rays in a microtomograph and the transmitted X-rays are detected giving a gray scale image. Base paper absorption effects are avoided by

the subtraction of an average absorption rate of the uncoated base paper. The gray scale image is finally transformed to a local coat weight map by the use of a calibration curve giving an average coat weight at an average gray level. An initial application of this technique is the estimation of coating coverage which was found to correlate with the burnout test. However, the limiting factor is that fillers and coating cannot be distinguished and therefore this technique is unsuited for coated papers with a higher filler content.

Similar to x-ray imaging are techniques like electrography by determining the local loss of energy of an electron beam by passing a sample [TOMIMASU ET AL., 1990], or the straight forward way using β -radiography by calculating the difference in standard deviations of the gray scales from the uncoated and coated sheet as a measure for coating layer uniformity [KARTOVAARA, 1989].

3.2.2 Analysis steps to extract coating thickness data

The development of fundamental analysis routines as well as first applications of automated serial sectioning in coating layer analysis were described by WILTSCHKE [2006]; WILTSCHKE ET AL. [2005]. This section gives a brief summary of the different process steps and parameters used to analyze coating layers.

Digitization of paper cross section and image pre processing

Digitization of paper samples for coating layer analysis is not performed at the highest resolution possible. Usually the 20 \times magnifying objective is chosen (pixel size: 0.402 μm , resolution: 0.84 μm). In special cases like board samples or extensively large sample areas, a lower resolution is applied in order to increase the field of view covered by a single image. The use of a higher magnification causes difficulties in image analysis because individual pigments become visible in the coating layer disturbing the homogeneous structure required for image analysis; see the comparison of cross section images obtained with incident light microscopy and scanning electron microscopy in section 3.2.3. The slice thickness in standard coating layer analysis is usually set to 12 μm , see section 3.3.1. The large thickness is important in order to speed up the analysis because digitization is still the time limiting factor.

A typical coating layer analysis is carried out on a 5 mm^2 paper sample. The sample geometry is defined by the length of the paper cross section which is usually set to 5 mm . 84 subsequent cross sections are required at a slice thickness of 12 μm to cover the sample area. Digitization of a 5 mm^2 sample with these parameters using the 20 \times magnifying objective takes 2 *hours*.

The sample size and the sample geometry were selected based on the experience from more than 500 analyzed samples because the effort in sample preparation, the time needed for digitization and the results obtained seemed to be well balanced. A

detailed discussion of the sampling procedure in section 3.3.1 supports the choices of sample size and sample geometry.

The coating layer(s) are extracted from the obtained digital representation of the paper sample for further analysis.

2nd generation image analysis

The first approach to detect coating layers from the cross section images was based on a pixel wise decision whether the pixel is coating or not [WILTSCHE, 2006]. Because the data sets were getting larger and larger, a faster segmentation approach had to be developed.

DONOSER ET AL. [2006] presented a modified approach to detect the coating layers from the cross section images which can be explained -from a paper makers point of view- by three subsequent steps:

1. First a typical region of interest has to be defined. This has to be performed by a user who has to extract a freeform-line or a rectangle from the first image of the image stack, indicating the color of the regions to be detected.
2. Calculation of a similarity measure between each pixel within a kernel of size $x \times y \times z$ (CD-pixel \times MD-pixel \times cross sections, odd numbers are required because the pixel of interest has to be in the center) in the cross section stack to be analyzed and the region of interest. This step covers the main improvement compared to the first image analysis approach which calculated the similarity measure for each individual pixel whereas now only one iteration step is necessary to analyze a whole image at once. This results in a gray scale map of similarity measures.
3. From this map of similarity measures, simply speaking the regions having a homogeneous gray scale and a high contrast to the background (maximally stable extremal region, MSER) are identified as coating layers. The steps 2 and 3 are repeated until the whole image stack defined by the number of cross sections is analyzed.

The calculation of the similarity measure considers a three dimensional kernel around the one pixel of interest. Taking into account also the neighboring pixels results in better segmentations because small irregularities like glare effects can be leveled out. The drawback of this approach is that the coating layer borders are smoothed which is especially the case for large kernel sizes. The use of a 3D kernel is very difficult for the large slice thicknesses used ($12 \mu m$, see section 3.3.1 for more details). The borders between coating and base paper change tremendously and this leads to a strong smoothing of this border line. Also the use of different kernels for

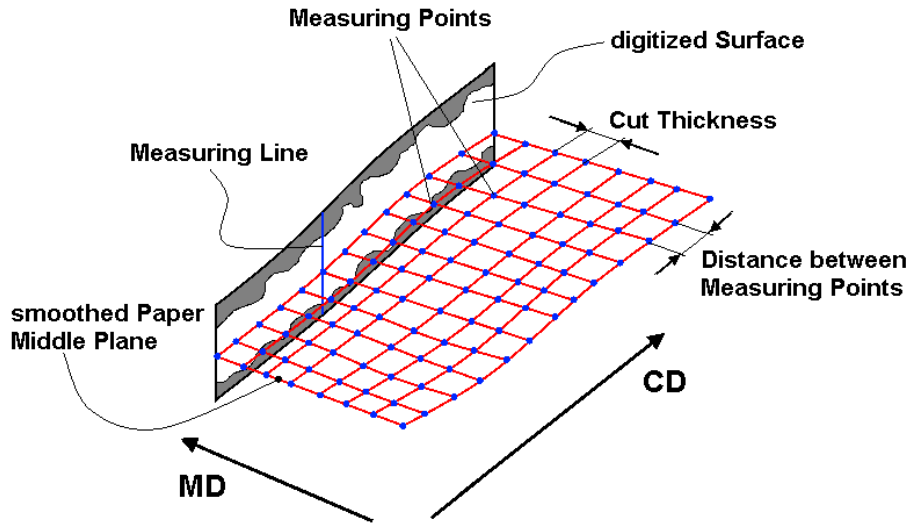


Figure 3.1 Definition of measuring points in the paper plane to extract thickness and topography data.

the segmentation of different papers to be compared is not recommended for the same reasons.

To avoid any influences from coating segmentation, the kernel size as a major influencing parameter was set to $7 \times 7 \times 1$ (CD-pixel \times MD-pixel \times cross sections). The segmentation finally results in a sequence of binary images highlighting the coating layers and regions with a similar appearance in the base paper.

Measuring of coating thickness and topography data

From the binary images highlighting the coating layer, several distance values representing local coating and base sheet thicknesses as well as base sheet and coated sheet topographies are extracted. The basic measuring concept was introduced by WILTSCHKE ET AL. [2005].

The thickness and topography data are obtained at the nodes of a virtual measuring grid which defines the final map of distinct measures, see Figure 3.1. This grid is thought to rest on a smoothed paper center plane, which is located in the middle between both paper surfaces, indicated by the coating layers in the exemplary cross section in Figure 3.1. The measuring grid is defined by the slice thickness and a distance between the nodes in the image plane. This distance is adjusted to the slice thickness, giving an almost square measuring grid.

The extraction of thickness and topography data is performed along measuring lines which are oriented perpendicular to the paper center line of a single cross section as can be seen in Figure 3.2. The different thickness and topography data obtained

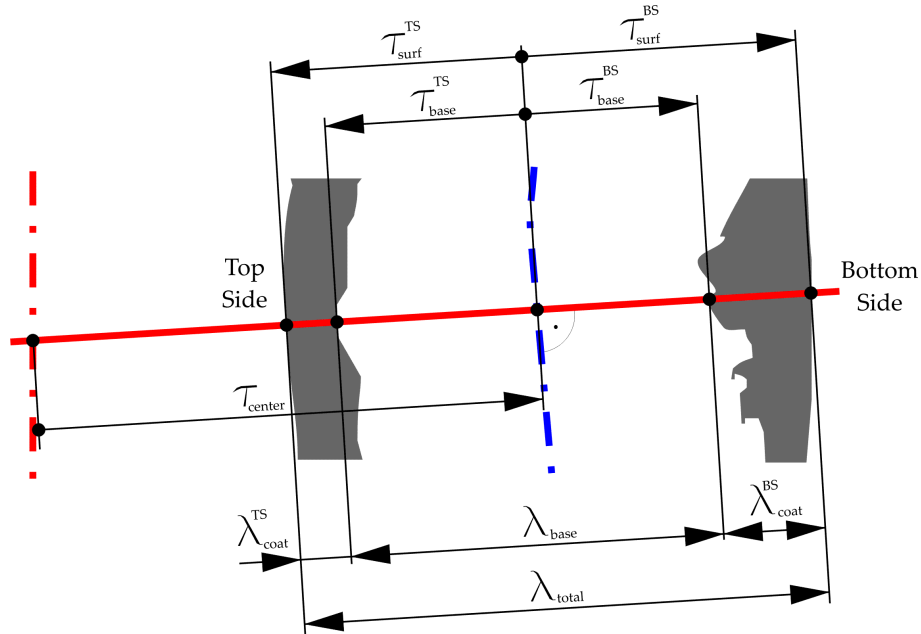


Figure 3.2 Definition of thickness and topography data obtained from the detected coating layers [WILTSCHKE ET AL., 2005]. The measures are explained in Table 3.1.

Abbr.	Explanation
λ_{coat}^{TS}	Top Side Coating Thickness
λ_{coat}^{BS}	Bottom Side Coating Thickness
λ_{base}	Base Sheet Caliper
λ_{total}	Total Sheet Caliper
τ_{surf}^{TS}	Top Side Surface Topography
τ_{surf}^{BS}	Bottom Side Surface Topography
τ_{base}^{TS}	Top Side Base Sheet Topography
τ_{base}^{BS}	Bottom Side Base Sheet Topography
τ_{center}	Center Plane Topography

Table 3.1 Thickness and topography data obtained with image analysis [WILTSCHKE ET AL., 2005].

along the measuring line are listed in Table 3.1. The final result is a stack of matrices (maps) containing the different measures at the same positions.

For a conventional coating layer analysis like the determination of a mean coating thickness or an estimation of the interaction between base paper topography and coating thickness, only the outermost regions detected as coating are evaluated. All separated regions denoted as coating in the paper are not considered. The reason is that only the outermost regions of the coating layer contribute to the basic goals of coating like the formation of an uniform surface and coating coverage. However, there is an option to consider all regions detected as coating and this will be used in an approach to evaluate coating holdout, see section 3.5.

A limitation of this measuring tool is that only papers coated on both sides can be analyzed because the calculation of the paper center plane requires a well defined surface at the paper top and bottom side. One side coated papers like e.g. board samples or a large number of pilot and laboratory coated papers cannot be analyzed. In order to overcome this limitation, another image analysis routine based on edge detection algorithms was developed to detect the paper surface which can then be used as an imaginary coating layer on the uncoated back side of the paper.

3.2.3 Validation

For a better understanding of the results obtained with serial sectioning and in order to validate results, several comparisons with other techniques used in coating layer analysis were carried out. Techniques for indirect mapping of coating structures as well as direct measuring of coating thicknesses in cross section images were considered.

Comparison of serial sectioning and burnout test

The burnout test is commonly used to estimate the uniformity of a coating layer [DOBSON, 1975; ENGSTRÖM AND LAFAYE, 1992]. Results obtained with the burnout test (parameters are summarized in Appendix A) and the serial sectioning technique were compared. Several different sample series like calendering studies (see Appendix B) were analyzed. Three randomly taken samples, each having a size of 5 mm^2 were analyzed with the serial sectioning technique for each sample specimen. The samples investigated with the burnout test covered an area of $2.1 \times 2.1\text{ cm}^2$. Figure 3.3 shows the results, a coefficient of variation of the coating thickness data on the y-axis and the coefficient of variation of the gray scale data obtained from the burnout tests on the x-axis.

The measures plotted in this graph show in general the expected overall trend that a higher coefficient of variation of the coating thickness data gives a higher coefficient of variation of the gray scale data from the burnout test. This is not a surprising result, but if one looks closer to individual sample groups this trend does not exist anymore.

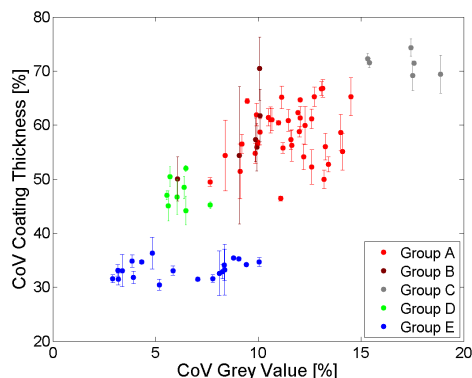


Figure 3.3 Coating uniformity determined with the serial sectioning technique (coefficient of variation in coating thickness data) and the burnout test (coefficient of variation in gray scale data).

This is obvious for sample group E indicated with blue dots representing a calendering study. The differences in the coefficient of variations of the coating thickness data obtained with automated serial sectioning technique do not show an obvious trend. The corresponding coefficient of variations of gray scale data can be divided into two groups: at low coefficient of variations (<5%) are the uncalendered samples and at higher values (~10%) the calendered samples. An extensive coating thickness analysis study of these samples has shown that coating thickness distribution (mean and standard deviation of coating thickness data) are hardly influenced by post calendering, see section 3.4.3. This leads to the conclusion that the burn out test does not give an accurate measure for the coating layer uniformity. These findings are supported by the other samples shown in the plot. For example, sample group A indicated with red dots was expected to result in remarkable differences because different base papers, different coating application systems and also the influence of calendering were analyzed in this study. These result are located in a small area without any obvious trend.

However, the validity of the results obtained with these very different methods is indicated by the general positive correlation shown in Figure 3.3. A more detailed comparison of serial sectioning and the burnout test is difficult because of the differences between both methods (sample size, resolution, sensitivity etc.). In addition there are some unsolved questions regarding the burnout test like the rapid change of the coefficient of variation induced in calendering or the influence of raw materials in the base paper (fillers, woodfree / woodcontaining base papers, etc.).

Comparison of serial sectioning and SEM

A measuring method more similar to the automated serial sectioning method is digitization with SEM [ALLEM AND UESAKA, 1999; PETERSON AND WILLIAMS, 1992]

A cross section of an embedded paper sample was imaged at the same position with the light microscopy (LM) approach in serial sectioning ($0.16 \mu\text{m}$ per pixel) and scanning electron microscopy ($0.056 \mu\text{m}$ per pixel), see Figure 3.4. Both cross sections show a strong agreement. Surface irregularities can be found in both cross section images. Also the penetration behavior of the coating color appears to be similar in both cross sections. The SEM-images allows the localization of individual pigments, which is generally not possible with the light microscopy technique. However, very large pigments seem to be visible in these images too. In some cases the boundaries between coating layer and some features in the base paper are not that clear in the image obtained with light microscopy.

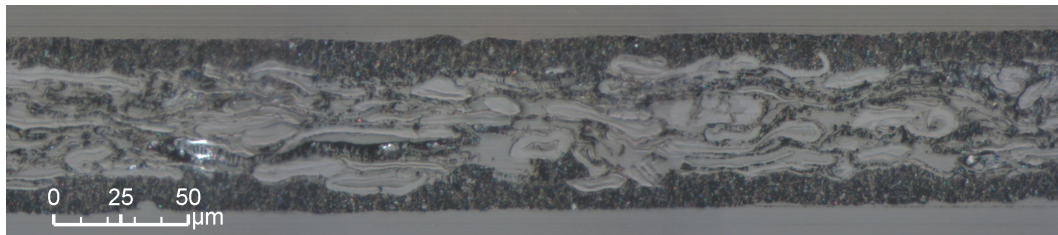
For a quantitative approach, a total cross section length of 2 mm was analyzed. Before the coating layers were detected manually, the image obtained with scanning electron microscopy was scaled down to a similar resolution as was used in light microscopy. The coating thickness measuring tool discussed in the previous section was applied to extract coating thickness data in both cases, coating thicknesses were measured at exactly the same positions. The results in Figure 3.5 present a strong correlation of coating thickness data obtained with the two different imaging techniques.

Comparison of serial sectioning versus X-ray microtomography

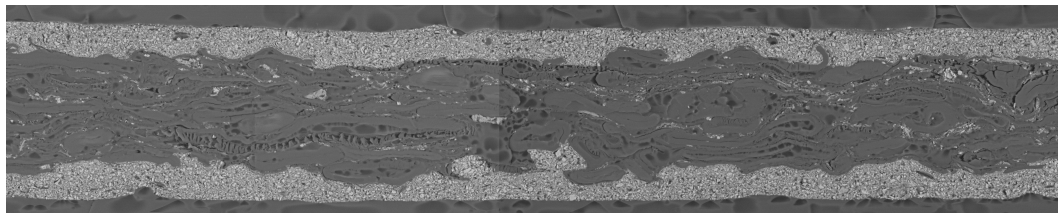
Three dimensional data sets obtained with the automated serial sectioning technique and X-ray microtomography (commercial desktop CT scanner Skyscan 1172, [CHINGA ET AL., 2007A]) were compared by the use of a registration concept introduced by HIRN ET AL. [2009].

A sample area of about 1 mm^2 of a 90 g/m^2 woodfree coated paper was first imaged with the microtomograph at a voxel size of $1.37 \times 1.37 \times 1.37 \mu\text{m}^3$. Imaging with the serial sectioning technique was done at a pixel size of $0.84 \mu\text{m}$ in the image plane and $3 \mu\text{m}$ between the subsequent cross sections. Typical cross section images from almost the same position in the paper sample are shown in Figure 3.6. The images obtained with light microscopy show more details of the coating layer and the fibrous materials. The high contrast between fibers and coating allows an easy distinction between those materials. The coating layer is observable in the cross section images obtained with X-ray microtomography due to the stronger absorbing behavior of X-rays of the inorganic pigments compared to organic materials. However, the whole image seems to be blurred and there are artifacts at the edges of the paper, both making a detection of coating layers in the cross section images more difficult. The hole visible in the cross section images is part of a pattern. These holes were applied with a laser and were used as landmarks to register the coating thickness maps obtained with serial sectioning and X-ray microtomography [HIRN ET AL., 2009].

Thresholding was used to extract the coating layer from the tomography data, giving as with serial sectioning a sequence of binary images where the coating layer



(a) Cross section obtained in serial sectioning.



(b) Cross section obtained with scanning electron microscopy.

Figure 3.4 Cross section image of the same paper cross section at the same position obtained with (a) light microscopy (automated serial sectioning concept) with a pixel size of $0.16 \mu\text{m}$ and (b) with scanning electron microscopy with a pixel size of $0.056 \mu\text{m}$.

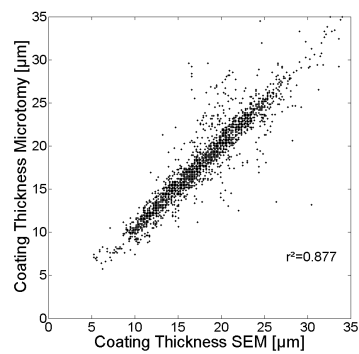
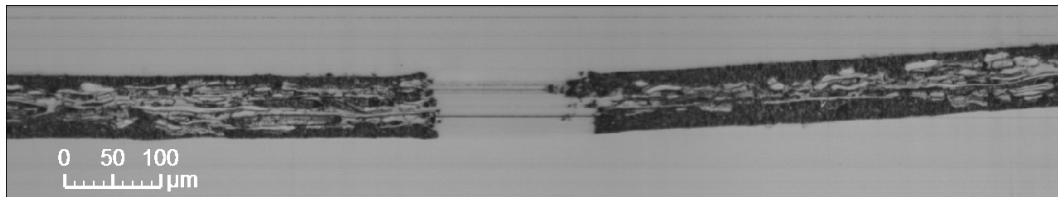
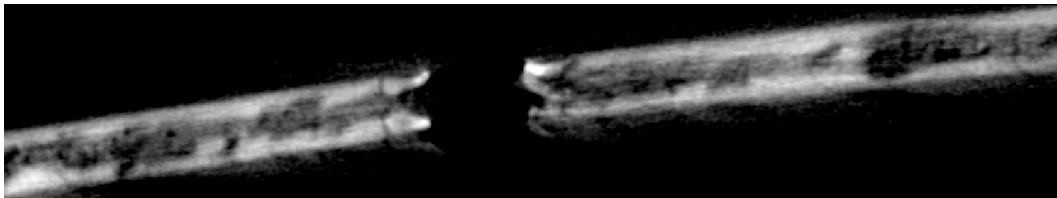


Figure 3.5 Correlation of coating thickness data obtained from exactly the same position at a 2 mm long cross section imaged with light microscopy (automated serial sectioning) and scanning electron microscopy.



(a) Cross section obtained with serial sectioning.



(b) Cross section image calculated from tomography data.

Figure 3.6 Cross section image of almost the same paper cross section obtained with (a) light microscopy (automated serial sectioning concept) with a pixel size of $0.84 \mu m$ and (b) X-ray microtomography (Skyscan 1172) with a voxel size of $1.37 \mu m$.

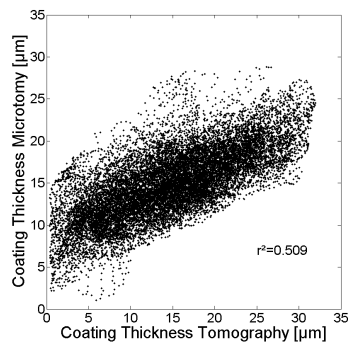


Figure 3.7 Correlation of coating thickness data from 3D data sets obtained with serial sectioning and X-ray microtomography at almost the same positions.

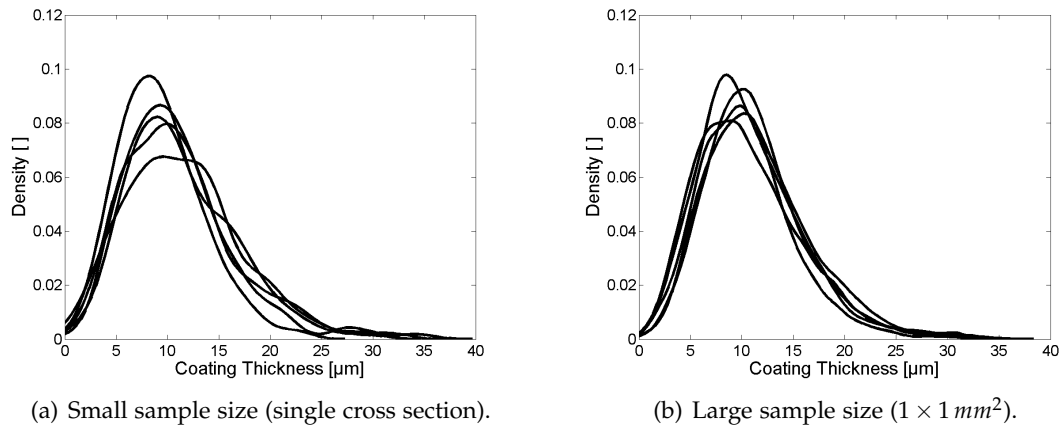


Figure 3.8 Similarity of coating thickness distributions from differently sized samples obtained from the same paper, using the serial sectioning technique. The distributions obtained from the smaller samples differ to a higher degree (a) than those obtained from larger samples (b).

is highlighted. 3D coating thickness maps were created, down scaled and registered to each other. The coating thickness data were then extracted at distinct positions. The correlation of the data obtained with both methods is shown in Figure 3.7. A trend to overestimate coating thicknesses in microtomography is observed at higher coating thicknesses. At lower coat weights, X-ray microtomography detects regions with no coating on a multiple coated woodfree paper. Nevertheless a correlation between these digitization techniques exists as also can be observed visually in the cross section images.

3.3 Sampling procedure for coating layer analysis

The need to define a sampling procedure in coating layer analysis

Coating layer analysis at a high resolution is usually restricted by the sample size. Thus, these techniques have a limited ability to cover the variations induced by the base paper, especially the large ones. The influence of base paper variations of different scales on spatial coating layer structures has been reported in literature, see for instance [GRÖN, 2000; HUANG AND LÉPOUTRE, 1995; TOMIMASU ET AL., 1990]. Therefore the validity of the results obtained has to be analyzed in more detail.

Figure 3.8 points out the subject of discussion in this section. The sample sizes used in the analysis of coating layer structures influence the shape and location of the resulting coating thickness distributions to a large extent. The data presented in this figure were obtained with the automated serial sectioning technique from different positions of a light weight coated paper. The coating thickness distributions for

the small samples in Figure 3.8 result from single paper cross sections, each having a length of 5 mm, about 400 coating thickness measures were extracted. These distributions differ a lot in their shapes and locations. The larger samples cover an area of $1 \times 1 \text{ mm}^2$. A total of more than 7000 coating thickness measures was extracted from 84 subsequent cross sections. These distributions are more similar compared to each other, but differences are still obvious.

Because the coating thickness distributions change their shape and location to a high degree, the analysis of several samples will be required for a representative analysis of coating layer structures. This finding implies also that a discussion of a representative elementary volume in coating layer analysis at a resolution in the micro-meter scale is not useful.

In this chapter an experiment is described which was designed to define a reasonable sampling procedure for a representative coating structure analysis taking into account the following influencing factors:

- A necessary resolution of the measuring grid
- A preferred sample size and sample geometry
- A reasonable number of samples

Paper grades

Two different paper grades were used. The first one was a glossy commercial 135 g/m^2 woodfree coated (WFC) paper with a total coat weight of 45 g/m^2 . This paper was triple coated on both sides, a precoat was applied with a film press and the second and third coating layer were applied with a blade. After coating application, this paper was calendered in a super calender. The coat weight on the back side was somewhat higher to level out irregularities of the base paper surface. The second paper was an industrially produced 70 g/m^2 light weight coated (LWC) paper. A total coat weight of 22 g/m^2 was equally applied on both sides in on machine blade coating units, but no calendering was performed. These two types of paper were chosen in order to cover a wide range of possible coating applications.

Statistical measures (similarity of distributions)

Besides the standard statistical measures - mean value, standard deviation and skewness of a coating thickness distribution - also a similarity measure indicating the similarity of coating thickness distributions to be compared was calculated. Because coating thickness values are usually not normally distributed data, nonparametric and distribution independent measures are recommended. Such a method is the calculation of the Kolmogorow-Smirnow - distance [SACHS, 2004]. It is defined as the

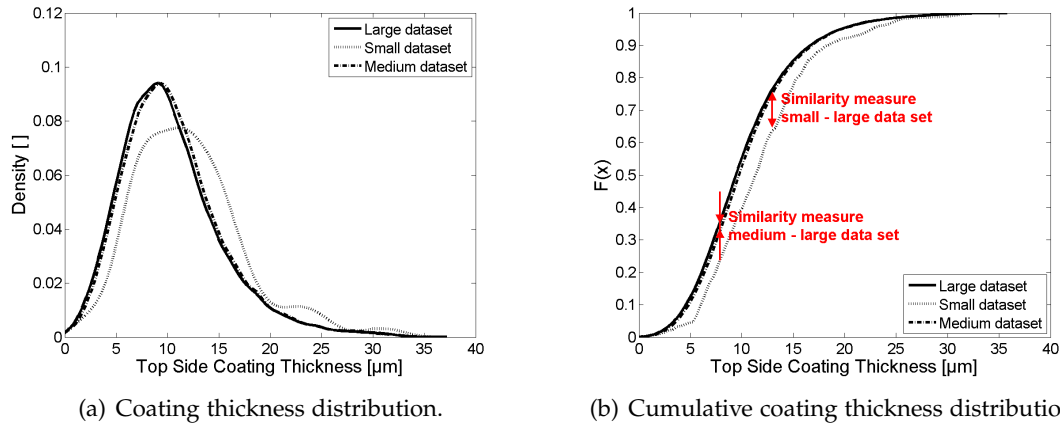


Figure 3.9 Similarity measure to compare distributions (Kolmogorow-Smirnow - distance): the maximum difference between the cumulative distribution functions \hat{F}_x (b). The corresponding density functions are shown in (a).

	large dataset	small dataset	medium dataset
Similarity []		0.163	0.029
Mean [μm]	10.37	12.10	10.62
Std.Dev. [μm]	5.03	5.37	4.97
Skewness []	1.05	0.99	1.01

Table 3.2 The similarity measure (Kolmogorow-Smirnow - distance) for similar and different distributions. Changes in the important statistical parameters are also visible in the similarity measure.

maximum difference between two cumulative distributions \hat{F}_1 and \hat{F}_2 :

$$D = \max|\hat{F}_1 - \hat{F}_2| \quad (3.1)$$

Figure 3.9 illustrates the Kolmogorow-Smirnow – distance. Kernel smoothed density functions of three samples are shown in (a), the original data were obtained with the serial sectioning technique. The large data sets covers a sample area of 10 mm^2 ($5 \times 2 \text{ mm}^2$ CD \times MD) and contains 70 056 coating thickness measures. Sub nsamples of this large data sets were used for comparison: the small data set (1 cross section, 5 mm, 420 data points) and a medium data set ($5 \times 1 \text{ mm}^2$, CD \times MD, 35 028 data points). As can be seen from Figure 3.9 (a) the locations of the distributions for the small and the large data set are very different. The medium data set is more similar to the large data set. The largest difference between the corresponding cumulative distributions, see (b), is the Kolmogorw-Smirnow - distance. The smaller this distance (similarity measure) the more similar are the compared distributions. Table 3.2 gives the associated similarity measure and shows that it covers the changes in the

	LWC			WFC		
	4 μm	12 μm	36 μm	4 μm	12 μm	36 μm
Resolution Measures [#]	63 504	7 056	784	63 504	7 056	784
Mean [μm] TS	10.84	10.77	10.50	17.54	17.49	17.30
Std.Dev. [μm] TS	4.61	4.60	4.45	5.03	5.02	5.07
Skewness [] TS	0.33	0.34	0.28	0.20	0.19	0.15
Similarity [] TS	0.00	0.00	0.01	0.00	0.01	0.01

Table 3.3 Characteristic statistical measures of coating thickness distributions at different resolutions of the measuring grid. Data given for LWC and WFC samples.

important statistical parameters (mean value, standard deviation and skewness). In the following, this similarity measure is used to represent the important statistical parameters.

3.3.1 Influential parameters on sampling and digitization.

Measuring grid size

The resolution of the measuring grid (defined by the slice thickness, see Figure 3.1) is the time controlling factor during digitization. For example, digitizing a sample area of $5 \times 1 \text{ mm}^2$ with a slice thickness of $4 \mu m$ requires double the time than with a slice thickness of $12 \mu m$ ($3 \times 4 \mu m$).

Figure 3.10 shows the effect of different measuring grid sizes having edge lengths of 4, 12 and $36 \mu m$ (see Figure 3.1) on coating thickness visualizations for a LWC – paper sample (a) and a WFC – paper sample (b). The color represents the coating thicknesses measured (in μm). The samples analyzed had an original measuring grid with an edge length of $2 \mu m$. The grids shown here were taken from the original grid considering only each second, sixth or eighteenth value in both directions. As expected the structural details diminish with decreased resolution. At a resolution of $12 \mu m$ impressions of individual fibers are still visible. At a resolution of $36 \mu m$ only large structures like fiber aggregates are preserved. This is not surprising because the fiber width is usually in a range of $20 \mu m$. The effect of different measuring grid sizes on quantitative parameters describing the coating layer structures are given in Table 3.3. The underlying samples cover an area of 1 mm^2 , see Figure 3.10. There are almost no differences in the major statistical parameters, the mean coating thickness as well as the standard deviation and skewness of the coating thickness distribution observable. There is also no influence on the similarity to the original sample distribution.

Further analysis of the coating layer structures with the automated serial sectioning technique is recommended at a measuring grid size having an edge length of

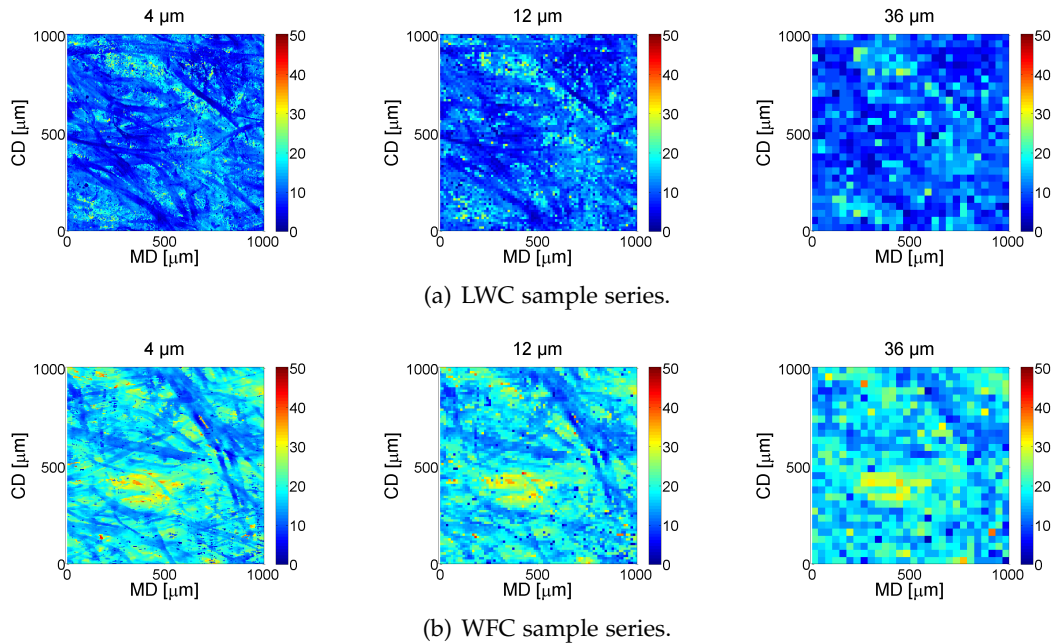


Figure 3.10 Effect of measuring grid size on distinguishability of individual objects.

$12 \mu\text{m}$. This length scale does not affect the calculated measures, visualizations still give reasonable information and digitization time is reasonable.

Influence of sample size and sample geometry

The sample size is usually fixed for a measuring system. As already mentioned, the serial sectioning technique is time efficient if a sample of 5 mm^2 ($5 \times 1 \text{ mm}^2$) is analyzed. The sample orientation can be chosen, with a preferred orientation in MD or CD (or randomly taken). To show the benefits of a large and anisotropic sample area, other sample sizes (1 mm^2 and 0.2 mm^2) as well as geometries (CD/MD ratio, including a preferred sample orientation in CD or MD) were analyzed. The basic populations used to point out the different influences of sample size and sample geometry were samples that cover an area of $5 \times 5 \text{ mm}^2$; using a measuring grid with an edge length of $12 \mu\text{m}$.

The coating thickness maps obtained for the top side coating layer are presented in Figure 3.11 (a) for the LWC paper sample and (b) for the WFC paper sample. Different structural features are observable. The LWC coating layer shows several impressions of fibers which are strongly oriented in MD. The coating thickness map for the WFC paper does not show these features. Structural features like local peaks with a thicker coating layer are more pronounced than for the LWC paper.

To analyze a possible influence of sample size and sample geometry, subsamples with a defined size (5 mm^2 , 1 mm^2 and 0.2 mm^2) and a defined CD/MD ratio were

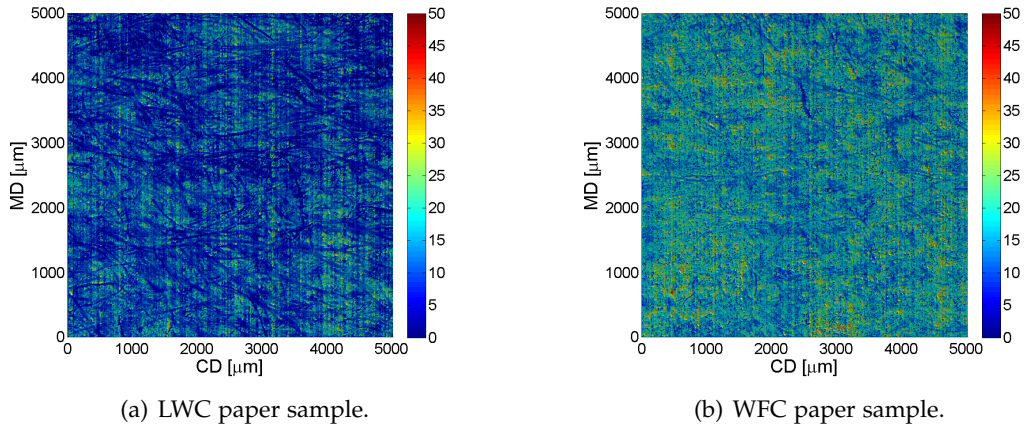


Figure 3.11 Coating thickness maps used to analyze effects caused by sample size and sample geometry; (a) LWC and (b) WFC.

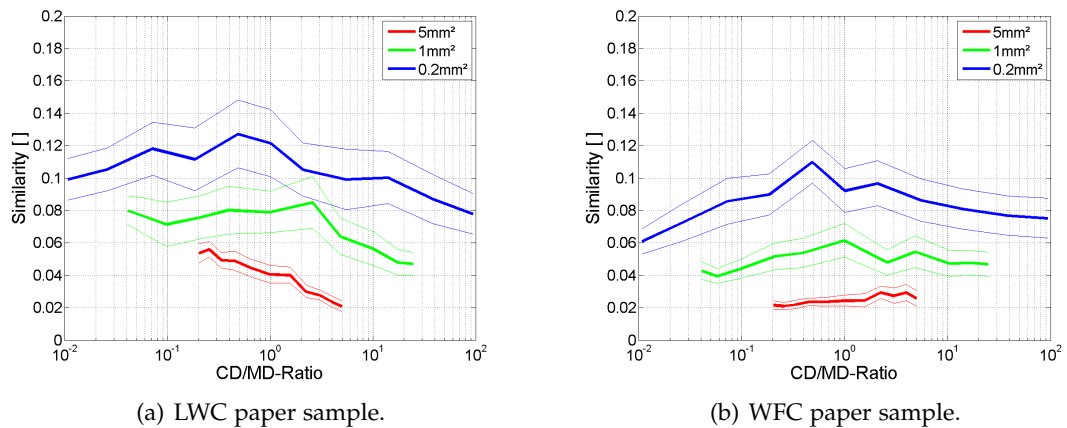


Figure 3.12 Influence of sample size and sample geometry on the similarity of coating thickness distributions between subsamples and total sample.

taken randomly from the total sample and then the similarities between the subsamples and the total sample were calculated. This procedure was repeated for all sizes and all possible sample geometries.

The resulting similarity measures are shown in Figure 3.12, (a) for the LWC paper sample and (b) for the WFC paper sample. As expected, the larger the analyzed samples are, the more similar are the obtained distributions (subsample and total sample).

The results for the LWC paper sample, Figure 3.12 (a), indicate a significant influence of the sample geometry for the large 5 mm^2 sample. At higher CD/MD ratios (~ 5) a very high similarity between the subsample and the underlying sample can be found. This is because the impressions of single fibers in the coating layer are oriented predominantly in machine direction causing a larger variation of coating thickness data along the paper cross direction. A higher CD/MD ratio is also preferred for samples with a size of 1 mm^2 . Smaller samples are not affected in that way; however an extreme geometry with a preferred orientation either in CD or MD should be chosen.

The large 5 mm^2 sample in the WFC paper is hardly affected by the CD/MD ratio used. Smaller samples with a size of 1 mm^2 or 0.2 mm^2 should be analyzed on samples having an extreme geometry with a preferred orientation either in CD or MD. This behavior was expected, since the dominant structures seem to be randomly distributed, Figure 3.11 (b).

In general, large sample areas as well as a high CD/MD ratio can be recommended for coating layer analysis. Using the serial sectioning technique, the analysis of 5 mm^2 samples with an anisotropic geometry and a preferred orientation in CD (5 mm) seem to be promising parameters for a reasonable analysis of coating layer structures.

Sampling procedure

Considering Figure 3.8, one has to conclude that a reasonable analysis of coating layer structures requires more than one sample to be analyzed. A suitable sampling strategy is important in order to avoid influences caused by e.g. pulsations in the paper making process.

The evaluation of a suitable sampling strategy requires a large number of samples from different positions on a sheet of paper. Therefore, three sheets of paper were taken from the same CD position at a reel, see Figure 3.13 (LWC and WFC). On four positions in machine direction (MD), four samples in cross direction (CD) were taken. All in all 16 samples of paper were investigated for each paper grade. The distance between the samples in CD was hold constant at 3 cm . The distance between the positions labeled with 1X and 2X was about 20 cm . The distance between the sheets 1 and 2 as well as the distance between sheet 2 and sheet 3 was about 4.4 m . Each of the 16 samples per paper grade covered an area of at least 5 mm^2 ($5 \times 1\text{ mm}^2$ CD \times MD).

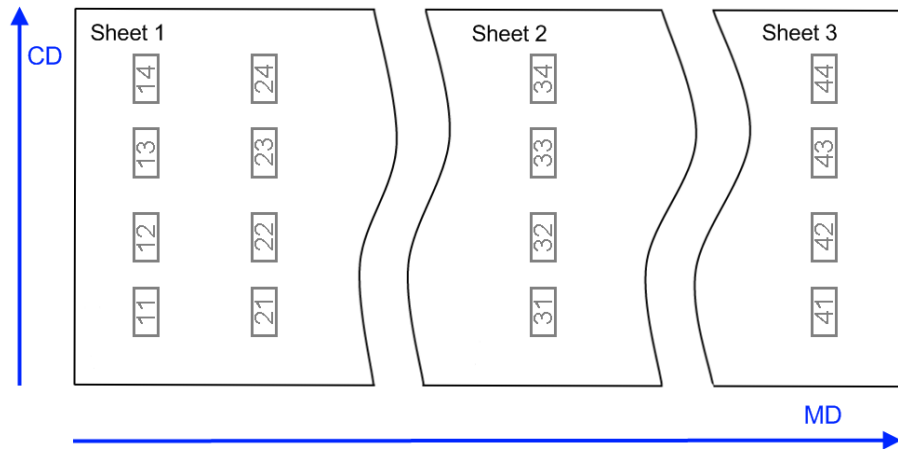


Figure 3.13 Sampling procedure on three different sheets to cover effects induced by CD and MD position on a paper web.

The slice thickness respectively the grid size of the measuring grid was set to $12 \mu\text{m}$. The data of all 16 samples was treated as the basic population.

Possible influences of sample positions are exemplarily shown in Figure 3.14 (a) for the LWC paper sample and (b) the WFC paper sample. These plots show the mean coating thicknesses at the distinct positions, the first letter of the numbers given in Figure 3.13 defines the MD position, the second letter the CD position. The coating thicknesses seem to be very uniform for the LWC paper sample. A closer look reveals rather constant CD profiles whereas the MD profiles show slight variations. This can be an indication for pulsations in the process. Differences in the coating thicknesses of the WFC paper seem to be more pronounced, but appear to be of random origin.

In order to find a suitable sampling procedure, three different approaches were evaluated in a quantitative way: only CD sampling (samples taken from different CD positions), only MD sampling (from different MD positions) and random sampling. Sample groups of 4 samples were created (e.g. CD sampling: all samples from one MD position - e.g. the samples with the ID's 11, 12, 13, 14 in Figure 3.13). The data of all samples within a group were then compared with the basic population (considering the data of all 16 samples) using the similarity measure described in Equation 3.1. Four sample groups were available at the different MD positions giving four similarity measures for the CD sampling. This was also done for the MD sampling and random sampling (four out of 16). In total 12 similarity measures were calculated ($4 \times \text{CD-sampling}$, $4 \times \text{MD sampling}$ and $4 \times \text{random sampling}$).

Figure 3.15 summarizes these results; the mean similarity measure for CD sampling, MD sampling and random sampling with 95% confidence intervals, (a) for the LWC paper sample and (b) for the WFC paper sample. The higher the bars, the more different are the sample groups from the basic population.

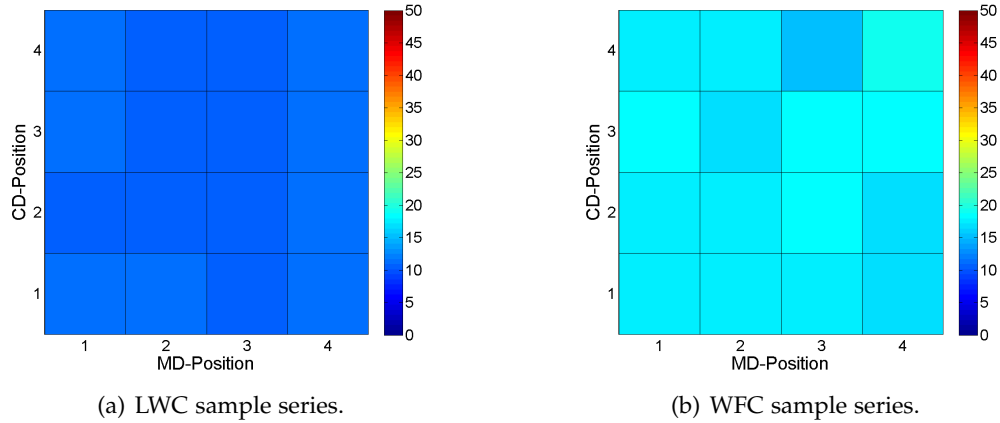


Figure 3.14 Map of mean coating thicknesses at different sample positions for (a) LWC and (b) WFC. No clear influence of sample position on mean coating thickness can be observed.

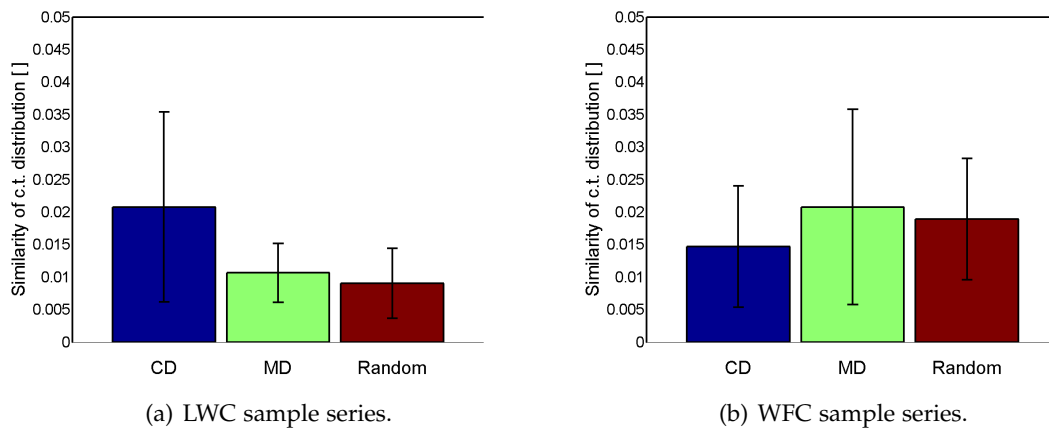


Figure 3.15 Influence of sampling procedure. The measure used to quantify the influence is the similarity of a subsample to the basic population.

In general, the differences are not significant and therefore no sampling routine can be recommended. However, in the case of the LWC paper, CD sampling shows a higher similarity measure indicating a larger difference between the sample groups and the basic population respectively between the individual sample groups. This can also be seen in Figure 3.14, where the MD profiles show slight variations whereas the CD profiles are rather constant.

Based on these findings random sampling is recommended in coating layer analysis. (This includes CD and MD sampling anyway.)

3.3.2 Expected confidence intervals

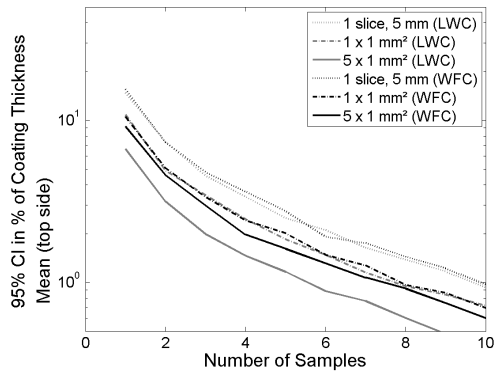
The last topic to be discussed in this section are expected confidence intervals (95%) for a different number of samples, a different number of sample sizes (single cross sections, $1 \times 1 \text{ mm}^2$ and $5 \times 1 \text{ mm}^2$ -CD \times MD- large samples) and for different coating layer properties; all measured with automated serial sectioning.

To be able to define an expected confidence interval, hundreds of combinations of up to 10 samples out of the 16 samples were analyzed for the two paper grades used in this study. The confidence intervals (CI) are given as a percentage of the values obtained by considering all 16 samples (basic population).

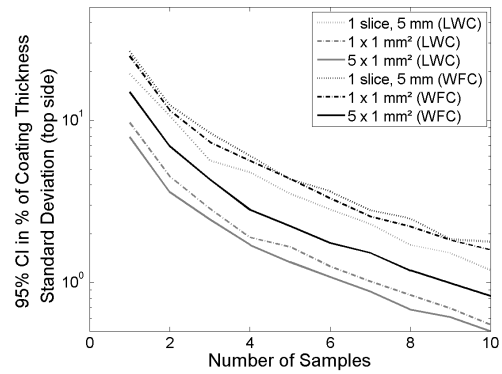
Figure 3.16 shows the expected confidence intervals for the coating thickness mean (a), the coating thickness standard deviation (b), the base sheet caliper mean (d), the base sheet roughness (e) and the coated sheet roughness (f). The similarity of coating thickness distributions to the basic population is shown in Figure 3.16 (c).

As an example, the expected confidence intervals are explained in more detail for the coating thickness mean. As can be seen in Figure 3.16 (a), the sample size shows an important influence. The smaller the samples to be analyzed, the higher the expected 95% confidence intervals are. If a defined confidence level has to be achieved, a higher number of small samples has to be analyzed. Also the coating thickness (LWC: thin coating layer, WFC: thick coating layer) has an influence on the expected 95% confidence interval. A thicker coating layer will always have larger confidence interval than a thinner one. A coating layer analysis with the automated serial sectioning technique (5 mm^2) gives an expected confidence interval of about $\pm 10\%$ of the mean coat weight for a thick coating layer and $\pm 6\%$ of the mean coat weight for a thin coating layer if only one sample was analyzed. This interval decreases if three samples were analyzed and gives $\pm 3\%$ for the thick coating layer and about $\pm 2\%$ for the thin one. If only single cross sections having a length of 5 mm are used for analysis, 6 to 7 samples are necessary to achieve these confidence levels.

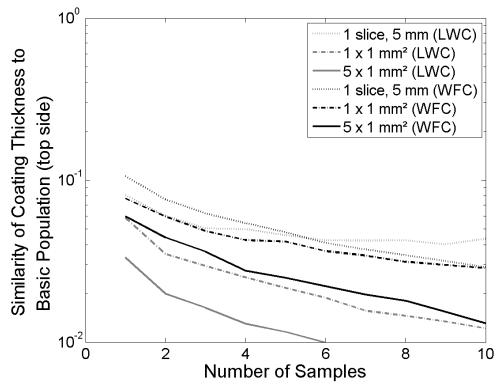
A surprising effect is that sometimes the analysis of a single cross section gives better results than the analysis of larger samples ($1 \times 1 \text{ mm}^2$) as it can be seen in the analysis of the base sheet caliper, Figure 3.16 (d), or the roughness of the coated sheet



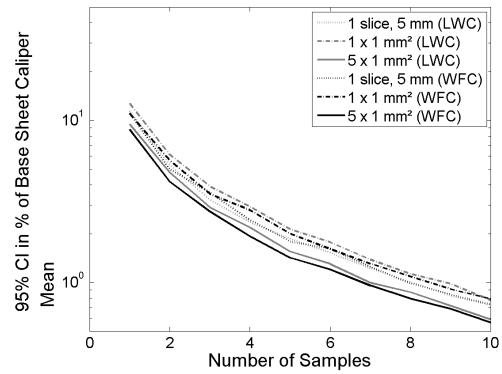
(a) Expected 95% CI for mean coating thicknesses.



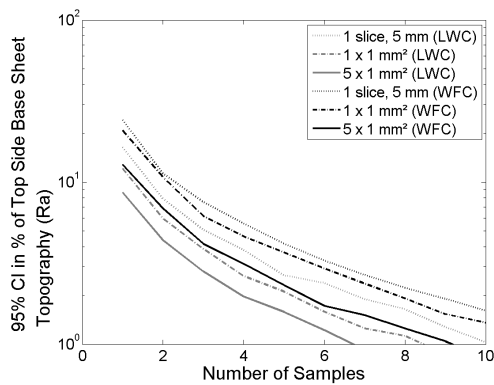
(b) Expected 95% CI for standard deviation of coating thickness data.



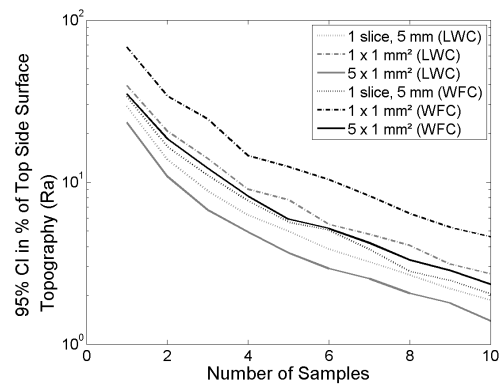
(c) Expected similarity for coating thickness data to basic population.



(d) Expected 95% CI for mean base sheet caliper.



(e) Expected 95% CI for base sheet roughness (Ra).



(f) Expected 95% CI for coated sheet roughness (Ra).

Figure 3.16 Expected confidence intervals (95%) and similarity measures for important properties of differently coated sheets at different number of samples and sample sizes.

(f). The reason for this might be the shorter edge length which of course is not able to cover the large sized variations caused by e.g. fiber flocs.

In order to standardize the coating layer analysis based on serial sectioning; three samples will be analyzed in a standard analysis of coating layer structures.

3.3.3 Summary

A valid analysis of coating thicknesses with high resolving measuring techniques requires a well defined sampling procedure. This approach focuses on the use of 3D measuring techniques like the automated serial sectioning technique. Valid conclusions can also be drawn for SEM imaging or the use of X-ray microtomography.

The edge length of a measuring grid applied does not effect the statistical parameters used for coating layer characterization. The impressions of fibers in the coating thickness map are still visible at a resolution of $12 \mu m$. The samples analyzed should have a rectangular shape, with the longer edge oriented in the paper cross direction. There is no preferred sampling procedure observable. Simple MD or CD sampling gives similar results to random sampling. In order to avoid failures, always random sampling on an A4 sheet of paper is recommended. The confidence intervals obtained can be strongly decreased if larger sample areas and a higher number of samples are analyzed.

All these observations lead to the following sampling procedure:

A standard coating layer analysis using automated serial sectioning is performed on three randomly taken samples having a size of $5 mm^2$ ($5 \times 1 mm^2$ CD \times MD). The edge length of the measuring grid used is set to $12 \mu m$.

3.4 Description of spatial coating layer formation

Print non-uniformities of coated papers are often attributed to a poor coating layer uniformity, see for instance [ALLEM, 1998; ENGSTRÖM, 1994; ENGSTRÖM AND LAFAYE, 1992; PRESTON ET AL., 2008].

Variations in the spatial formation of a coating layer can be caused by the base paper topography. A rough surface of the base paper results in a wide range of coating thicknesses, whereas a smooth paper surface gives a uniform coating mass distribution [ALLEM AND UESAKA, 1999; HUANG AND LEPOUTRE, 1995; STEFFNER AND NYLUND, 1995; ZOU ET AL., 2001]. In that way, also the base paper formation can influence the coating layer uniformity [HEDMAN ET AL., 2003; TOMIMASU ET AL., 1990].

An important parameter controlling the spatial formation of a coating layer is the application system [ENDRES AND TIETZ, 2007]. One would expect remarkable coating thickness variations in blade coating because irregularities of the base paper surface are leveled out during the metering action [KARTOVAARA, 1989; WILTSCHKE ET AL., 2006]. This results in the so called leveling coat which is indicated by a strong cor-

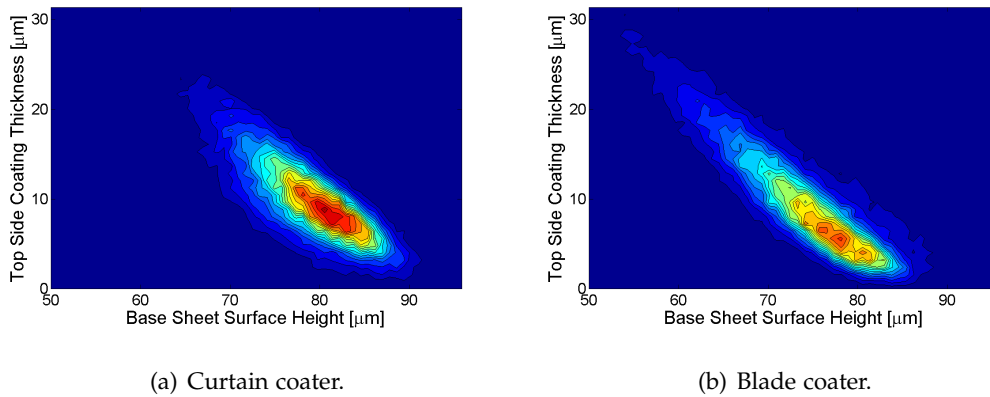


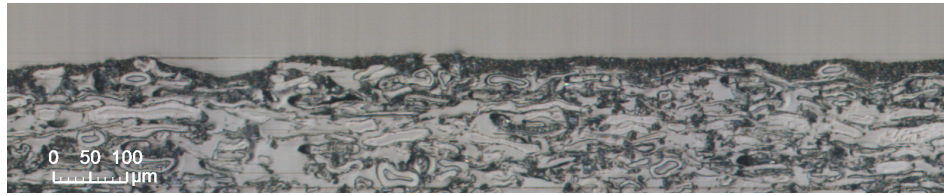
Figure 3.17 Local correlation of coating thickness data and base sheet surface height (base sheet topography) for (a) curtain coater and (b) blade coater. The same type of base paper has been coated with all carbonate containing coating color in both cases.

relation between coating thickness and base sheet topography. Curtain coating is expected to give a uniform coating mass distribution because no metering action is needed [ENDRES AND TIETZ, 2007; WILTSCHKE ET AL., 2006]. The coating thickness of this so called contour coat is hardly influenced by the base sheet topography [FORSSTRÖM ET AL., 2003].

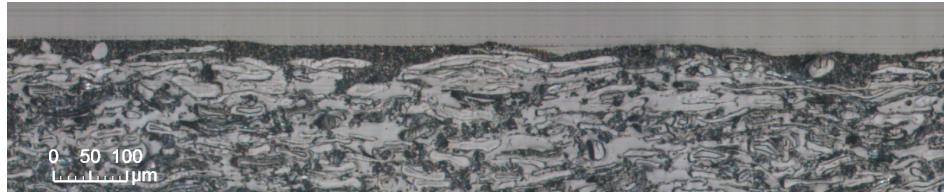
Different techniques can be applied in the analysis of coating layer uniformity. The most common one is the burnout test, e.g. [ENGSTRÖM AND LAFAYE, 1992; GRÖN AND AHLROOS, 2001; HUANG AND LEPOUTRE, 1995; WIKSTRÖM AND GRÖN, 2003]. This test indicates differences in the spatial formation of coating layers from different samples, but it cannot be used to analyze the impact of base paper properties on coating layer non-uniformities.

A way to analyze the effect of base sheet topography on coating layer uniformity is the use of imaging techniques like e.g. scanning electron microscopy [ALLEM, 1998; ALLEM AND UESAKA, 1999; PETERSON AND WILLIAMS, 1992; ZOU ET AL., 2001], X-ray microtomography [TURPEINEN ET AL., 2005] or serial sectioning combined with optical light microscopy [WILTSCHKE ET AL., 2006]. The measuring principle is basically the same for all of these methods: local coating thicknesses and base sheet topography data are extracted from a digital representation of the paper sample to be analyzed. These methods differ only in their resolution and the sample size to be investigated; the results obtained show similar trends, see section 3.2.3.

As an example, Figure 3.17 shows two typical local correlations between coating thickness and base sheet surface height data, (a) for a curtain coater and (b) for a blade coater, coated on the same base paper. The data were obtained with automated serial sectioning and coating layer analysis, see section 3.2.2. The base sheet topogra-



(a) Curtain coated.



(b) Blade coated.

Figure 3.18 Cross section images of (a) a curtain coated paper sample and (b) a blade coated sample.

phy is given as height from a paper middle-plane. Red areas in Figure 3.17 (a) and (b) indicate a high number of measurement values, blue areas a low number. Both application systems result in a quite similar correlation of coating thickness and base sheet surface height data. Against the expectation for an ideal contour coating process the coating thickness applied with a curtain coater also shows a strong dependency from base sheet topography. In this case, the only difference between the two coating aggregates is that for the curtain coater the same coating thickness values can be observed over a wider range of base sheet heights, giving a somewhat wider distribution. The better coverage of a curtain coater compared to a blade coater becomes evident in Figure 3.17 from the low number of areas with a low coating thickness.

However, despite these differences a clear differentiation based on the spatial coating layer formations is not possible from the plots shown in Figure 3.17. Therefore a measure to clearly distinguish between coating structures has to be developed. Indirect measures of differences in the coating structure like a higher roughness of curtain coated papers compared to blade coated papers were already reported in literature [ENDRES AND TIETZ, 2007].

3.4.1 Approach

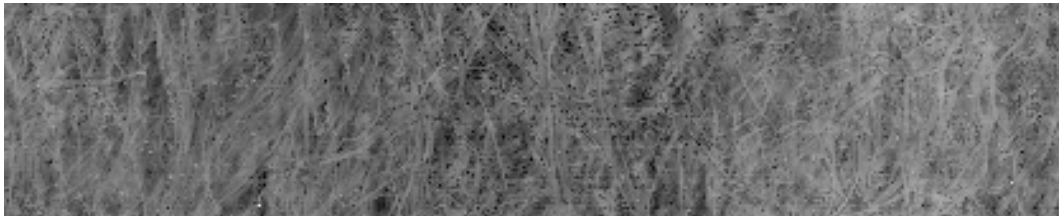
Figure 3.18 shows paper cross sections of (a) a curtain coated sample and (b) a blade coated sample. The obtained coating layers are supposed to be quite different for the two application systems, but in both cases a clear void filling effect is observable. A leveling or contouring behavior of the coating layer cannot be observed from these small cutouts.

An explanation for this observation was given by DAHLSTRÖM AND UESAKA [2009]; DAHLSTRÖM ET AL. [2008]. They used frequency analysis to study the effect of different length scales of base sheet surface heights variations on local coating thicknesses. The samples used in these studies were coated with a laboratory coater equipped with a blade metering system. The structure of the coating layer was found to follow two mechanisms. At shorter wavelength or small structures the coating layer behaves like a leveling coat where small voids at the paper surface are filled with coating color creating a small scale uniform surface. At larger wavelength or larger structures of the base sheet, the coating layer thickness is not that strongly influenced by the base sheet surface height. They assumed that random deposition of coating color is a dominating effect at larger length scales of base sheet surface height, resulting in a contour coat like structure of the coating layer.

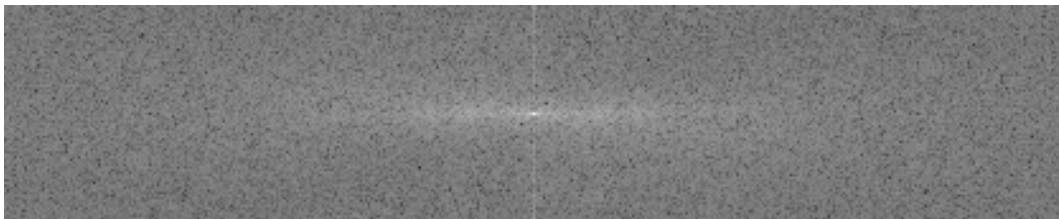
Here a similar approach is used. The idea is that small structures in the base sheet surface (e.g. fibers) are filled with coating color independent from the application system. Different to the work of DAHLSTRÖM AND UESAKA [2009]; DAHLSTRÖM ET AL. [2008], an interrelation between base sheet topography and coating thickness is expected at larger structures (e.g. fiber flocs). For example, the type of application system is awaited to influence the obtained coating layer structures, void filling respectively leveling in blade coating as well as a contour coat in curtain coating.

The analysis is based on coating thickness maps and base sheet surface height maps, both obtained with the automated serial sectioning technique. These maps are filtered in a frequency domain, where a predefined cutoff wavelength is used to differ between small structures (highpass-filtering) and large structures (lowpass-filtering). The filtered coating thickness and base sheet surface height data are then correlated. The coefficient of determination (R^2) and the slope of the regression line are calculated and used as measures to describe the spatial coating layer formation. A low coefficient of determination indicates a low influence of base sheet topography on coating thicknesses and this is expected for a contour coat. A value close to 1 indicates a leveling coat like behavior of a coating layer. The slope of a regression line between coating thickness and base sheet topography is expected to be mostly negative, an elevated base paper region will be covered with a thin coating layer and vice versa. A slope close to 0 again indicates an independency of local coating thickness from base sheet topography or a contour coat like structure.

Filtering in the frequency domain is performed in MATLAB by the use of standard operations [GONZALEZ ET AL., 2004]. Figure 3.19 (a)-(d) shows the main processing steps, (a) an original map of data, (b) a corresponding frequency domain image after 2D-discrete Fourier transformation and the shift of zero-frequency components of the transformation to the center of the spectrum, (c) a filter applied to the frequency domain image – lowpass (large structures/wavelength with low frequencies are considered) in this case and (d) the retransformed map of data.



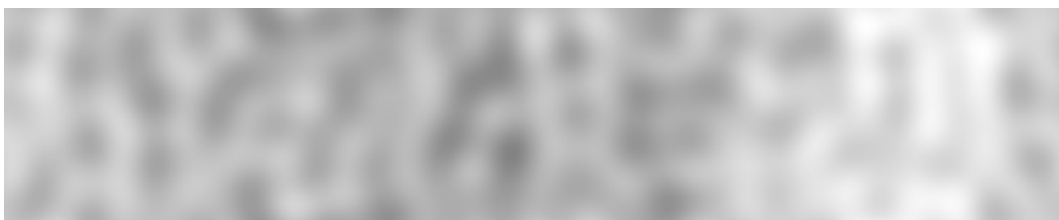
(a) Original map of base sheet topography (surface height).



(b) Frequency domain image after Fourier transformation and the shift of zero-frequency components to the center of the spectrum.



(c) Lowpass-filtering, all frequencies above a cutoff-frequency are set to zero.



(d) Reconstructed image.

Figure 3.19 Filtering in the frequency domain - basic operations.

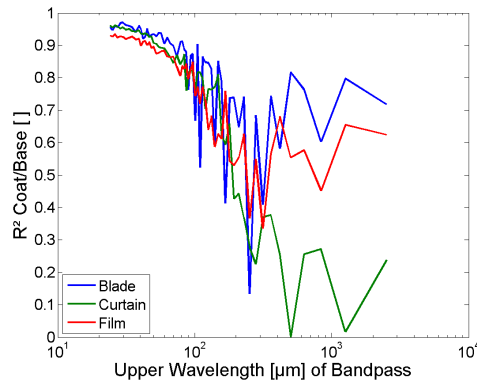


Figure 3.20 The coefficient of determination (R^2) between coating thickness and base sheet surface height as a function of the upper wavelength used in bandpass-filtering. At shorter wavelengths, a high R^2 can be observed for all coating aggregates. If larger structures, having a wavelength above 250-300 μm , are analyzed differences between the coating aggregates are observable.

The cutoff wavelength used to differentiate between the void filling effect of small base sheet structures and the coating layer structure at larger scales was determined by the calculation of R^2 values for correlations of bandpass-filtered coating thicknesses and bandpass-filtered base sheet surface heights. Figure 3.20 shows the R^2 values as a function of the upper wavelength of the bandpass filter kernels used; the lower wavelength was in all cases set to the upper wavelength of the filter kernel of the previously used smaller filter kernel. At shorter wavelengths, a high R^2 can be observed for all coating aggregates analyzed. This is an indication for the void filling effect which occurs with all coating application systems. Above a wavelength range of 250 – 300 μm , the calculated R^2 values for correlations of coating thicknesses and base sheet surface heights begin to differentiate between the coating aggregates. Blade coating still results in a high R^2 of about 0.5-0.7 while curtain coating gives R^2 values of 0-0.3. Further differentiation between small scale and large scale structures is performed at a cutoff wavelength of 275 μm .

Figure 3.21 (a) and Figure 3.22 (a) show a typical base sheet surface height map respectively coating thickness map of a blade coated sample. The mean value was subtracted for visualization purposes in each case. The application of the filtering steps at a predefined cutoff-wavelength gives the following results:

- Highpass-filtering to preserve only the small structures below a defined cutoff-wavelength, see the reconstructed maps in Figure 3.21 (b) and Figure 3.22 (b). The shapes of individual fibers are the dominating structures in these images.
- Lowpass-filtering to preserve only the large structures, see the maps in Figure 3.21 (c) and Figure 3.22 (c). Fiber aggregates in the base sheet are apparently an origin of the base sheet topography variations. In this example an interrela-

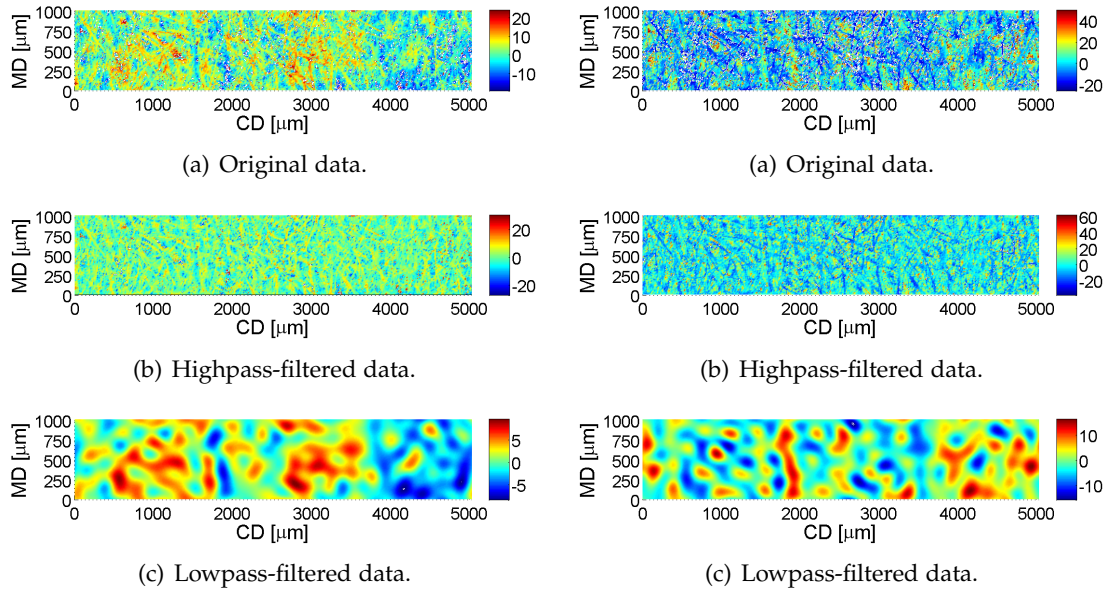


Figure 3.21 Base sheet height maps of a blade-coated paper. Remaining structures after (b) highpass-filtering and (c) lowpass-filtering.

Figure 3.22 Coating thickness maps of a blade-coated paper. The original map in (a) and remaining structures after (b) highpass-filtering and (c) lowpass-filtering.

tion between coating thickness and base sheet topography is observable. As it is expected for blade coating, a thicker coating layer can be found on a lower base sheet topography in the CD region above $4\,000\ \mu\text{m}$.

The effect of frequency filtering on the correlation of coating thickness and base sheet surface height (topography) for the samples presented in Figure 3.17 is shown in Figure 3.23 (a) for a curtain coater and (b) for a blade coater. For visualization purposes, the mean values of coating thickness and base sheet surface height were subtracted from the original data. Blue dots in Figure 3.23 correspond to the original input data. As already discussed, differences between blade and curtain coating are hardly observable. The highpass-filtered data is indicated by the green dots. Both, curtain and blade coating show a strong correlation between coating thickness and base sheet surface height. This behavior is interpreted as void filling or leveling of small scale base sheet structures with coating color. The red dots indicate the correlations of lowpass-filtered coating thickness and base sheet surface height data. Differences between curtain and blade coating become obvious. In curtain coating the large scale base sheet surface height variations have a weak influence on coating thickness data, whereas the influence is more pronounced for blade coating. These findings are supported by the calculated measures R^2 and slope of the regression line between coating thickness and base sheet surface height, given in Table 3.4.

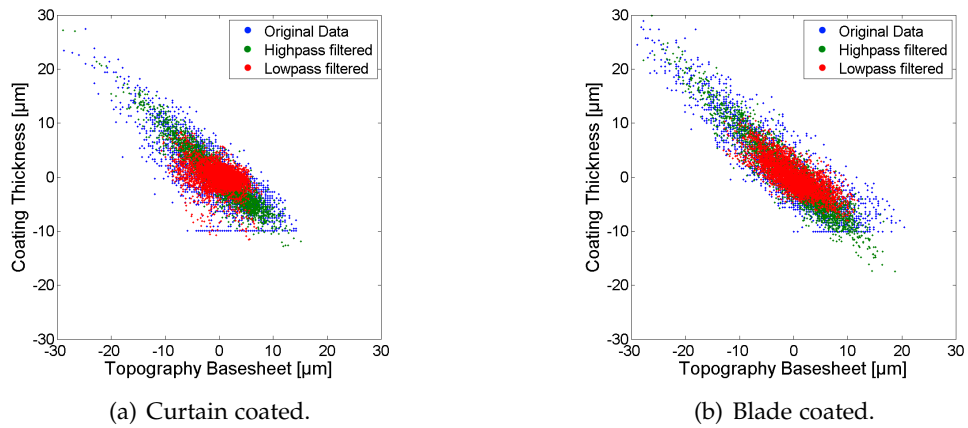


Figure 3.23 Effect of highpass- and lowpass- filtering on correlation between coating thickness and base sheet surface height. The same data as presented in Figure 3.17 are used.

Curtain	Original data	Highpass-filt.	Lowpass-filt.
R^2	0.6851	0.8564	0.1680
Slope	-0.6957	-0.8408	-0.2640
Blade	Original data	Highpass-filt.	Lowpass-filt.
R^2	0.8050	0.8754	0.5802
Slope	-0.7909	-0.8646	-0.5558

Table 3.4 Measures defining coating layer structures (curtain and blade coated).

In the following, two additional measures are considered. Besides the coefficient of determination and the slope of the regression line, also the variance of base sheet surface height data and the variance of coating thickness data are calculated. The variance of base sheet surface height is used as a measure for the uniformity (roughness) of the base sheet surface. The idea is that a uniform surface of the base sheet will give a more uniform coating thickness, or a lower variance of coating thicknesses. A higher variance of coating thicknesses is expected for leveling coat like coating structures because irregularities in the base sheet topography are filled with coating creating a uniform and smooth surface. This leveling like structure is expected in blade coating. Contour coating, as it would be achieved with a curtain coater, is expected to give a more uniform coating layer thickness resulting in a lower variance of the coating thickness data.

3.4.2 Example I: Pilot coating trial with different application systems

A parameter controlling the spatial coating layer formation is, as already mentioned, the application system. The coating layer thickness obtained in blade coating can be expected to be strongly dependent from the base sheet topography because of the metering action of the blade resulting in a smooth surface [KARTOVAARA, 1989; WILTSCHE ET AL., 2006]. Film press coating is expected to give a more contour coat like structure because a premetered film is transferred to the base paper [DICKSON ET AL., 2002; FORSTRÖM ET AL., 2000; GRÖN AND AHLROOS, 2001; TREFZ, 1996]. Curtain coating should give the most uniform coating layer because no metering action is necessary [ENDRES AND TIETZ, 2007].

The first application of the presented approach is the quantification of the spatial formation of coating layers obtained with different application systems. A wood-free base paper was coated at the Center of Excellence for Paper and Board Coating of DOW Europe GmbH (now Styron Europe) with blade, film press and slide curtain application systems. Two coating colors, the first contained 100% carbonate and the second 100% clay, were used. The same coat weight was applied in each case. Detailed trial data is given in Table 3.5. Previous work on these samples [SALMINEN ET AL., 2010] has shown that curtain coating results in a more uniform coating thickness distribution indicating a contour coat like formation of the coating layer. A higher porosity of the coating layer was obtained when clay is used. Blade coating was found to give a denser coating layer and a high surface smoothness. The wider coating thickness distribution indicates the stronger leveling tendency of this application system. The spatial formation of a coating layer obtained in film coating is located between that of curtain and blade coating.

The sample series was not perfect, since the blade coating was applied on the rougher back side of the paper while the curtain and film coating were applied on the top side. Another important restriction is that similar coating colors were used

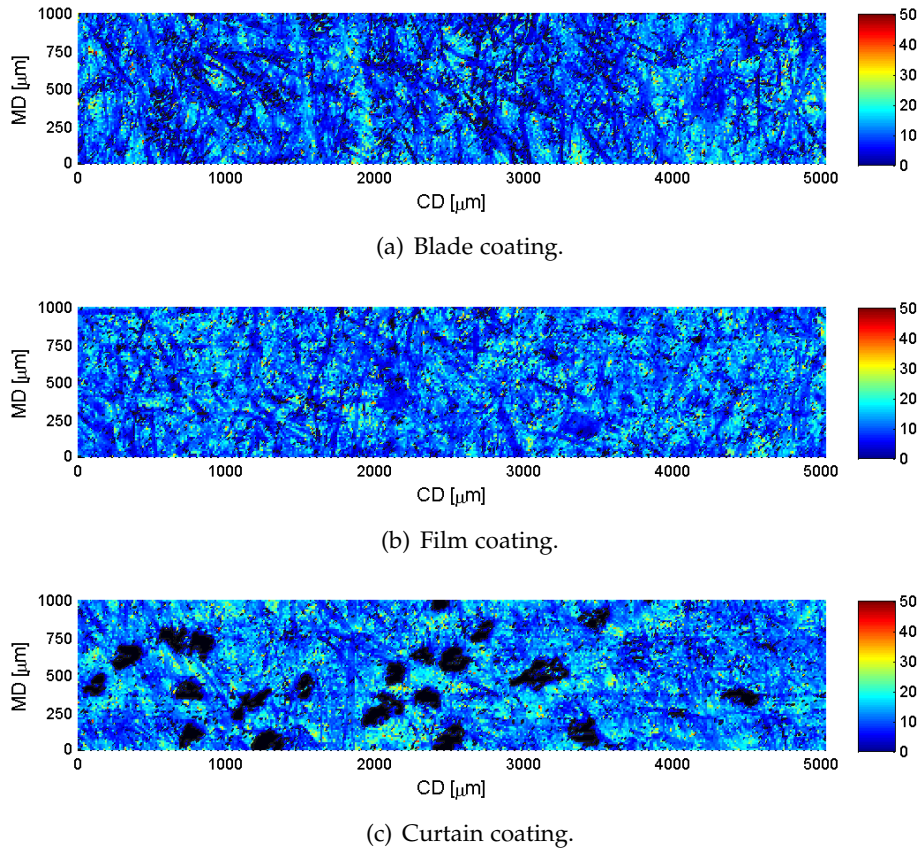


Figure 3.24 Coating thickness maps obtained from different application system by the use of the same all clay containing color. The rheological limitations especially in curtain coating are easy to observe.

for the three different application systems without adapting the rheology and surface chemistry. This was especially a problem with the clay containing colors, as can be seen at the coating thickness maps presented in Figure 3.24, (a) for blade coating, (b) for film coating and (c) for curtain coating. In the last case (c), the coating color does not spread over the base paper leaving large uncoated regions which is indicated with the large uncoated spots highlighted as black regions. This strongly influences the variance of coating thicknesses and influences also the correlations of coating thickness data versus base sheet surface height data.

In accordance to chapter 3.3, three samples each covering an area of 5 mm^2 were analyzed per paper sample. The coefficient of determination (R^2) and the slope of the linear regression model considering coating thickness and base sheet surface height data were then calculated for each individual sample for the original data and the lowpass- as well as highpass-filtered data. In addition, also the coating thickness variance as a measure for the coating layer uniformity and the variance of the base

	Clay	Carbonate
Delaminated Clay	100	0
Carbonate (90% < 2 μm)	0	100
SB Latex	10	10
CMC	0.5	0.3
Solids, %	60	68
pH	8.5	8.5
Viscosity (Brookfield 100 rpm, cP)	710	1060
Coat weight, g/m^2	12	
Coating speed, m/min	1200	
Base paper basis weight, g/m^2	143	

Table 3.5 Coating formulations used to study the influence of application systems on the coating layer formation.

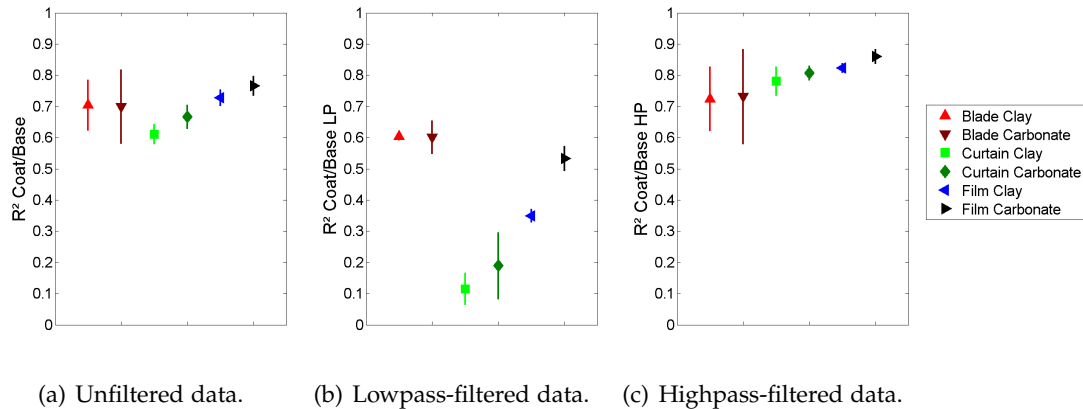


Figure 3.25 Coefficient of determination (R^2) between coating thickness and base sheet surface height data, (a) for the original data, (b) for lowpass-filtered data and (c) for highpass-filtered data.

sheet surface height as a measure for the base paper surface smoothness were analyzed. The 95% confidence intervals are shown.

Coefficient of determination (R^2)

Figure 3.25 shows the R^2 values for the correlations between coating thickness and base sheet surface heights, (a) for the original data (b) for the lowpass-filtered data and (c) for the highpass-filtered data. In the case of original data, the obtained R^2 values are located within a small range between 0.6 and 0.8. There is a significant difference between curtain and film coating for the individual pigment systems, but blade coating cannot be distinguished from the others due to a higher variability in the data expressed by the larger confidence intervals. Lowpass-filtering widens the range of R^2 values, which are now in a range between 0.1 for curtain coating and

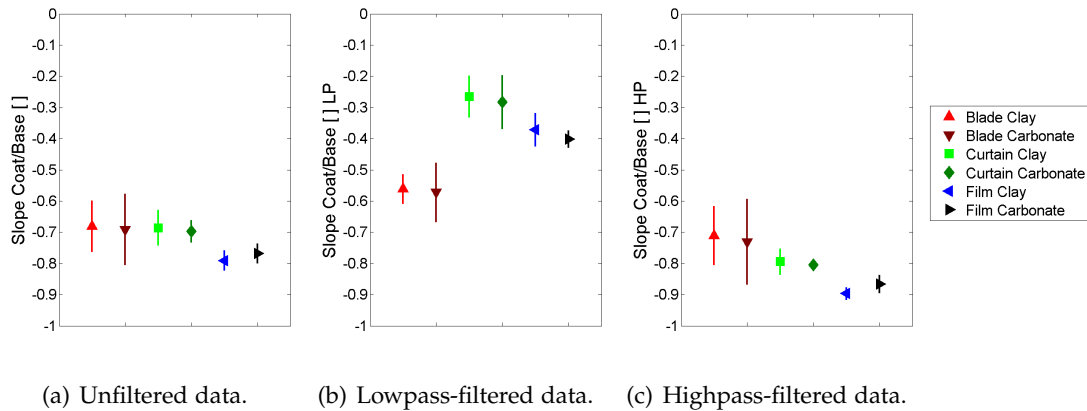


Figure 3.26 Slope of the correlation between coating thickness and base sheet surface height data, (a) for the original data, (b) for lowpass-filtered data and (c) for highpass-filtered data.

0.6 for blade coating. The weak correlation in curtain coating is an indication for a contour coat like behavior, which is slightly more pronounced for clay coatings than for carbonate coatings. The high R^2 in blade coating is an indication for a leveling coat like behavior, as expected for blade coatings. The different pigments do not show an influence on the obtained coating structure. The values for the coating layers applied with the film-press are between those of a curtain coater and a blade coater. As with curtain coating, the clay containing coating color gives a more contour coat like structure than the carbonate containing color. For the highpass-filtered data a small difference between the coating application systems as well as the pigment systems is observable, at least for curtain and film coating. These differences could be induced by the application system (forces acting,...) but detailed reasons have not been identified so far. However, the high R^2 values above 0.7 indicate the filling of small sized voids in the paper surface independent from the application system.

Slope of the linear regression

Similar conclusions can be drawn for the slopes of the regression lines obtained from the correlations of coating thickness and base sheet surface height data, which are shown in Figure 3.26(a) for the original data and (b) for the lowpass-filtered data. The range of slopes obtained in the original data is even narrower than the R^2 values discussed before. After lowpass-filtering, the correlations of the remaining structures of coating thicknesses and base sheet surface heights give gradients of about -0.6 for blade coatings -0.2 to -0.3 for curtain coatings and -0.4 for film-press coatings. The closer to zero the slope the less pronounced is the correlation between coating thickness and base sheet surface height. A distinction between clay and carbonate containing coatings is not possible in this case. Figure 3.26 (c) presents the results obtained in

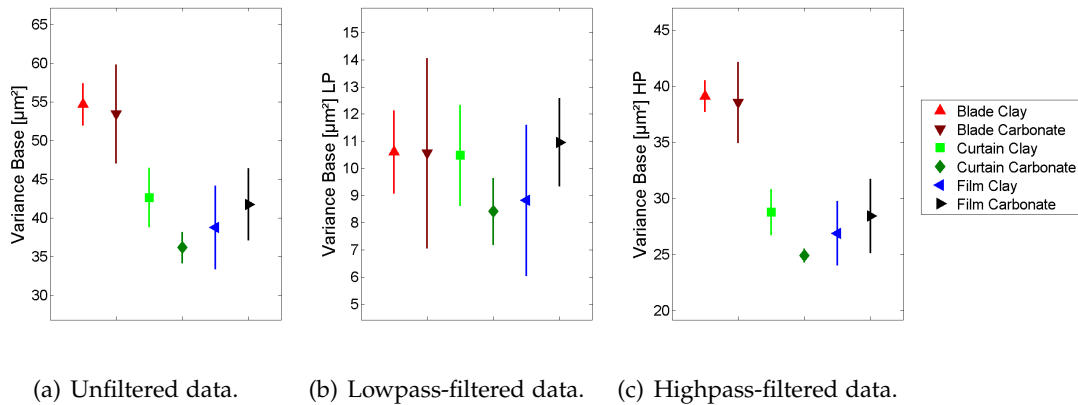


Figure 3.27 Variance of base sheet surface height data (a) for the original data, (b) for lowpass-filtered data and (c) for highpass-filtered data.

highpass-filtering. Again, the value close to -1 indicates a strong correlation between coating thickness and base sheet topography at the small structures indicating the void filling effect independent from the application system. The differences observable only result from the application system. Film press coating gives the strongest correlation between coating thickness and base sheet surface height, whereas blade coating give the weakest correlation. A reason for this might be the fact that the blade coating was applied on the rougher side of the base paper.

Variance of base sheet surface heights data

The variances of the original base sheet surface height data are presented in Figure 3.27 (a) and show a clear difference between the blade coated samples and the film and curtain coated samples. Blade coating was applied on the rougher backside of the paper while curtain and film coating were applied on the smoother paper top side. This difference in roughness is not evident in the larger structures obtained in lowpass-filtering because - as can be seen in Figure 3.27 (b) - the variance of the lowpass-filtered base sheet surface height is similar for all samples analyzed. The small structures obtained in highpass-filtering, see Figure 3.27 (c) show higher variance for the blade coated samples, indicating a difference between the top and the bottom side of the base paper. In this particular case, the differences in base sheet roughness originate from structures having a size lower than $275 \mu m$ (cutoff wavelength), whereas larger structures do not show significant difference in base paper roughness.

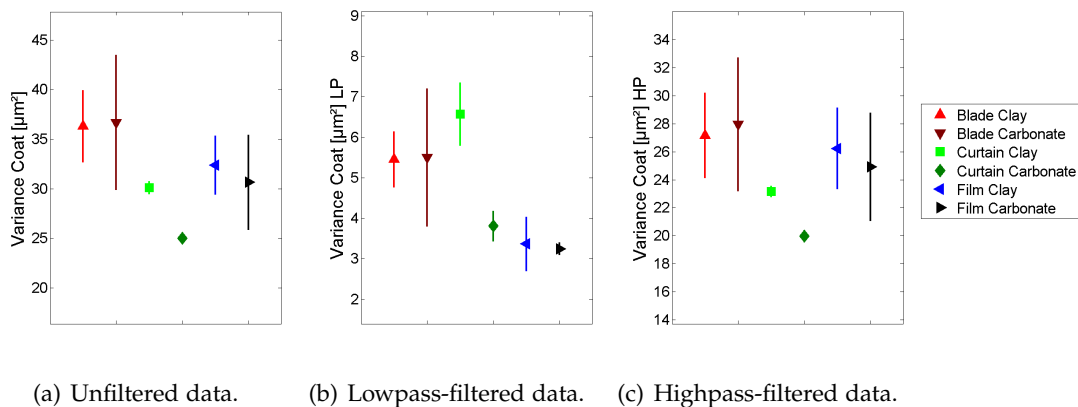


Figure 3.28 Variance of coating thickness (a) for the original data, (b) for lowpass-filtered data and (c) for highpass-filtered data.

Variance of coating thickness data

Figure 3.28 presents the calculated variances of the coating thickness data, (a) for the original data, (b) for the lowpass-filtered data (large structures) and (c) for the highpass-filtered data (small structures). The coating layers applied with a curtain coater show a significantly lower variance of coating thicknesses in the unfiltered case compared to the coating layers applied with the other application systems. Film and blade application cannot be distinguished statistically, however a trend to a more uniform coating layer in film coating can be observed. Lowpass-filtering of the data results in a narrower range of the variations observed, see Figure 3.28(b). The lowpass-filtered data seemingly show higher variations of the coating thicknesses obtained with blade coating. This agrees with the assumption of a leveling coat like structure obtained in blade coating. The expected contour coat obtained in curtain coating giving a uniform coating thickness can only be seen for the carbonate containing coating color. The variance of coating thickness data obtained in curtain coating - especially for the clay coated sample - has to be treated with care, see the coating thickness maps e.g. Figure 3.24.

Summary of influences caused by application systems

This example demonstrated that different types of application systems - blade coating, film coating and curtain coating - fill the small voids at the base paper surface caused by e.g. individual fibers with coating colors in all cases. Differences between the application systems were observed if larger structures at a length scale larger than $275 \mu m$ were considered. The influence of the different pigments analyzed, clay and carbonate, was less pronounced compared to the influence of the application system.

One can obtain a more leveling coat like structures with carbonate pigments, whereas clay seems to have a better covering ability.

3.4.3 Example II: Pilot calendering trial on curtain coated samples.

Pre-calendering is discussed as an option to reduce the variance in coating thickness distributions [GRÖN AND AHLROOS, 2001] which again leads to an improved print quality, e.g. [AHLROOS ET AL., 1999; KOYAMOTO AND OKOMORI, 2006; ZOU, 2007]. Different effects were observed in previous studies. A more uniform coating layer after pre-calendering was reported [GANE AND HOOPER, 1989; GRÖN AND AHLROOS, 1998; STEFFNER AND NYLUND, 1995], but an inverse trend was found too [ENGSTRÖM AND LAFAYE, 1992]. The different relaxation behavior during rewetting was discussed as a possible reason for this behavior [GRÖN, 2000]. Post-calendering is believed to have no influence on coating layer structures [STEFFNER AND NYLUND, 1995]. A reduction in the void volume of the coating was observed [LEPOUTRE AND MEANS, 1978], but no thickness reduction of the coating layer was measured after post-calendering [LARSSON ET AL., 2007]. However, the pigments hardly change their position in the paper plane during post-calendering indicating a compression only in z-direction [BHARDWAJ ET AL., 2006].

This brief literature overview indicates the wide variety of possible results obtained in pre- and post-calendering of coated paper samples. The approach to estimate the spatial coating layer formation was applied to study influences of pre- and post-calendering.

The samples used in this study were all curtain coated. A coat weight of 12 g/m^2 was applied on the top and the bottom side of a woodfree base paper having a basis weight of 44 g/m^2 . Three calendering steps with different pre- (softnip) and post-calendering (super calender) linear loads were analyzed. The different parameters used as well as the main results obtained are summarized in Table 3.6

Again, at least three samples having a size of 5 mm^2 were analyzed per sample in order to obtain statistically meaningful results.

Coefficient of determination (R^2)

The influence of pre- and post calendering on the coefficient of determination (R^2) for a correlation of coating thickness and base sheet topography is given in Figure 3.29, (a) for the original data, (b) for the lowpass-filtered data and (c) for the highpass-filtered data. The results show the expected trend for curtain coated samples - void filling of small structures (high R^2 for highpass-filtered data) and a contour coat like formation of the coating layer for the larger structures (low R^2 for the lowpass-filtered data). A difference between top and bottom side is observed in the original data and the lowpass-filtered data, the contour coat like behavior is less pronounced on the top side. The differences between top and bottom side are not observable if only the

Pre-calendering Post-calendering	25 kN/m		100 kN/m		100 kN/m	
	0 kN/m		0 kN/m		225 kN/m	
	TS	BS	TS	BS	TS	BS
Mean coating thickness [μm]	9.39	9.42	9.42	8.82	9.203	8.90
CI coating thickness [μm]	0.38	0.65	0.25	0.22	0.31	0.83
Caliper (ser.sect.) [μm]	59.12		57.11		54.69	
CI Caliper [μm]	3.99		1.10		2.24	
Caliper (ISO 534) [μm]	69		66		59	
CI Caliper [μm]	1.35		0.71		0.97	
Rq (coated, ser.sect.) [μm]	2.71	2.56	2.30	2.14	1.82	1.82
CI Rq [μm]	0.07	0.06	0.28	0.24	0.36	0.43
PPS (ISO 8791-4) [μm]	3.50	2.30	3.16	1.96	1.41	0.87
CI PPS [μm]	0.15	0.13	0.10	0.07	0.06	0.05

Table 3.6 Parameters changed and the basic results obtained in the calendering study using woodfree curtain coated samples.

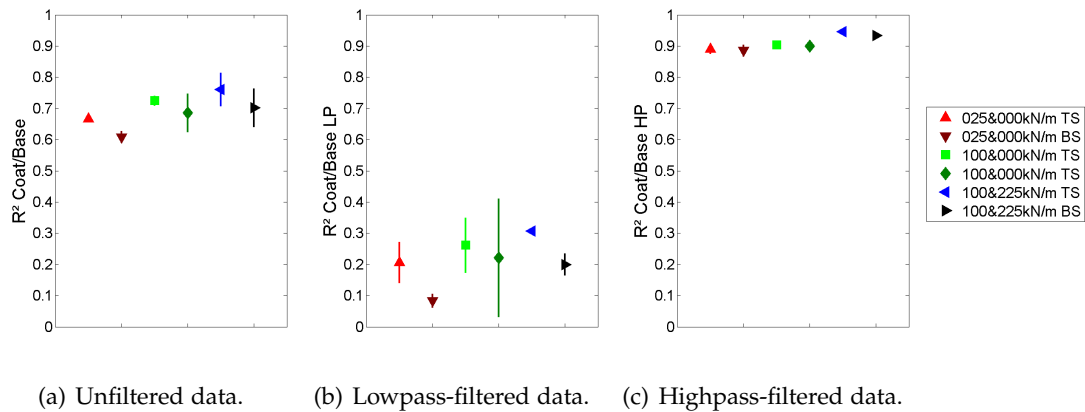


Figure 3.29 Coefficient of determination (R^2) obtained in correlating coating thickness and base sheet topography data, (a) original data, (b) the lowpass-filtered data and (c) the highpass-filtered data of pre- and post-calendered samples.

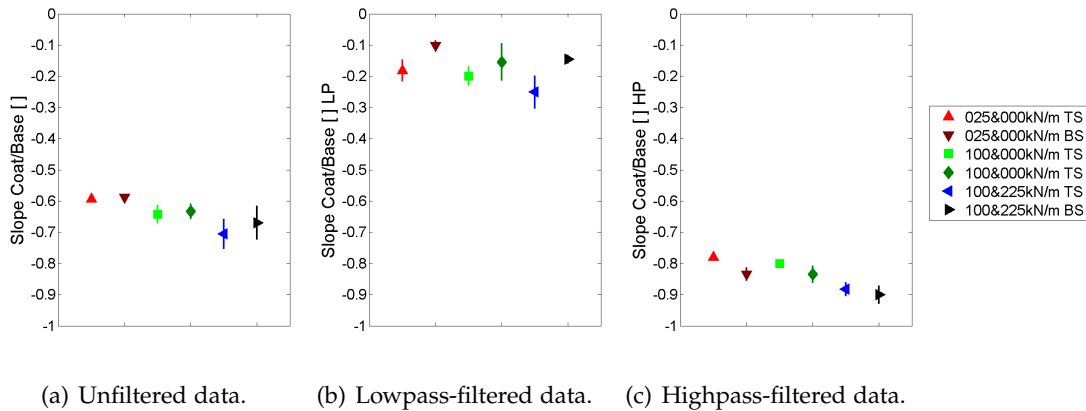


Figure 3.30 Slope of a linear regression model for the correlation between coating thickness and base sheet topography data influenced by pre- and post-calendering for (a) original data, (b) lowpass-filtered data and (c) highpass-filtered data.

small structures (fibers) are considered. Pre-calendering shifts the spatial formation of the coating layer seemingly to a less pronounced contour coat like formation of the coating layer. An influence of post-calendering is hardly observable. Post-calendering affects the highpass-filtered data at an already high level of the coefficient of determination, being always close to 1. This indicates a strong leveling tendency of structures at length scales below $275 \mu\text{m}$.

Slope of the linear regression

The slopes of the linear regressions obtained from the correlations of coating thickness and base sheet topography data are indicated in Figure 3.30, again for the original data (a), the lowpass-filtered data (b) and the highpass-filtered data (c). The twosidedness is less pronounced in the original data. Pre- as well as post-calendering slightly shift the spatial coating layer formation towards more leveling coat like structure. Considering the large structure, only the twosidedness is observable. Pre- and post calendering do not have a significant influence on the coating layer formation. A shift towards leveling coat like structures can be observed for the highpass-filtered data at increased linear loads especially in post-calendering. The slope close to 1 again indicates the strong leveling tendency.

The coefficient of determination (R^2) and the slope of the linear regression between coating thickness and base sheet topography show only weak influences on the spatial formation of the coating layers. Increased loads in pre- and post-calendering shift the coating layer structure to more leveling coat like structures. However, this changes are seemingly not important compared to the roughness improvements in calendering.

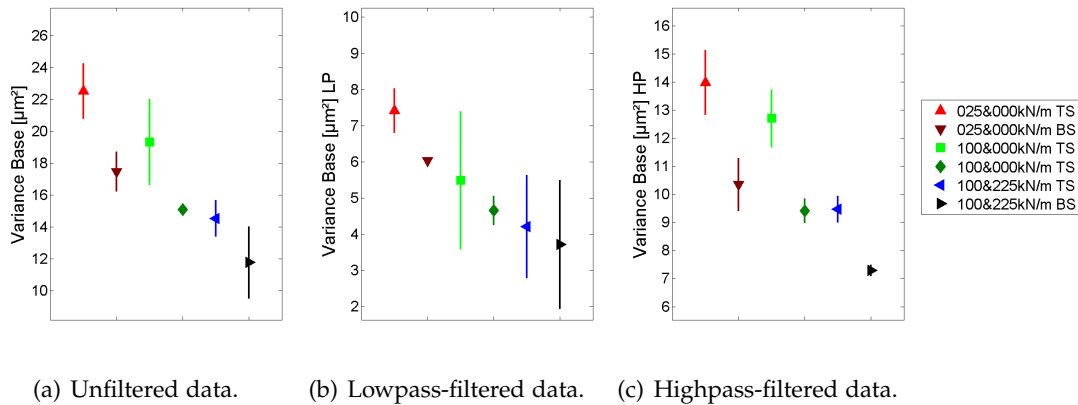


Figure 3.31 Variance in base sheet structures affected by pre- and post calendering, (a) representing the original data, (b) the lowpass-filtered data and (c) the highpass-filtered data.

Uniformity of base sheet surface and coating thickness

Both, pre- and post-calendering reduce the variance of base sheet surface height values (roughness), see Figure 3.31, (a) for the original data, (b) for the lowpass-filtered data and (c) for the highpass-filtered data. The differences between the top and bottom side of the analyzed papers are caused mainly by the small scale structures. Pre-calendering seems to reduce the variance of the large structures above a length scale of $275 \mu\text{m}$, whereas post-calendering effects mainly the small scale structures. A similar trend is found for the coating layer uniformity, expressed as reduced variance of the coating thickness distributions after pre- and post-calendering operations, see Figure 3.32

Summary of the calendering study results

Regarding the influence of pre- and post-calendering on coating structures of a curtain coated woodfree paper, one has to conclude that in this case the coating layer formation was hardly affected by calendering. Only a slight trend towards a less contour coat like formation of the coating layer at increased linear loads (pre- and post-calendering) was observed. The uniformity of the base sheet surface as well as the coating layer distribution were improved. Pre-calendering influenced mainly large structures probably originating from fiber flocs at length scales larger than $275 \mu\text{m}$, the threshold used to differ between void filling and coating layer formation. Structures having a size below this threshold were affected mainly in post-calendering. This can be explained with the compression of individual fibers, creating a more uniform surface of the base paper and therefore reducing also the non-uniformity of the coating layer.

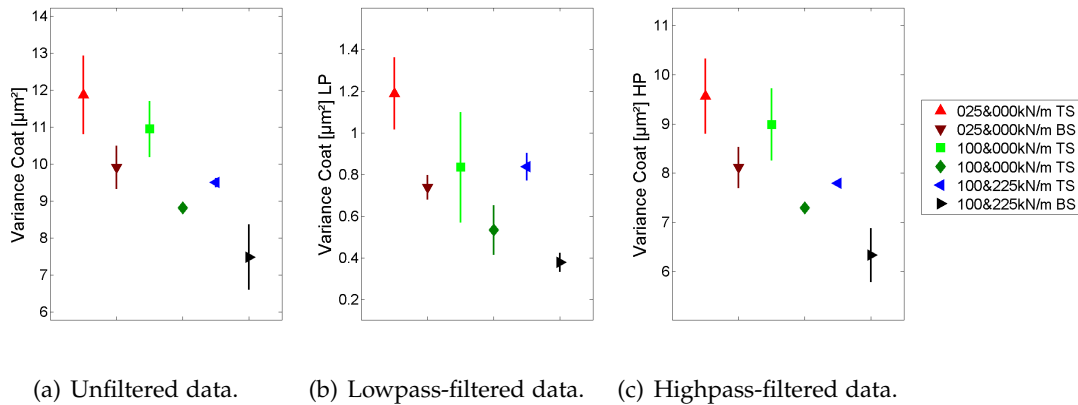


Figure 3.32 Variance of coating thickness distributions affected by pre- and post-calendering. The original data are represented in (a), the lowpass-filtered data in (b) and the highpass-filtered data in (c).

3.4.4 Summary

The spatial formation of a coating layer represented by the interrelation of coating layer thickness with the base sheet topography changes at different length scales. The hypothesis that small structures at the base paper surface (valleys between individual fibers) are filled with coating layer independent from the application system, pigments systems or calendering operations was confirmed. Mainly at larger structures (e.g. fiber flocs) the distinction between a leveling coat or a contour coat like formation of the coating layer becomes possible.

Filtering in the frequency domain was applied to analyze spatial coating layer formation at distinct length scales. The differentiation between small and large structures was performed at a cutoff wavelength of $275 \mu\text{m}$.

Four measures were calculated to quantify the coating layer formation at different length scales. The coefficient of determination (R^2) and the slope of a regression line for a correlation of local coating thickness and local base sheet surface height data were used as measures. In addition, the variance of the base sheet surface height data as a measure for base sheet roughness and the variance of the coating thickness data as a measure for coating layer uniformity were calculated.

The first example presented revealed that blade coating clearly gives a leveling coat like structure whereas curtain coating results in a contour coat like coating layer formation. The small scale structures were found to be hardly affected by the application system. The most obvious differences occurred at the larger scales.

The second example examined the influences of pre- and post-calendering on the spatial coating layer formation for a curtain coated woodfree base paper. In the presented case, pre- as well as post-calendering were found to shift the coating layer formation slightly to a less pronounced contour coat like structure. Pre- and post-

calendering were found to be more important in the development of a uniform base sheet surface as well as coating layer thickness. Small structures were affected in post-calendering, whereas larger structures were altered in pre-calendering.

3.5 Relevance and evaluation of coating holdout

Coating holdout is generally defined as the base paper's resistance to coating solids penetration [HUANG AND LÉPOUTRE, 1998]. ENGSTRÖM [2005] summarized the literature regarding coating holdout in one sentence, indicating the need for a closer look at the influencing parameters and the definition of coating holdout: *"The research world disagrees on whether coating hold-out is a relevant problem or not."*

Coating holdout is important because coating pigments penetrating into the base sheet do not contribute to the goal of surface treatment like covering surface fibers [GRÖN AND AHLROOS, 2001] or the contribution to the final gloss [TREFZ, 1996]. Also expensive brightening and hiding pigments penetrated into the base paper do not perform the desired function to the full extent [ADAMS, 1983; HIRAI AND BOUSFIELD, 2006].

Coating solids penetrate beneath some of the top fibers, but normally not deeper than 15 to 20 μm , or the thickness of about two fibers [HUANG AND LÉPOUTRE, 1998]. A key issue for coating solids penetration is the pore size, which has to be large enough to be entered by solid pigments [HUANG AND LÉPOUTRE, 1998]. FORSTRÖM AND PAJARI [2009] found that coating color penetrated totally into big pores of model substrates (larger than 3 μm), but no bulk coating color penetration was observed at pore sizes below 1.2 μm . Altering the pore size by enhanced fiber swelling [AKINLIKOKAK ET AL., 2002] or the application of a pre-coat to plug the pores and valleys of the base paper [KIM AND BOUSFIELD, 2003] prevents extensive coating penetration. An increased filler content (20%) reduces the pore volume of the base paper, but increases water penetration due to a higher number of small pores and higher capillary forces, leading to a faster immobilization of the coating layer [GRÖN AND AHLROOS, 2001]. The addition of water retention agents and flow modifiers to the coating color or sizing of the base paper are used to control coating penetration into the base paper [ADAMS, 1983]. The application system influences coating penetration too, a high pressure in the nip at metered size press coating was found to facilitate coating penetration [ENGSTRÖM, 2005].

Also totally opposing views on this topic were discussed in the literature stating that the fraction of coating color entering the base paper is not a problem at all [LÉPOUTRE AND DE SILVEIRA, 1991; LÉPOUTRE ET AL., 1986].

A proper characterization of coating holdout respectively an evaluation of the coating solids fraction inside the paper is necessary in order to decide whether coating

holdout is a relevant problem or not. But there is no method available up to now which provides reliable measures:

- Coating holdout is usually inferred from the properties of a coated sheet, like oil absorption [HUANG AND LEPOUTRE, 1998; TREFZ, 1996], brightness gain [ADAMS, 1983] or roughness and porosity [DICKSON AND LEPOUTRE, 1997].
- The reflectance of burnouts is used to evaluate coating holdout [HUANG AND LEPOUTRE, 1998]. The idea is an enhanced contribution to brightness if the coating remains on the paper surface. This approach implies that coating holdout and coating layer uniformity are not independent from each other.
- Another way to evaluate coating holdout is the analysis of the coating backside with roughness measurements or in more detail with electron microscopy. To expose the coating backside, the fibrous material has to be removed either with low temperature ashing techniques [ADAMS, 1983] or by dissolving in a solution with CED [AKINLI-KOÇAK ET AL., 2002; DICKSON AND LEPOUTRE, 1997; KIM AND BOUSFIELD, 2003].
- CLSM is also used to estimate coating holdout [HIRAI AND BOUSFIELD, 2006]. Base paper and coating binders are stained with different fluorescent dyes. Intermixed regions in the obtained images indicate areas where coating penetrated into the base paper.
- Also cross section images of the paper samples are used to analyze coating holdout [FORSSTRÖM AND PAJARI, 2009; GRÖN AND AHLROOS, 2001; HUANG AND LEPOUTRE, 1998]. LLOYD ET AL. [2003] presented an image analysis tool to characterize coating holdout. They divided regions indicated as coating into three types: trapped coating (discrete regions in the base paper), hidden coating (visibly connected to a coating layer, but separated by a layer of fibers) and the coating on the paper surface. Relationships between these three types are calculated and used as a measure for coating penetration and coated paper quality.

This section introduces automated serial sectioning as a measuring technique capable to quantify coating penetration into the base paper in a representative way based on the approach presented by LLOYD ET AL. [2003]. A laboratory scale coating trial was carried out in order to evaluate the relevance of coating penetration and to analyze several possible influencing parameters: base paper porosity and coating formulation.

3.5.1 Measuring principle

The measuring principle can be summarized as follows. The analysis of coating holdout starts with a set of subsequent paper cross section images obtained from a paper

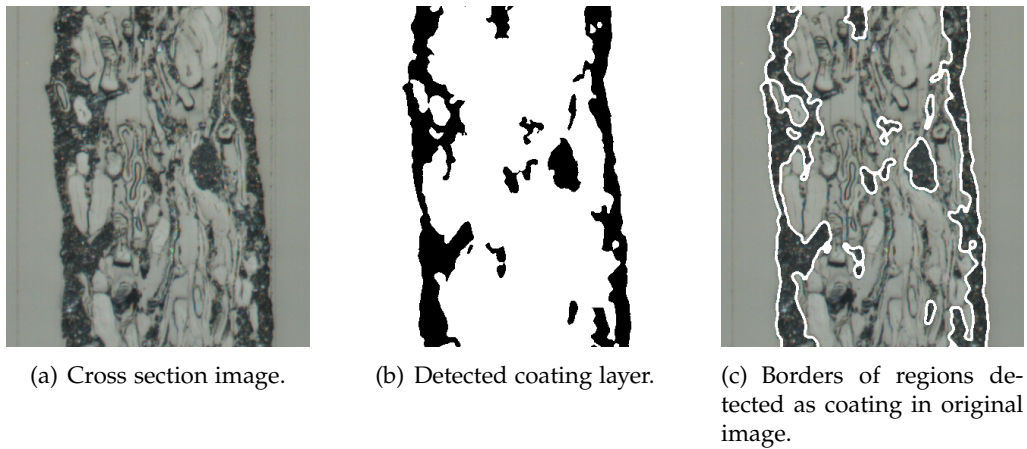


Figure 3.33 Detection of coating regions in cross section images.

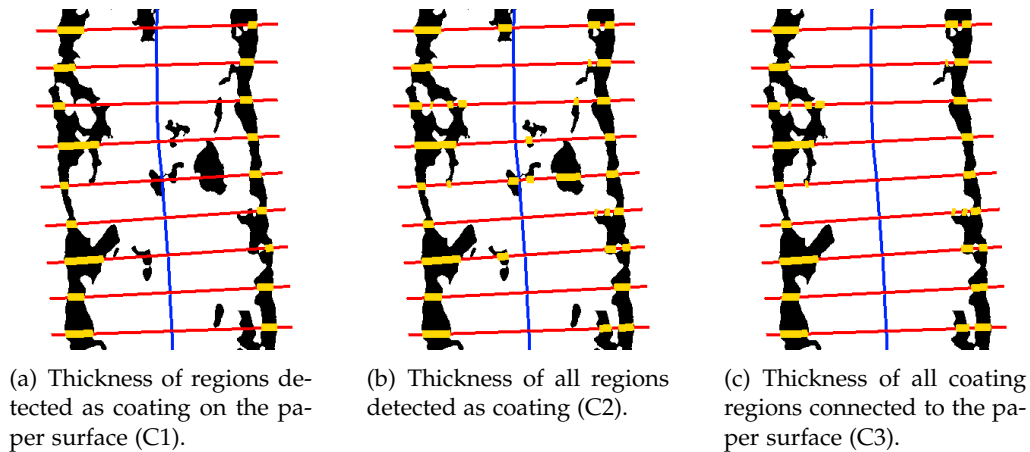


Figure 3.34 Definition of the different coating thicknesses used to quantify the fraction of penetrated coating into the base paper.

sample with automated serial sectioning, see section 3.2.2 for more details. Image analysis is used to detect all regions in the cross sections that have a similar color information as the coating layer, see Figure 3.33.

Similar to the approach presented by LLOYD ET AL. [2003], three types of coating regions were defined and are measured from the binary images highlighting the regions detected as coating, see Figure 3.33 (b). Coating thickness measurement is performed by selecting different options in the image analysis routine to extract the distance values representing coating thicknesses (indicated as yellow regions in Figure 3.34) and other properties, see section 3.2.2. The following types of coating and their thicknesses are extracted:

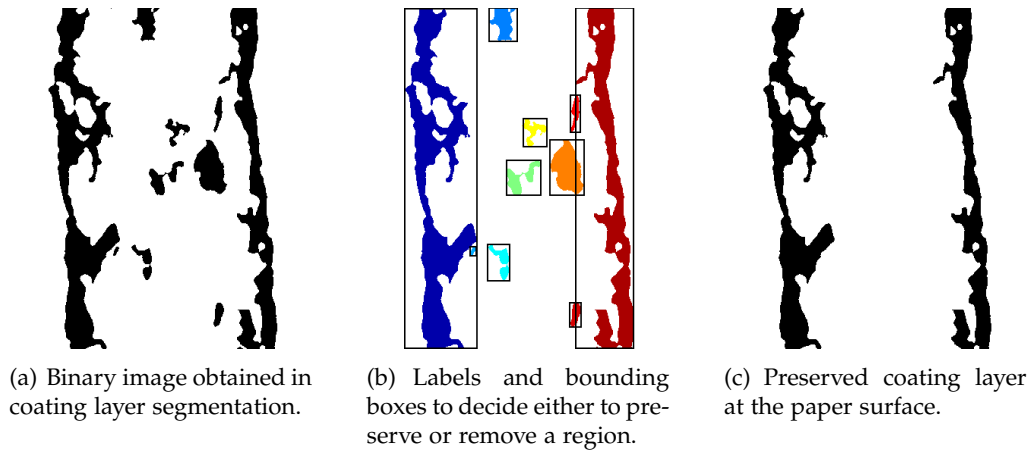


Figure 3.35 Removal of separated regions denoted as coating layers in the paper. If an outermost edge of a region is identical with the paper surface, then it will be preserved as coating

- Thickness of regions detected as coating on the paper surface (C1)
Only coating on the paper surface is considered in this case. The coating thickness is determined by counting pixels. Counting starts at the outermost coating pixel on a measuring line (paper surface) and moves towards the paper center line. The distance to the first interruption is counted, see Figure 3.34 (a). This is the standard coating thickness measurement procedure which is applied to quantify the different other coating layer properties presented in this thesis, see section 3.2.2.
- Thickness of all regions detected as coating (C2)
All regions detected as coating are considered. The coating thickness results from a summation of the individual thicknesses (obtained by coating pixels) of all regions detected as coating along a measuring line - from the paper surface to the paper center line, see Figure 3.34 (b). According to LLOYD ET AL. [2003], this measure includes the coating on the paper surface, hidden coating and trapped coating. But also filler agglomerates detected as coating regions are included.
- Thickness of all coating regions connected to the paper surface (C3)
This coating thickness is obtained in a way similar to the measurement of C2, but separated regions detected as coating in the base paper are not considered, see Figure 3.34(c). In accordance with LLOYD ET AL. [2003] the coating layer on the paper surface and hidden coating are included.
Figure 3.35 presents an additional processing step which is applied to remove all separated regions detected as coating in the base paper from the binary images for an accurate analysis of the third type of coating layer. All individual coating regions in the binary cross section are labeled with a unique ID, indicated as

a unique color in Figure 3.35(b). This allows direct access to each individual region. The outermost edges of each region are calculated and represented as boxes in Figure 3.35(b). This is the basis of the decision criterion whether the individual region is preserved as coating or removed. If an outermost edge of a region is identical with the paper surface, then it will be preserved as coating, otherwise it will be removed.

The three coating thicknesses - coating thickness on the paper surface ($C1$), thickness of all regions denoted as coating ($C2$) and the thickness of all regions linked to the paper surface ($C3$) - are used to define measures to quantify the coating penetration. In this first approach, the mean values of the measured coating thicknesses are used and two relations are calculated:

- All regions detected as coating below the paper surface (hidden and trapped coating) are defined as penetrated coating. This includes also the fillers in the paper since a distinction between penetrated coating and fillers is not possible. The coating in the paper is given as a fraction of the total detected coating ($C2$, see Figure 3.34 (b)):

$$Upper\ Limit = \frac{C2 - C1}{C2} \quad (3.2)$$

The fraction obtained indicates the upper level of penetrated coating solids into the base paper.

- From the paper surface separated but visibly connected regions (hidden coating) are treated as penetrated coating. The coating hidden in the base paper is given as a fraction of total detected coating connected to the paper surface ($C3$, see Figure 3.34 (c)):

$$Lower\ Limit = \frac{C3 - C1}{C3} \quad (3.3)$$

The fraction obtained indicates the lowest level of penetrated coating solids into the base paper.

In general, the higher the calculated value, the more coating color has penetrated into the base sheet. The true fraction of penetrated coating color is somewhere between the two measures. A closer quantification of the true fraction is difficult because this requires knowledge regarding the amount of detected fillers considered as trapped coating ($C2$). In the following, these measures will be used to analyze the penetration behavior of coatings into the base paper.

	Solids [%]	S1S & S1Z	S2S	S3S	S4S	S5S & S5Z	S6S
Hydrocarb 90	78	100		80	80	60	
Covercarb 75	72		100				
Omyaprime HO 40	74						100
Hydragloss 90	73			20	20	40	
PVA BF-05 (6-98)	25			0.40			
CMC Finnfix 10	12			0.50			
Styronal D 628	50			11.0			
Leucophor VM fl	100			0.50			
Solids Content		71.4	67.0	71.0	67.1	68.7	68.3
Coat Weight g/m^2		15.3 & 14.2	13.9	18.8	13.5	18.7 & 14.3	16.5

Table 3.7 Coating formulations used for sample series to evaluate influencing parameters of coating hold out.

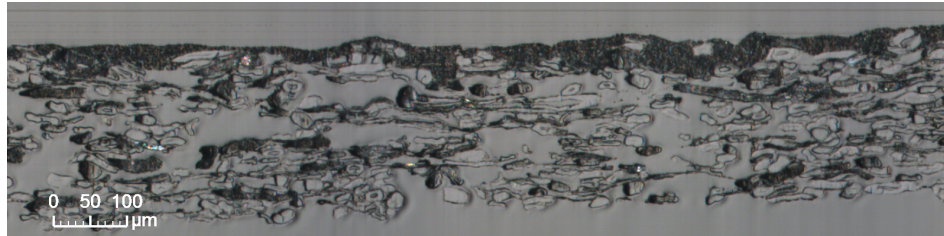
3.5.2 Relevance of coating holdout and influencing parameters

The influence of base paper porosity and coating color formulation on coating solids penetration into the base paper was analyzed. Two sample series with different kinds of base paper have been prepared, see Table 3.7 for more details. The coating was applied with a laboratory web coater on one side of the base paper. The base paper in the first sample series contained only eucalypt pulp (S1Z, only carbonate containing coating and S5Z, 40% clay in coating color) and was used to study the effects of base paper porosity and basic pigment variations on coating penetration without the presence of fillers in the base paper. An industrially produced base paper containing fillers and coated broke was used in the second trial (S1S - S6S) that was designed to study the effects caused by pigment variations in more detail.

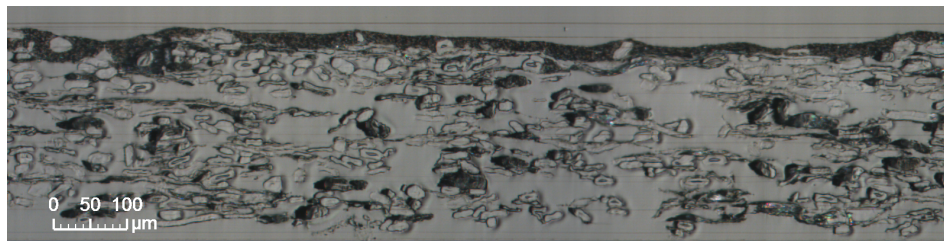
Influence of base paper porosity

The pure eucalypt pulp containing base paper was produced on a pilot paper machine. Strong variations in base paper porosity were found, a closer evaluation revealed a distinct pattern visible in the look-through which most probably resulted from a suction roll in the production process. The large differences in base paper porosity are difficult to measure directly due to the small size of the suction roll pattern, but these are clearly obvious from the paper cross section images, see Figure 3.36; (a) and (b) represent an open structure with large pores between the fibers, (c) and (d) a dense structure.

Small samples (65 slices with a distance of $4 \mu m$ and a length of $2 mm$ giving a total area of $0.5 mm^2$) were digitized and prepared for coating layer analysis. This sample size was chosen because of the small size of the regions with high and low base paper porosity caused by the suction roll pattern. To get statistically meaningful results, 3



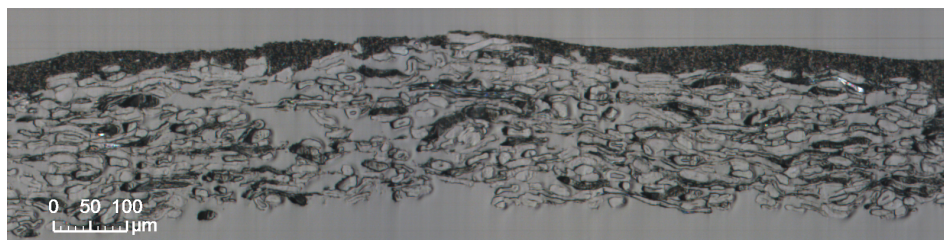
(a) S1Z - Only carbonate containing coating color, high base paper porosity.



(b) S5Z - 40% clay in coating color, high base paper porosity.



(c) S1Z - Only carbonate containing coating color, low base paper porosity.



(d) S5Z - 40% clay in coating color, low base paper porosity.

Figure 3.36 Effect of base paper porosity and coating formulation on coating hold out.

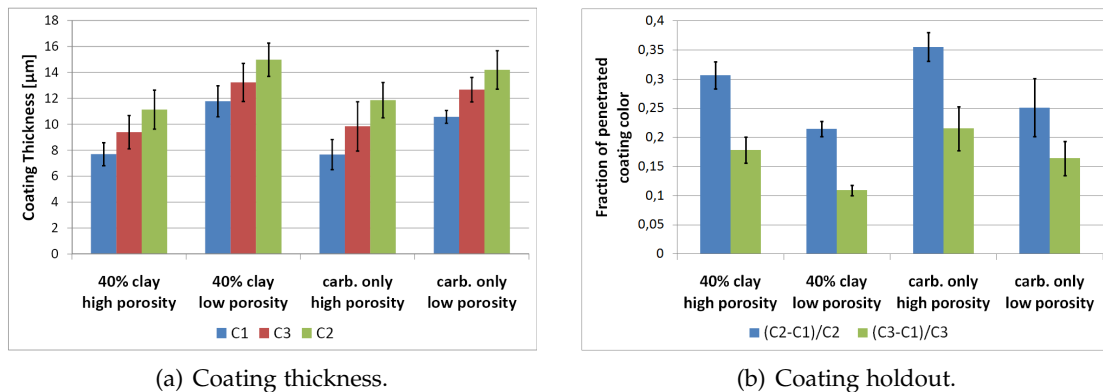


Figure 3.37 Influence of base paper porosity on measured coating thicknesses (a) and coating holdout (b).

samples were analyzed for each paper sample. Because of the reduced sample size, the 90% confidence intervals were calculated.

Figure 3.37(a) shows the measured coating thicknesses - 1) coating thickness at the paper surface (C1), 2) the thickness of all regions connected to the surface (C3) and 3) the thickness of all regions detected as coating (C2). The coating layer on the paper surface is significantly thinner on the regions with an open sheet structure than on regions with a dense structure. This difference is also true for the other thicknesses (C2 and C3) measured although they are not significant for the only carbonate containing color. Both coating colors give similar results for the particular measures and are therefore difficult to distinguish. The difference between the coating thicknesses C2 and C3 indicates a noticeable but not significant fraction of distinct regions detected as coating in the base paper. But a detailed look at the cross section images presented in Figure 3.36 reveals that there are hardly separated coating regions in the base paper. There are some fiber cross sections observable that have a similar appearance to coating and these are detected as coating during image analysis as well. For this reason, C2 clearly overestimates the fraction of coating penetrated into the base paper. However, the increase from C1 to C3 indicates a remarkable coating penetration into the base paper in each case.

The measures used to explain the penetration of coating solids into the base paper are presented in Figure 3.37(b). In general, a minimum of 10 - 20% of the total detected coating has penetrated into the base paper. A more detailed look at the results reveals a higher fraction of penetrated coating solids for the paper regions with the more open structure for both coating colors. The differences between dense and open base sheets are more obvious for the clay containing coating color, both measures calculated indicate a significant lower fraction of penetrated coating solids in the base region with a low porosity. The only carbonate containing color shows significant differences between the open and the closed base paper structures at the

upper limit of penetrated coating. The measure defined as the lower limit indicates also a better holdout at dense sheet regions but this is not significant anymore. There are also small differences between the coating colors observable. The clay containing color gives a somewhat better holdout than the only carbonate color. This leads to a first conclusion that base sheet porosity clearly influences the penetration behavior of coating solids into the base paper, whereas the coating formulation is less important in this particular case. Since a high fraction of coating color cannot contribute to paper surface enhancement, coating holdout / coating penetration has to be treated as serious challenge in paper coating.

Influence of pigment variations

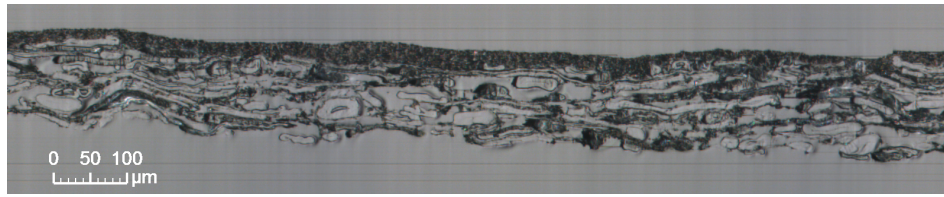
The second sample series was designed to study the influence of different coating color compositions on the coating solids penetration into an industrially produced base paper, see S1S - S16 in Table 3.7. A limitation of this sample series were the different coat weights applied.

As with the first experiment, 3 samples having a size of 0.5 mm^2 (65 slices with a distance of $4 \mu\text{m}$ and a length of 2 mm) have been analyzed per paper sample. The results are presented with 90% confidence intervals.

Cross sections of the papers analyzed are very similar, see Figure 3.38. The largest differences obtained from visual inspections can be found in the coating thicknesses and the uniformity of the coating layers.

The first results again show the coating thicknesses for the different samples, see the bar plot in Figure 3.39(a). In agreement with the cross section images (Figure 3.38) and the coat weights given in Table 3.7, the thickest coating layer were found on the samples S3S (20% clay and high solids content) and S5S (40% clay). A still undetermined but possible influence of coat weight on penetrated coating solids has to be kept in mind for the next step of analysis.

The fraction of penetrated coating color is presented in Figure 3.39(b). Coating formulation S1S (100% Hydrocarb 60) gives a poor coating holdout. The other formulations considered (S2S - S6S) show a significant improvement of coating holdout compared to S1S. Only small and hardly significant differences can be observed between the coating formulation S2S to S6S. Having the same coating color, a higher solids content seems to give a better coating holdout than the lower solids content (S3 and S4 respectively, both contain 80% Hydrocarb 60 and 20% Hydragloss 90). The color with the highest clay content seems to give the best coating holdout (S5S). Because of the overlapping confidence intervals, there are no statistically significant differences in the results and one has to conclude that in this particular case the coating formulation (changes in the pigment system) do not result in major improvements in the coating penetration behavior.



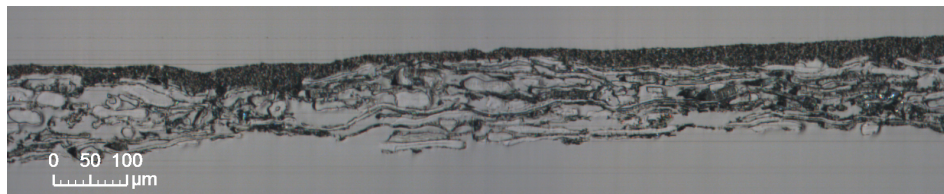
(a) S1S - Coating color 1, industrially produced base paper.



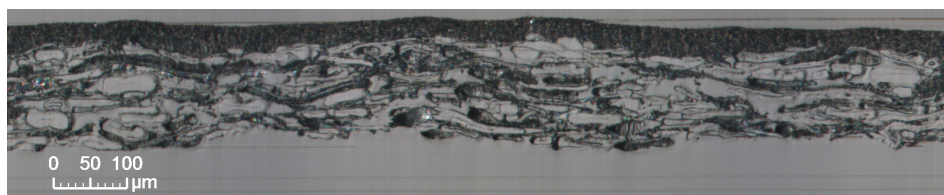
(b) S2S - Coating color 2, industrially produced base paper.



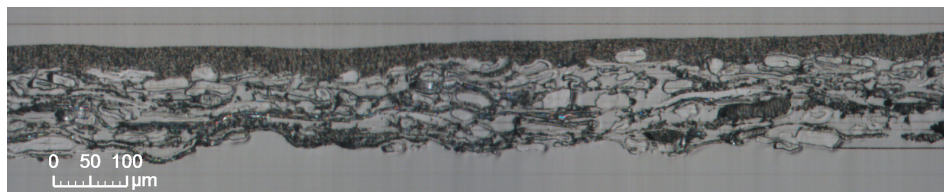
(c) S3S - Coating color 3, industrially produced base paper.



(d) S4S - Coating color 4, industrially produced base paper.



(e) S5S - Coating color 5, industrially produced base paper.



(f) S6S - Coating color 6, industrially produced base paper.

Figure 3.38 Cross section images of a similar industrially produced base paper coated with different coating colors.

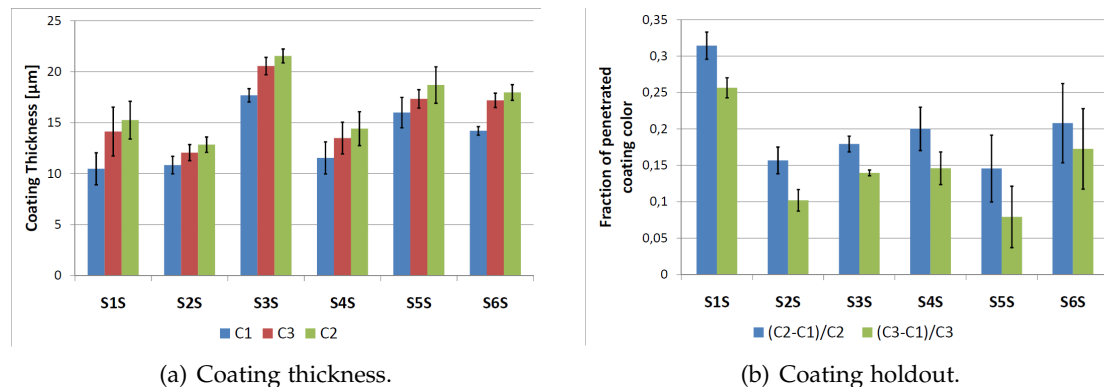


Figure 3.39 Influences of different coating colors applied to an industrially produced base paper on coating thickness and coating holdout.

3.5.3 Summary

The question whether coating holdout is a relevant problem or not was discussed. Measures which span the range between the maximum and the minimum penetration of coating color solids into the base paper were defined.

The effects of base paper porosity and coating color formulations (changes in the pigment system) on the coating holdout respectively coating penetration into the base paper were analyzed. The results revealed that base paper porosity (remarkable changes in the base paper porosity) has a clear influence on the fraction of coating solids penetrating into the base paper. Changes in the pigment system of a coating color can be used to alter the coating penetration behavior. All in all, each case analyzed has shown a large fraction of the coating color penetrated into the base paper and for this reason coating holdout should be discussed as a relevant problem.

The results presented here were first trials and have to be validated with other methods and samples in the future work. Also other approaches to analyzed coating holdout based on serial sectioning have to be developed. For example, currently the means of coating thickness data are used for evaluation. The next step could be the use of local data (individual coating thicknesses at a measuring line) which should result in a distribution of coating solids fractions penetrated into the base paper.

3.6 New ways to analyze coating coverage

The goal of coating is a sufficient coverage of the base paper even at low coat weights [WIKSTRÖM AND GRÖN, 2003]. A surface of a base paper that is not covered well will give a poor quality paper [DICKSON ET AL., 2002]. The general definition of coating coverage refers to the fraction of the surface of coated paper that is well covered by

the coating layer [AZIMI ET AL., 2009] and finally gives a measure about how well the coating covers the base paper [ENGSTRÖM, 1999].

Coating coverage can be influenced in different ways. Pre-calendering improves coating coverage because a more uniform coating layer can be obtained, see for instance [GRÖN AND AHLROOS, 2001; STEFFNER AND NYLUND, 1995]. Coating coverage can be improved by reducing the openness of the base paper. This can be achieved by the use of fillers [GRÖN AND AHLROOS, 2001], refining of pulp or a higher fines content [FORSSTRÖM ET AL., 2003]. Also the coating color can be an influencing parameter, a higher level of clay gives a better coverage as does a higher solids content of the coating color [DICKSON ET AL., 2002; FORSSTRÖM ET AL., 2000]. A coat weight of 12 g/m^2 was found to give complete coverage in blade coating [KARTOVAARA, 1989]. Coating application with a metered size press gives a better coverage than blade coating [WIKSTRÖM AND GRÖN, 2003].

A common method to estimate coating coverage is the burnout test [ENGSTRÖM, 1999; FORSSTRÖM ET AL., 2003; STEFFNER AND NYLUND, 1995]. Surface imaging with scanning electron microscopy is an important method and gives direct access to the fraction of the uncoated surface area [DICKSON ET AL., 2002; ENGSTRÖM, 1999; FORSSTRÖM ET AL., 2003; KARTOVAARA, 1989]. Also novel techniques like x-ray imaging (transmission of x-rays through a paper sample) are used to estimate the fraction of uncoated / coated area [AZIMI ET AL., 2009].

In this section, the benefits of a 3D digitization technique like the automated serial sectioning technique in the analysis of coating coverage are presented. Coating coverage is defined as a fraction of uncoated area and as a fraction of areas with low coat weight. Influencing parameters on these measures are discussed. Novel approaches like local analysis of uncoated spots and their surrounding areas are presented. This field of research is one of the youngest in coating layer analysis based on data obtained from automated serial sectioning and therefore only first approaches are discussed.

3.6.1 Determination of uncoated areas

The fraction of uncoated areas can easily be determined from the data obtained with serial sectioning. A straightforward way is the definition of a reasonable threshold level, as it is presented exemplarily in Figure 3.40. The graph shows cumulative distributions of coating thicknesses obtained from blade and curtain coated samples. Two threshold levels are highlighted, at coating thickness of $1 \mu\text{m}$ and $3 \mu\text{m}$.

The first threshold at a coating thickness of $1 \mu\text{m}$ seems to be a proper measure for the areas not covered with coating. This is because the cumulative distribution functions keep almost unchanged in the range between 0 and $1 \mu\text{m}$. The second threshold at a coating thickness of $3 \mu\text{m}$ is defined to analyze regions with a very thin coating layer which are assumed to be located around uncoated spots.

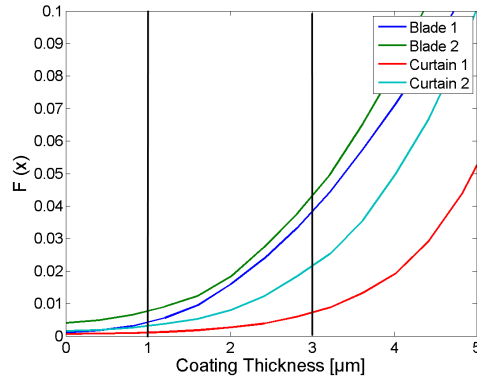
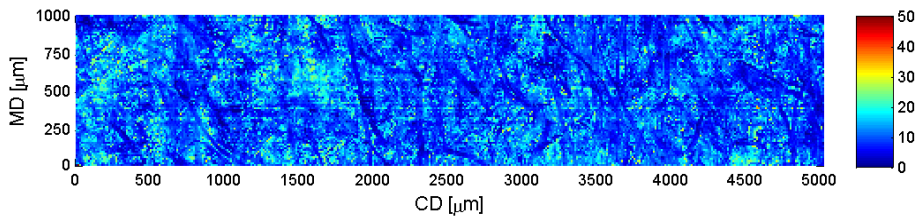
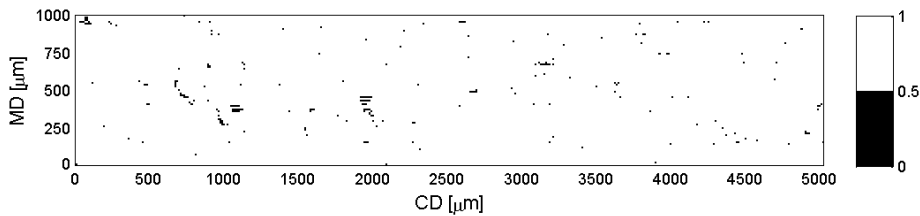


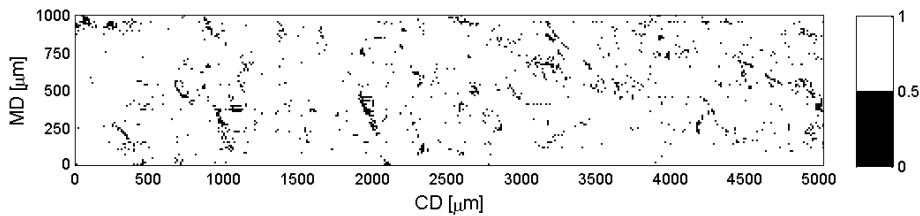
Figure 3.40 Definition of threshold levels for uncoated areas and areas with low coat weight on cumulative coating thickness distributions.



(a) Original coating thickness map.



(b) Areas below 1 μm coating thickness.



(c) Areas below 3 μm coating thickness.

Figure 3.41 An original coating thickness map (a) and the corresponding areas with a lower coating thickness than 1 μm (b) and 3 μm (c).

Figure 3.41 gives a closer look on how the thresholds are used. An original coating thickness map is shown in (a). The thresholds are then used to point out the regions with the different coating thicknesses. Regions covered with a thinner coating thickness than $1 \mu\text{m}$ are shown as black spots in Figure 3.41 (b). Regions with coating thicknesses below $3 \mu\text{m}$ are highlighted in (c). These results (b) and (c) can be used to calculate the fraction of uncoated areas respectively areas with a low coat weight. In addition, all other data obtained in serial sectioning e.g. base sheet topography and surface topography can be extracted for these highlighted regions and used for further analysis.

Also the visual evaluation of the binary pattern obtained allows to gain some knowledge regarding coating coverage, see Figure 3.41. Several small and seemingly randomly distributed spots with no coating on the paper surface can be observed. A few larger regions with no coating can be linked to exposed fibers at the base paper surface. Also the regions with a low coat weight can be found at exposed regions at the base paper.

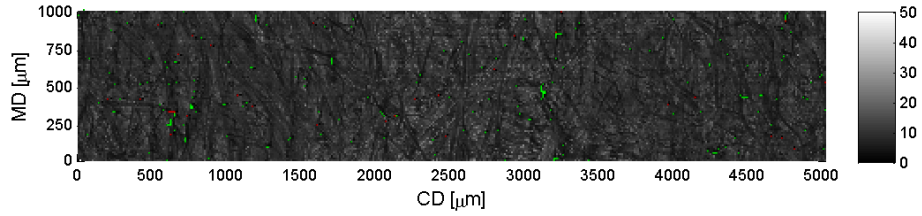
Using this approach, differences between application systems become obvious, see Figure 3.42. These graphs show the coating thickness maps, bright regions represent a thick coating layer, dark regions a thin coating layer. Uncoated areas are highlighted in red, areas with a low coat weight in green. Figure 3.42 (a) shows the result for the curtain coater and (b) the result for the blade coater. Discontinuities in the coating layer obtained from curtain coating are rare. Those appearing are caused mainly by individual fibers at the paper surface. The regions highlighted are very small in size. In blade coating, the discontinuities in the coating layer are larger and again caused by fibers at the paper surface. It is easy to imagine that these larger region originate from the metering action in blade coating, where excess coating color is removed from the elevated regions in paper surface. A conclusions from these plots is that the base sheet topography could be an important influencing parameter in coating coverage.

3.6.2 Discussion of influencing parameters

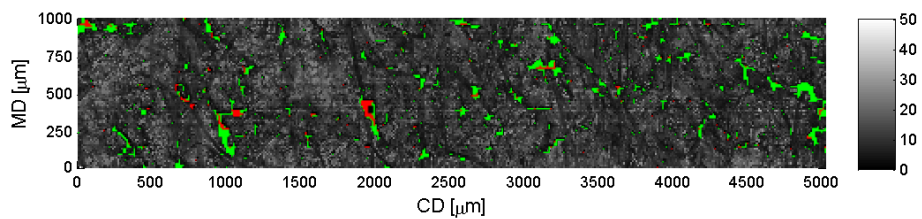
During the course of this thesis, numerous samples were analyzed, see Appendix B. Here, the influences of coating layer properties (mean coating thickness, roughness of the base sheet and the coating thickness coefficient of variation) on the fractions of uncoated areas and areas with a low coat weight are shown in the Figures 3.43 - 3.45. A comparison to results obtained with the burnout test is given in Figure 3.46. A general fact observable from these plots is that the different sample groups (see Appendix B) are usually located within a small range of measured property.

According to section 3.3, at least three samples having an area of 5mm^2 were analyzed per sample specimen.

The influence of the mean coating thickness on the fraction of uncoated areas is presented in Figure 3.43(a). As expected, a general trend to a larger fraction of un-

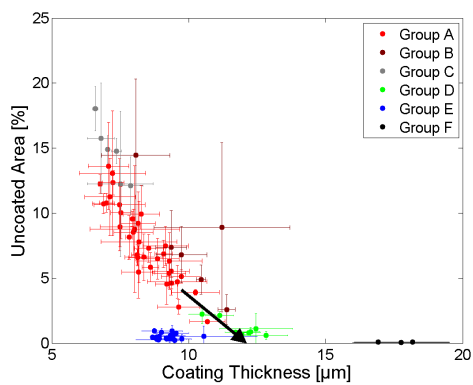


(a) Curtain coated.

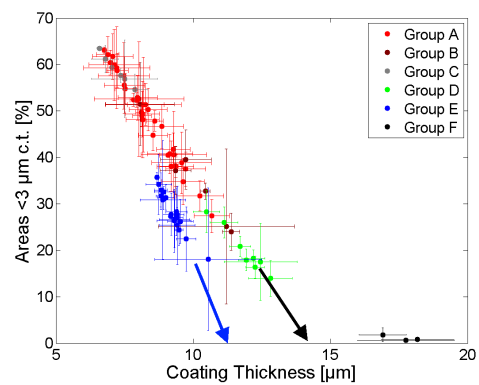


(b) Blade coated.

Figure 3.42 Coating thickness maps obtained with different application systems; (a) curtain coated and (b) blade coated. A low fraction of uncoated areas or areas with low coat weight indicates the better coverage obtained in curtain coating.



(a) Uncoated regions.



(b) Low coat weight.

Figure 3.43 Influence of coating thickness on coating coverage.

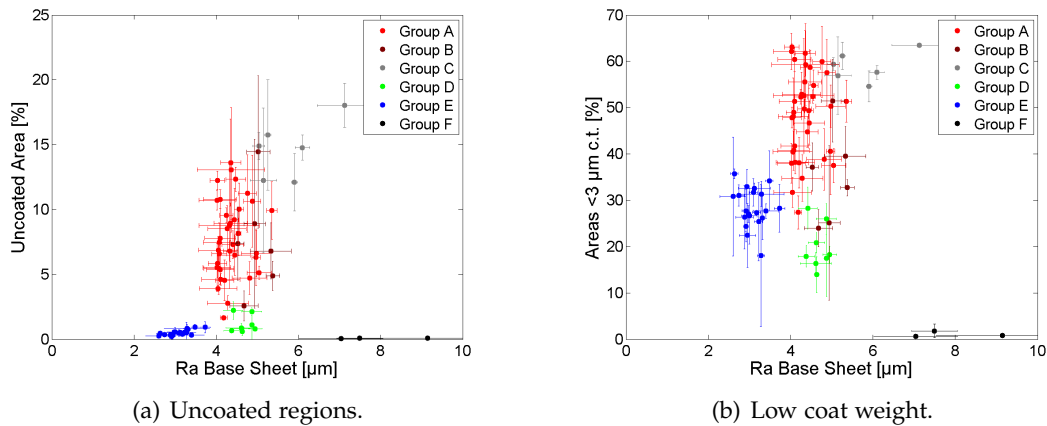


Figure 3.44 Influence of base sheet roughness on coating coverage.

coated areas can be observed for thinner coating thicknesses. Curtain coated samples (Group E, blue dots) seemingly cover the base paper entirely; even with thin coating layers of about $9 \mu\text{m}$. Blade and film coated samples (e.g. Group A, red dots and Group D, green dots) require a higher mean coating thickness of about $12 \mu\text{m}$ for a total coverage (indicated with the black arrow) of the base paper. This value is significantly higher than previous findings discussed in literature, e.g. KARTOVAARA [1989].

Coating thicknesses also influence the fraction of thin coating layer regions, see Figure 3.43(b). Two seemingly independent correlations can be observed. Curtain coated samples (Group E, blue dots) give the fraction of uncoated regions at thinner coating layers compared to blade and film coating. An extension of the trends reveals a mean coating thickness of $14 \mu\text{m}$ to cover the base paper entirely with a coating layer of at least $3 \mu\text{m}$ in blade and film coating (Group A, red dots or Group D, green dots). About $11 \mu\text{m}$ are necessary in curtain coating.

Figure 3.44 shows the influence of the base sheet roughness (Ra) on coating coverage. As mentioned in the beginning of this sections, the different sample groups are located within a small range of the measured property, but the base papers used in the sample groups A, B, C and D are different. There is no obvious influence of the base sheet roughness on the fraction of uncoated areas Figure 3.44 (a) and the fraction of areas with low coat weight Figure 3.44 (b). It seems like the coating application system, curtain or blade and film coating, is a more important variable than the base paper roughness. An important limitation of these plots is that the differences in the applied coat weight are not considered, see the graphs in Figure 3.43.

The influence of coating thickness variations (coating layer uniformity) on the fractions of uncoated regions and the fractions of regions with a low coat weight are shown in Figure 3.45 (a) and (b) respectively. There is an obvious influence of coating

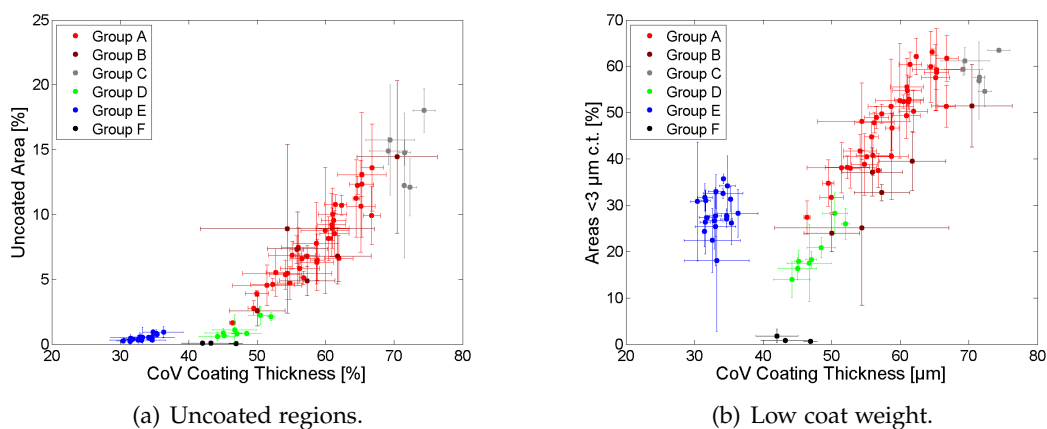


Figure 3.45 Influence of coating thickness uniformity on coating coverage.

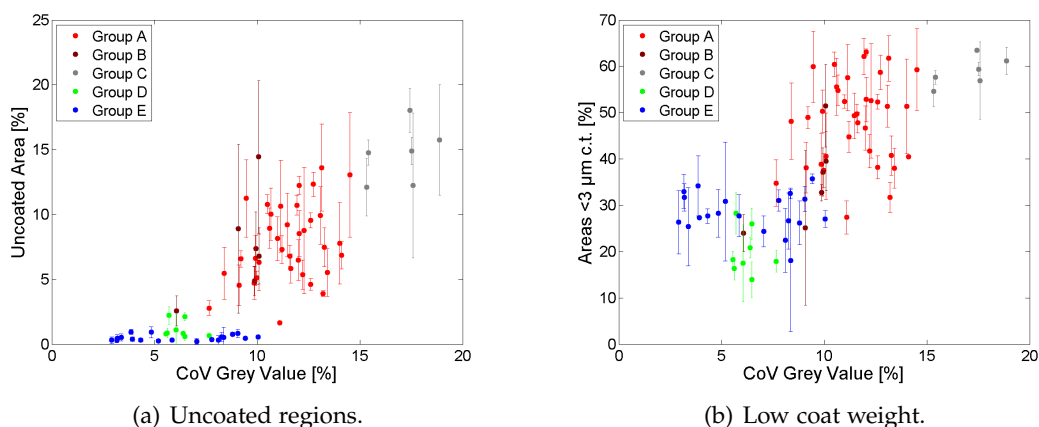
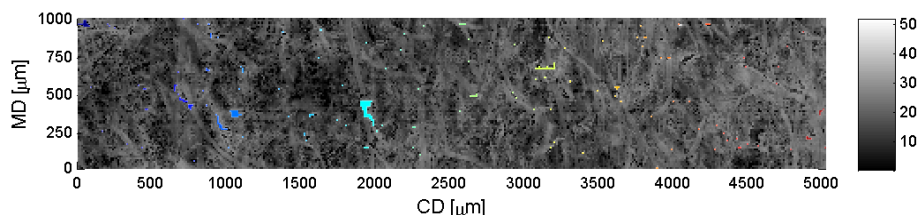


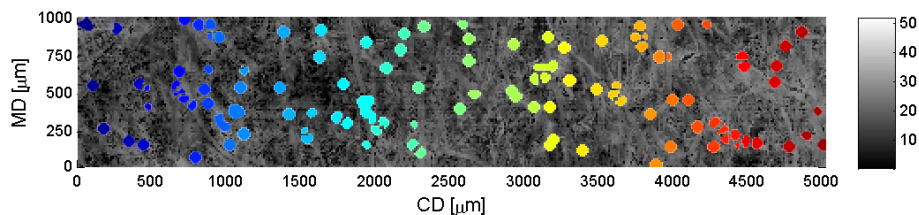
Figure 3.46 Influence of coating thickness uniformity (burnout) on coating coverage.

layer uniformity on the fraction of uncoated regions. A uniform coating layer, as it is obtained in curtain coating (e.g. Group F, black dots) results in an almost fully covered paper surface. A larger variation of coating thicknesses, as it is obtained in blade and film coating, results in larger fractions of uncoated areas. This trend can also be observed for the fraction of areas with low coat weight.

Figure 3.46 shows the influence of coating layer uniformity determined as variance of gray scale data, measured in the scanned images of samples after burnout treatment (Appendix A), on (a) the fraction of uncoated regions and (b) the fraction of regions with a thin coating layer. A slight trend to a higher fraction of uncoated areas can be seen at higher variations in the gray scale data. Looking at the samples of Group E (blue dots, calendering study, woodfree base paper) large difference between the individual samples can be found in the results obtained with the burnout test, but the fractions of uncoated areas keep almost unchanged. The same is observed for the



(a) Topography map with uncoated regions highlighted.



(b) Topography map with indications of surrounding regions of the uncoated spots.

Figure 3.47 Extraction of base sheet topography data at and around uncoated spots.

relation between the fraction of areas with a low coat weight and the variations in the gray scale data. The reasons for this weak correlations are possible limitations of the burnout test as these are discussed in section 3.2.3.

3.6.3 Analysis of individual uncoated spots

A concept of a novel approach to quantify coating coverage is presented in this section. The idea is to analyze different properties e.g. the base sheet topography locally at the uncoated spots and in the surroundings of uncovered areas. Figure 3.47 (a) presents an example showing the base sheet topography, bright regions indicate a hill, dark regions a valley on the paper surface. The uncoated spots are highlighted with different colors (a). These colors represent a label of each individual uncovered area. This allows the analysis of each individual uncoated region independent from the others. Figure 3.47 (b) indicate the surrounding regions of the uncoated spots. To analyze the topography at the uncoated spot and in the surrounding of the uncovered areas, three topography measures (surface heights data) are extracted from the data sets; 1) the topography at the uncoated spot, 2) the topography around the uncoated spot (+1 pixel) and 3) the topography farther away (+2 pixel). Besides the topography data, also the area of uncoated spots is examined.

Figure 3.48 shows typical results, (a) for a blade coated sample and (b) for a curtain coated sample. The y-axis gives the measured local topography standardized by dividing with the mean topography of the sample examined. (Topography is defined as local surface height from a paper middle plane, see section 3.2.2). The individual uncoated spots observed on a 5 mm^2 sample area are placed one after each other on

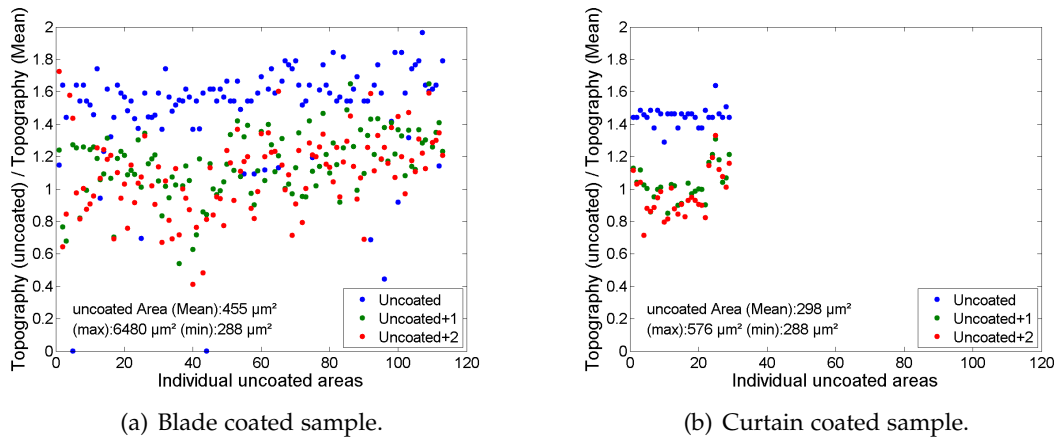


Figure 3.48 Influence of elevated base paper topography on uncoated spots. Data were extracted from 5 mm^2 samples.

the x-axis. The blue dots represent the topography at the uncoated spots. Green and red dots represent the topography around the uncoated spot (+1 pixel and +2 pixel respectively). In both cases, the uncoated spots are mostly exposed regions on the base paper surface because the surrounding areas have usually a lower base sheet surface heights. Coverage seems to be influenced by surface irregularities, even if these cannot be determined with a mean roughness measure as it was presented in Figure 3.44 (a). In addition, a mean as well as a minimum and maximum area of the uncoated spots is calculated. As expected and shown before (Figure 3.42), curtain coating gives a lower number of uncoated spots than blade coating on the same sample area. The average size of the uncoated spots in curtain coating is about $300 \mu\text{m}^2$ and lower than the average size of uncoated spots in blade coating ($\sim 450 \mu\text{m}^2$).

3.6.4 Summary

The data obtained in serial sectioning were found to be well suited for the analysis of coating coverage. The fractions of uncoated areas (areas with a coating thickness below $1 \mu\text{m}$) and the fraction of areas with a low coat weight (coating thickness below $3 \mu\text{m}$) were calculated and used as measures.

A mean coating thickness of $9 \mu\text{m}$ for curtain coating and $12 \mu\text{m}$ for blade and film coating was found to be a prerequisite for good coverage as would be a uniform coating layer. The base sheet roughness appeared to be less important, but uncoated spots are mostly elevated regions on the base paper surface.

Curtain coating was found to cover the base paper better than blade coating. Only a small number of small sized regions were not covered in curtain coating, whereas in blade coating a large number of uncoated areas having different sizes were observed.

These first approaches clearly demonstrated the potential of serial sectioning in the analysis of coating coverage issues.

3.7 Conclusions

Based on the work of DONOSER ET AL. [2006]; WILTSCHKE [2006]; WILTSCHKE ET AL. [2005] several new measuring concepts to analyze properties of coating layers have been developed. The benefits of automated serial sectioning were used: the fast accessibility of large sample areas at high resolution. The analysis of coating layer structures is currently the most important application of the automated serial sectioning technique.

The validity of results obtained with automated serial sectioning was proven by comparisons with other techniques used in coating layer analysis. An extensive discussion of a recommended sampling procedure completed the work regarding the validity of the obtained results. A statistically meaningful analysis of coating layer structures with high resolving measuring equipment was the main outcome of the recent work in the field of coating layer analysis.

Several structural features of the coating layer were discussed showing also future potential for further works in this field of research:

The coating layer formation in terms of an interrelation between coating thickness and base sheet topography was analyzed at different length scales. A threshold level was defined to distinguish between void filling effects at small scale structures like voids between fibers and the spatial formation of coating layers at larger structures like fiber flocs. Differences between application systems as well as influences caused by calendaring were found in first experimental studies.

The second structural feature analyzed in more detail was coating holdout. The first measures presented to quantify coating holdout were fractions of coating penetrated into the base paper. Both, porosity of the base paper as well as changes in the pigment system of a coating color influenced the penetration of coating solids into the base paper.

Coating coverage was another developed approach. In a first step, the fraction of uncoated area was calculated from the data obtained with serial sectioning. First experiments show that the coating thickness applied was a major influencing parameter on the fraction of uncoated areas whereas the base sheet roughness was not that important. However, a local analysis of the surrounding of uncoated spots reveals that these were exposed on the paper surface.

The beginning work in the analysis of coating holdout and coating coverage clearly demonstrated further potential of the automated serial sectioning technique. The current approaches considered basically cumulative measures. The local data available from serial sectioning have not been used extensively and these data invite to spend further thoughts on these tasks.

Analysis of Fiber Cross Section Properties

An alternative way to use data obtained with serial sectioning is the analysis of fiber cross section properties. The relevance and origins of variations in fiber cross section properties are discussed in section 4.1. Analysis of fiber cross sections in the dry state requires several considerations. These as well as a basic layout of a measuring concept and the different imaging techniques used are summarized in section 4.2. This section is followed by a detailed look at the different processes required to measure fiber cross section properties from data obtained with serial sectioning, see section 4.3. The presented approach is then used for several studies, section 4.4; the effect of laboratory beating on fiber cross section properties, the influence of fiber cross section properties on dewatering and sheet properties and finally a comparison of fiber cross section properties obtained in dry and wet state.

4.1 Introduction

The basic network of paper is built up from individual fibers, which show strong variations in their shapes and dimensions. The fiber dimensions in a range of $1\ \mu\text{m}$ (cross sectional dimensions) to $10\ \text{mm}$ (fiber length) were found to be key parameters for structures and properties in the final sheet of paper [KORTSCHOT, 1997]. Measurement of longitudinal fiber properties - length, kink and curl - is well established e.g. [CARVALHO ET AL., 1997; HIRN AND BAUER, 2006; ROBERTSON ET AL., 1999; TREPANIER, 1998; TURUNEN ET AL., 2005]. These measurements are usually performed in flow cells where images of fibers in highly diluted suspension are analyzed. Also fiber width, fiber flexibility [ECKHART ET AL., 2009] and fiber wall damage [ECKHART ET AL., 2006, 2007] can be analyzed in flowcells.

Analysis of fiber cross sectional morphology - e.g. fiber collapse or fiber perimeter - requires significantly higher resolution and thus more sophisticated measurement techniques. Most of the techniques used are performed in the dry state and are time consuming and challenging. However, the determination of fiber cross section properties is of high importance since these properties have serious effects on paper quality:

Changes in the cross sectional dimensions affect mechanical properties of a fiber like fiber strength [HARTLER AND NYREN, 1970]. Reduced fiber wall thickness in combination with the removal of lignin causes easier fiber collapse making the fibers more flexible [JANG AND SETH, 1998]. For both, chemical and mechanical pulps, fiber collapse is important [JANG ET AL., 1996]. The increase in flexibility and conformability of fibers as well as the fiber collapse are strongly related to fiber cross sectional dimensions. Thin walled fibers collapse easier than thick walled ones. Collapsed fibers, which in general are more elastic, form denser fiber networks [GREGERSEN AND NISKANEN, 1999]. This has an impact on the final paper in terms of higher paper strength, a lower paper thickness and increased paper smoothness e.g. [DINWOODIE, 1965; OLUWAFEMI AND SOTANDE, 2007]. Cracks in the fiber wall, induced in mechanical pulping, are an important quality issue for paper making fibers. These cracks cause changes in paper properties like the light scattering coefficient or surface smoothness [NESBAKK ET AL., 2001]. A cracked fiber occurs more often for earlywood fibers [REME AND HELLE, 2001].

Besides the measurable influence of fiber cross section properties on paper properties a detailed knowledge about these properties is also required in the current efforts of modeling and simulating paper properties. A typical example is a recently published model to explain air permeability of paper as a function of fiber width and fiber thickness [SHALLHORN AND GURNAGUL, 2009].

Cross sectional properties of pulp fibers exhibit large variations due to a multitude of reasons. The most important are:

- Most of the wood species used for pulp and paper making contain earlywood (springwood) and latewood (summerwood) fibers. Earlywood fibers have large fiber diameters and thinner cell walls compared to latewood fibers e.g. [EDER ET AL., 2009; HUANG ET AL., 2008; REME ET AL., 2002].
- Different species of trees have different fibers. Softwoods like spruce or pine are almost fully composed of tubular tracheids with an average length of 2 to 3 mm and a width of 20 to 30 μm . Hardwoods tracheids are significantly smaller than those in softwoods e.g. [HORN, 1974, 1978; PULKKINEN ET AL., 2006; SETH ET AL., 1997]
- The growing conditions of wood. For instance, a high plantation density may lead to less distinction in fiber diameter and fiber wall thickness [ZHU ET AL., 2008]. Narrow crowned trees show lower variations in fiber properties compared to normal crowned trees [ZUBIZARRETA GERENDIAIN ET AL., 2008]. Fertilization of trees leads to a decrease in fiber wall thickness and to an increase in fiber width [LUNDGREN, 2004; MÄKINEN ET AL., 2002]. Also the provenance and growing site were found to be a source of variation of fiber dimensions [MIRANDA AND PEREIRA, 2002].
- Technological parameters during pulping and stock preparation. Fiber wall area as well as fiber wall thickness are strongly related to the pulp yield in chemical pulping [JANG ET AL., 2003]. Beating of fibers increases the elasticity and fibrillation and causes fiber collapse [HUANG ET AL., 2008; KANG ET AL., 2008]. Fiber cross section dimensions are also affected by the number of recycling loops the fibers have already passed [JANG ET AL., 1995].
- Also the papermaking process induces changes in fiber cross sectional dimensions. An increased degree of fiber collapse during wet pressing and calendaring was reported in literature [DICKSON ET AL., 2006; HE ET AL., 2003A; NESBAKK AND HELLE, 2002].

4.2 Analysis of fiber cross section properties in the dry state

4.2.1 Considerations regarding analysis in the dry state

A high resolved analysis of fiber cross section properties is usually accomplished in the dry state on images revealing the shape of fiber cross sections. Several influencing parameters like the fiber orientation and the heterogeneous population of fiber cross sections have to be considered and adequate precautions have to be taken.

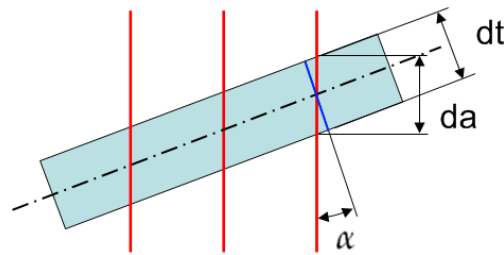


Figure 4.1 Measurement of cross sections from individual images overrates the true fiber dimensions. The red line indicates the image plane. An apparent fiber diameter d_a is measured instead of the true fiber diameter d_t . In order to correct this error the tilting angle α between the fiber main axis and the image plane has to be known.

Unbiased measurement of fiber cross section properties

An extraction of fiber cross section properties from cross section images leads to the problem that fibers are usually oriented non-perpendicular to the image plane and the dimensions directly extracted from cross section images are overrated, see Figure 4.1. If the fiber axis is tilted to the image plane by an angle α an apparent fiber diameter d_a is measured instead of the true fiber diameter d_t . To avoid or correct this error, different approaches have been developed, like aligning of individual fibers or bundles of parallel fibers to the image plane in a 2D case [JANG ET AL., 1992; REME ET AL., 2002] as well as a correction of the measured results obtained from 3D data sets [HE ET AL., 2003B].

A full restoration of true fiber cross sectional geometry from cross section images is impossible because the information between individual image planes is lost during digitization. Still, implementation of a cross sectional shape reconstruction procedure is an important advancement on the way to accurate and unbiased measurements.

Representative analysis of an unbiased fiber population

A statistically meaningful evaluation of fiber cross section properties is an absolute need in order to analyze effects of pulping and stock preparation on fiber properties and to determine the influence of fiber properties on dewatering and final sheet properties. Several techniques use either individual fibers, e.g. [JANG ET AL., 1992], or fiber bundles [CHINGA-CARRASCO ET AL., 2009; REME ET AL., 2002] which have to be prepared before digitalization. The fiber preparation process affects the results obtained, it can be expected that large fibers - which are easier to manipulate - are over-represented in the examined population. For this reason it is more desirable to measure fiber cross section properties in hand sheets, e.g. [HE ET AL., 2003B; KANG ET AL., 2008], which exhibit a more complete sample of the fiber population to be

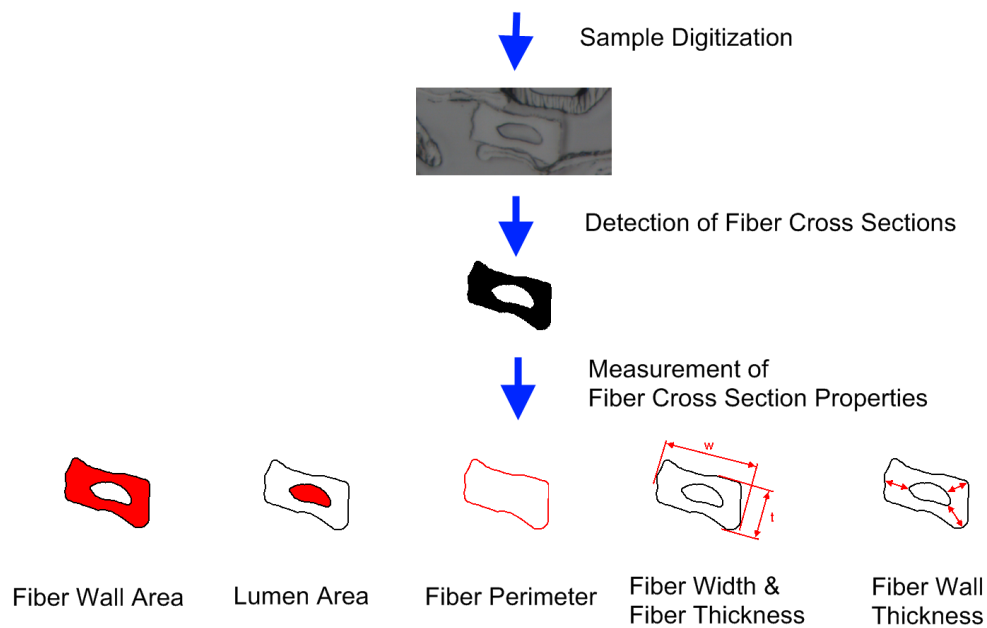


Figure 4.2 Analysis steps for measuring fiber cross section properties in the dry state. First digital images of the sample are acquired. Second the fiber cross section is detected in the image. Third morphological parameters are measured from the detected cross section.

examined and are close to the real population of fibers in a sheet of paper. 1 000 cross sections are recommended in order to obtain a representative analysis of TMP fiber cross sections properties [REME ET AL., 2002].

Outline of a general analysis procedure in the dry state

Analysis of fiber cross section properties can be divided into three subsequent steps, see for instance [CHINGA ET AL., 2007B; DICKSON, 2000B; HE ET AL., 2003B; JANG ET AL., 1992; REME ET AL., 2002], Figure 4.2. First fiber cross sections are digitized by acquiring a single image or a series of images along the fiber main axis. The major differences between the applied analysis routines originate from the imaging process. From these images, the fiber cross sections are extracted by the use of image processing approaches like thresholding or edge-detection functions. The detected cross sections are used in a third step to calculate several morphological properties like fiber wall area, fiber perimeter, fiber width, fiber wall thickness or a degree of collapse. This is commonly straightforward and can be accomplished with standard image analysis routines.

4.2.2 Digitization techniques used for analysis in the dry state

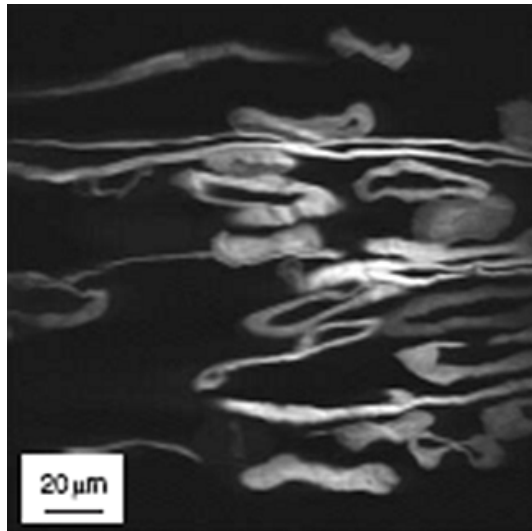
KIBBLEWHITE AND BAILEY [1988] were the first who introduced a semi-automatic image analysis concept for the estimation of fiber cross section dimensions from cross section images. Images were obtained with transmitted or bright field light microscopy from 2 to 3 μm thick cross sections. Today, the main methods are confocal laser scanning microscopy (CLSM) [BATCHELOR ET AL., 2006], see Figure 4.3 (a), scanning electron microscopy (SEM) (b) [CHINGA ET AL., 2007B], x-ray microtomography (c) [ANTOINE ET AL., 2002] and serial sectioning techniques in combination with light optical microscopy (d) [WILTSCHE, 2006].

Confocal laser scanning microscopy (CLSM)

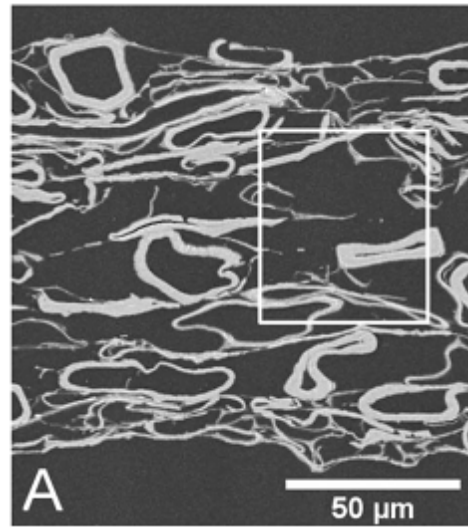
A key feature of confocal laser scanning microscopy (CLSM) is its ability to produce images from different focal planes, thus delivering 3D datasets of the sample. Fiber cross section analysis is performed in two different ways, optical sectioning through the fiber thickness of individual fibers mounted on a microscope slide [JANG ET AL., 1991, 1992] and digitization of prepared paper cross sections [DICKSON, 2000A,B].

Preparation of individual fibers require several sample preparation steps in order to achieve a good image quality [JANG ET AL., 1992; WEISE, 1993]. Because of the low auto-fluorescence of pulp fibers, the samples have to be dyed with a fluorochrome dye. CLSM images usually exhibit low contrast, varying gray scales within the fiber wall and a weakened signal with increasing depth of scanning; all resulting in blurred fiber edges. From the obtained images, the fiber cross sections are extracted with edge detection algorithms. The time needed for digitization of one fiber cross section is in the range of 30 seconds. This technique has been used recently to determine the flexibility of fibers, which is strongly related to fiber cross section properties [YAN AND LI, 2008].

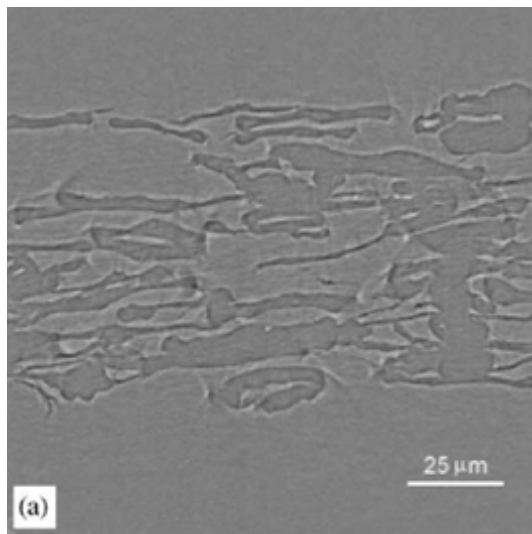
The second important CLSM-technique used to analyze fiber cross section properties is based on the digitization of paper cross sections of embedded paper samples [DICKSON, 2000A,B]. After embedding several surface treatment steps like polishing and etching away of resin have to be carried out. The final surface is then stained with a fluorochrome dye. Digitization of paper cross section and subsequent measurement of fiber cross section properties is performed in two different ways. One mode is the digitization of few cross sections at a small depth range [DICKSON, 2000A,B]. This technique requires the analysis of oriented sheets, which delivers cross sections perpendicular to the fiber main axis. The second mode is the digitization of several cross sections at different depth, from 0 to 10 μm [HE ET AL., 2003A,B], allowing the determination of a fiber orientation trend which can be used to transform overestimated fiber cross sections to their real size. The problem here is a rapid diminishing of the signal intensity with increasing depth of the focal plane. A problem for both techniques is that fibers that touch each other have to be separated manually because in



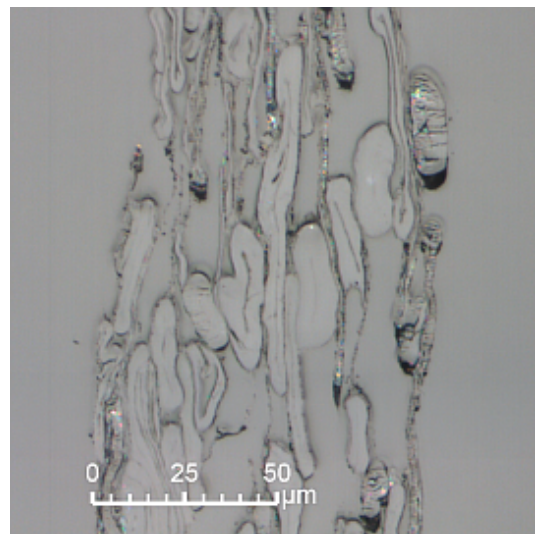
(a) CLSM [BATCHELOR ET AL., 2006].



(b) SEM [CHINGA ET AL., 2007B].



(c) x-ray microtomography
[ANTOINE ET AL., 2002].



(d) sectioning and episcopic imaging
[WILTSCHKE ET AL., 2010].

Figure 4.3 Fiber cross section images obtained with different digitization techniques: (a) CLSM, (b) SEM, (c) x-ray microtomography and (d) automated serial sectioning with light optical microscopy.

many cases the boundaries between the fibers are not visible in the gray scale images, see Figure 4.3(a).

Scanning electron microscopy (SEM)

Another well known digitization method for estimating fiber cross section properties is scanning electron microscopy (SEM) in backscatter mode. The most important benefit of this technique is the digitization with very high resolution and good image quality, Figure 4.3(b).

The common way is the digitization of individual cross sections [GREGERSEN AND NISKANEN, 1999; NESBAKK AND HELLE, 2002; NESBAKK ET AL., 2001; REME ET AL., 2002]. It is important that the individual fibers are oriented perpendicular to the image plane. Therefore, individual fibers are aligned in a fiber bundle. This bundle is embedded in resin and after curing, the block is cut perpendicular to the fiber direction. The created surface is prepared with grinding and polishing steps for digitization [REME ET AL., 2002]. Also single cross sections of papers are used to estimate fiber cross section properties [CHINGA ET AL., 2007B]. Fiber cross sections are obtained by binarization with an automatically selected threshold value [CHINGA ET AL., 2007B; REME ET AL., 2002]. Like for CLSM images, image analysis is difficult in the case of touching fibers as they show no visible borderline. In this case, the images are edited manually [REME ET AL., 2002]. Recently CHINGA-CARRASCO ET AL. [2009] proposed a method to tackle the main image analysis problems.

There are also some attempts to analyze fiber cross section properties from 3D data sets obtained with SEM. These data sets are created with serial grinding [CHINGA ET AL., 2004] or serial sectioning [ARONSSON ET AL., 2002]. The large effort needed for digitization limits these techniques to very small sample sizes.

X-ray microtomography

Compared to the other techniques used for estimation of fiber cross section properties, X-ray microtomography is the only non destructive technique. Tomography can be performed directly on the sample material without the need to enhance contrast by the application of chemical agents or to embed the sample. The data set obtained is usually a set of gray scale images, see Figure 4.3(c). Two different methods are available. Synchrotron radiation based digitization gives best image quality [ANTOINE ET AL., 2001, 2002; ROLLAND DU ROSCOAT ET AL., 2005]. Easier to handle, are commercial fan-beam microtomographs, which, on the other hand, do not provide sufficient resolution. Thus only synchrotron micro CTs are used for fiber cross section analysis [GOEL ET AL., 2006; HOLMSTAD ET AL., 2006; LUX ET AL., 2006]. Recent approaches show the possibility to analyze the structures of single fibers [HAGEN ET AL., 2004; WALTHER ET AL., 2006]. Again, image analysis is difficult because the gray scale images usually

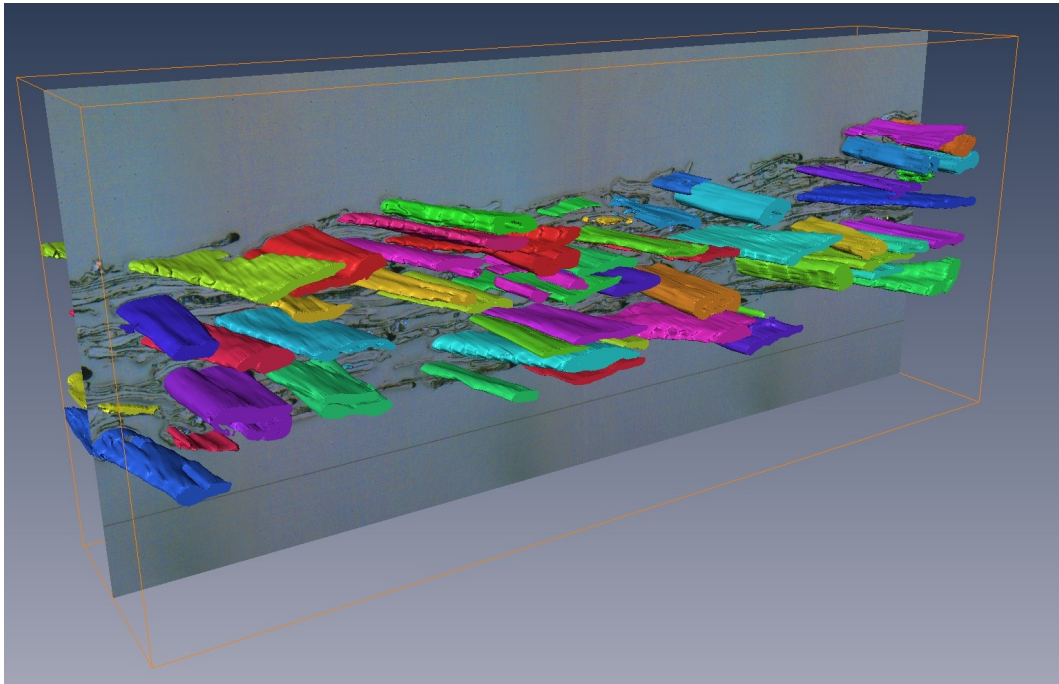


Figure 4.4 First 3D reconstructions of detected fibers giving an impression about the fiber network [WILTSCHKE, 2006].

do not show boundaries of touching fibers. High resolution digitization is limited to small sample volumes.

Serial sectioning

The preparation of slices and imaging are time consuming processes and sources of failures [KIBBLEWHITE AND BAILEY, 1988]. Compared to CLSM, serial sectioning is difficult because the individual images have to be aligned for a true three dimensional representation of a sample, but it has the advantage of much greater imaging depth providing a larger sample size [DONALDSON ET AL., 2007]. On block imaging does not require difficult handling of individual slices but requires more sophisticated image analysis routines.

WILTSCHKE [2006] gave an overview about applications of automated serial sectioning to analyze fiber cross section properties. Novel image analysis routines were applied to extract individual fiber cross sections from cross section images [DONOSER AND BISCHOF, 2006], see section 4.3.1 for more details. The segmentation results were used in two ways. The first was an analysis of the fiber network, like the calculation of a fiber mass distribution or a partial reconstruction of the network, see Figure 4.4. The second way was the calculation of fiber cross section properties, as e.g. the fiber wall thickness of collapsed fibers and of fibers with visible lumen directly from the obtained binary images.

Conclusions on sample digitization

While SEM imaging clearly provides the best image quality, the main disadvantage is its limited ability to acquire 3D datasets due to limited image size and time consuming sample preparation. X-ray microtomography yields reasonable image quality and specimen preparation is simple, however synchrotron radiation allowing the high resolution required is not available in day to day research to quantify fiber cross section properties. The best suited methods are confocal laser scanning microscopy and automated serial sectioning. The quality of images obtained with CLSM suffer at deeper regions in the paper [HE ET AL., 2003B] which makes it difficult to track fibers in a network over a longer distance. Automated serial sectioning [WILTSCHKE, 2006] is able to acquire large fiber data sets because it is fast, efficient and image quality is not affected by a large sample size. 3D data sets obtained from paper samples can be used directly for analysis thus avoiding manipulation of individual fibers for specimen preparation.

4.3 Quantification of fiber cross section properties in serial sectioning

4.3.1 Analysis steps to obtain fiber cross section properties

Because of the many influencing parameters and different ways to process fiber cross section morphology data, a discussion considering the subsequent process steps is necessary:

1. Digitization of fiber cross sections.
2. Detection of fiber cross sections.
3. Transformation to true sized cross sections.
4. Evaluation of basic cross section properties.
5. Classification of fiber cross sections.
6. Calculation of fiber wall thickness.
7. Measures and ratios for a closer analysis of fiber cross section properties.

Digitization of fiber cross sections

The samples used for the analysis of fiber cross section properties are digitized at the highest resolution available in the image plane to preserve as many structural features as possible ($50\times$ magnification; pixel size: $0.16\ \mu\text{m}$, resolution: $0.60\ \mu\text{m}$). Several subsequent images of paper cross sections are prepared to enable a true estimation

of fiber cross section properties. The distance between the cross section is chosen between 1 and 3 μm ; the thinner the cross section the easier is the tracking of fibers through an image sequence as will be discussed later in this section.

The fibers to be analyzed are prepared in hand sheets because these are almost randomly oriented. In theory, one can expect that each class of fibers appears in every direction. This allows the analysis of all fibers occurring in a fiber network without the restriction to some fiber classes.

Detection of fiber cross sections

A typical color image provided by the serial sectioning technique is shown in Figure 4.3(d). The difficulties in detecting fiber cross sections are obvious, a wide variability of shapes can be observed and only contour information can be considered for segmentation since fiber wall and background have a similar color. Trials with dyed resins to get a better contrast between fibers and background were not successful [WILTSCHKE, 2006].

The basic method used to track fiber cross sections is based on Maximally Stable Extremal Regions (MSERs, regions having a homogeneous gray scale and a high contrast to the background) [DONOSER AND BISCHOF, 2006]. Fiber cross sections are detected as MSERs and then robustly tracked through the images sequences, in order to provide a 3D representation of individual fibers. Several attempts were done in order to improve tracking robustness [DONOSER ET AL., 2008].

Nevertheless, tracking of individual fibers has to be initialized in the first frame with a user drawn mask containing the fibers to be tracked. This requires cumbersome and time-consuming user-interaction. Besides the mask, the currently used algorithms can not detect a fiber lumen which has to be drawn manually in the detected cross sections. Tracking of fibers along a large number of paper cross sections as well as large distances between the individual cross sections reduces the quality of the segmentations, which then also have to be edited manually. Furthermore, MSER detection only finds well shaped cross sections limiting the diversity of detected fibers.

A skilled user is able to extract about 2500 fiber cross sections within a day. The segmentation results are binary cross sections, where the detected fiber cross sections are highlighted. The cross sections of an individual fiber are denoted with a unique ID, a so called label which allows the analysis of individual fibers in the following processing steps.

Transformation to true sized cross sections

The segmentations of individual fiber cross sections are usually not oriented perpendicular to the fiber main axis giving overestimated cross section dimensions, see Figure 4.1. To extract true cross section dimensions, the individual segmentations have to be transformed to true sized ones. This is done by calculating a misalignment

between the visible cross section in the image plane and the true one perpendicular to the fiber center line.

A fiber center line is estimated with the fiber's center of mass coordinates, calculated for each cross section in each image of the sequence with the MATLAB function (*regionprops*) [GONZALEZ ET AL., 2004]. These center of mass coordinates are fitted with a polynomial of the third degree. The third order fit was found to be well suited to cover changes in orientation along a 10 to 20 frame cross section sequence. The polynomial is used to estimate a slope of the fiber center line at the individual image planes. The misalignment between the slope of a fiber center line and the individual image planes is the basis for transformation.

Currently a simplified approach is used, see Figure 4.5. The third order polynomial representing the fiber center line is separated into two polynomials of the second order. The slopes of the fiber center line projected to the CD/MD - plane and the ZD/MD - plane are calculated for each cross section; starting at the second frame and ending up at the penultimate frame. These slopes are used to estimate the misalignment angles of the true fiber center line in the CD/MD - plane (α_{CDMD}) and the ZD/MD - plane (α_{ZDMD}). Two scaling operations are applied to the segmentations of individual fiber cross sections. Single columns (scaling in CD direction) and lines (scaling in ZD direction) are removed from the matrix representing the original image.

Estimation of basic properties

A ready to use MATLAB function (*regionprops*) [GONZALEZ ET AL., 2004] is applied for the calculation of the main cross sectional properties see Table 4.1. This straight forward approach requires only resized label images and returns a matrix of results in pixels which are transferred to a reasonable length scale by multiplying with the pixel size.

Classification of fiber cross sections

A typical cross section of a commercially available kraft paper is shown in Figure 4.6. Besides the strong variations in the size of fiber cross sections also large differences between the cross sectional shapes can be observed. The shapes can be divided into three basic groups: fibers with visible lumen, collapsed fibers and fibers with a broken fiber wall. This classification is important for the two following reasons:

- Influence on paper properties:
The individual groups are assumed to enforce distinct paper properties. For example, fibers with a visible lumen are considered to give a porous sheet with a high bulk as is desirable for board or filter paper. Collapsed fibers on the other hand are more flexible thus giving larger contact areas between the fibers

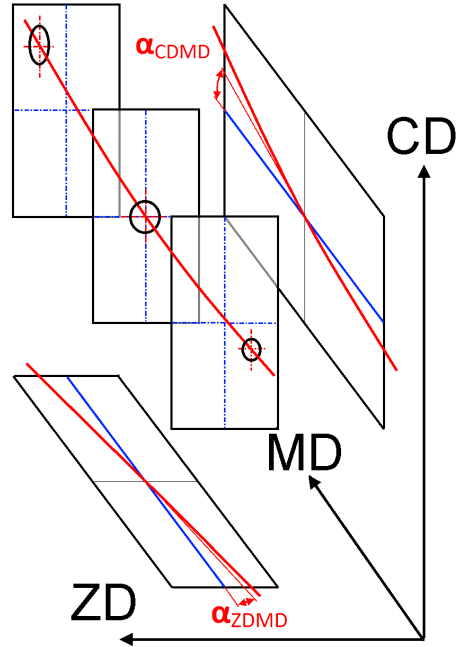


Figure 4.5 Definition of the straining measures (α_{CDMD} and α_{ZDMD}) used to re-scale fiber cross sections to true dimensions.





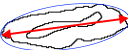

	Property	Definition
	Wall area	The number of pixels defining a region.
	Lumen area	The number of pixels defining a region with all holes filled minus the fiber wall area.
	Perimeter	The number of connected pixel at the outermost surface of a region.
	Width	The length of the major axis of an ellipse with the same second moments as the region.
	Thickness	The length of the minor axis of an ellipse with the same second moments as the region.

Table 4.1 Definition of basic fiber cross section properties and their estimation.

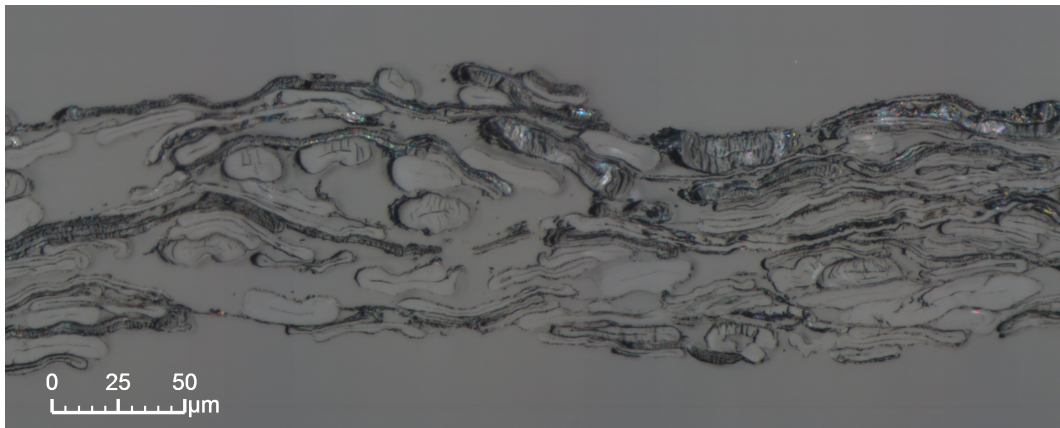
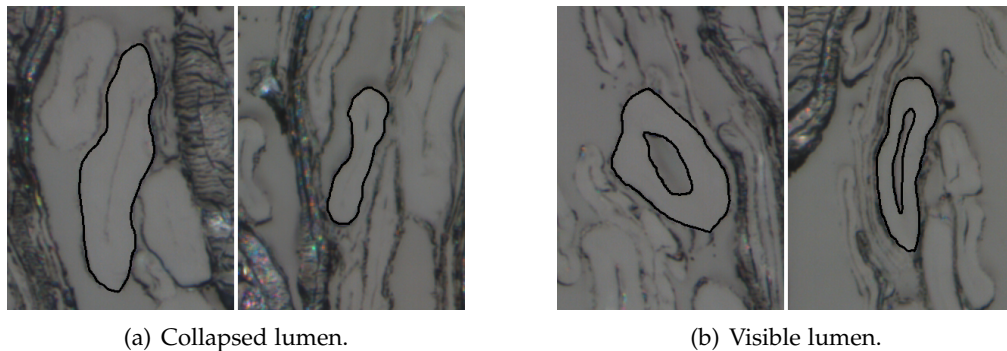


Figure 4.6 Paper cross section of a kraft paper sample showing the wide range of different fiber cross section shapes as well as the different classes of cross sections.



(a) Collapsed lumen.

(b) Visible lumen.

Figure 4.7 Decision either collapsed or visible lumen.

and finally a higher paper strength [DINWOODIE, 1965; OLUWAFEMI AND SOTANDE, 2007]. Fibers with a broken fiber wall influences light scattering coefficient or surface smoothness [NESBAKK ET AL., 2001]. Therefore, the fractions of the individual classes are measures of interest.

- Quantification of cross section properties:
The proposed way to quantify fiber wall thicknesses requires an adaption of analysis parameters for the different fiber classes. A fast and reliable classification of cross sections is required.

Only the previously defined cross section properties - fiber wall area, lumen area, fiber perimeter, width and thickness; see Table 4.1 - can be employed to separate the fiber cross sections into individual classes. Figures 4.7-4.10 show typical examples that have to be classified. The manually drawn borders indicate the segmentation results and the properties available for classification.

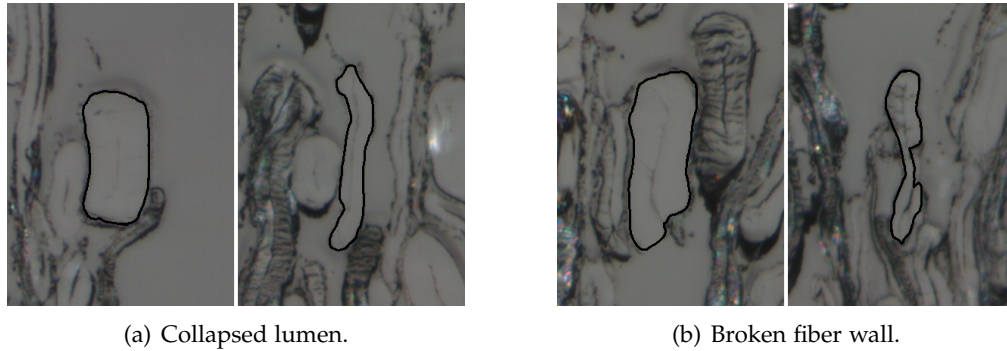


Figure 4.8 Decision either collapsed lumen or broken fiber wall Part I.

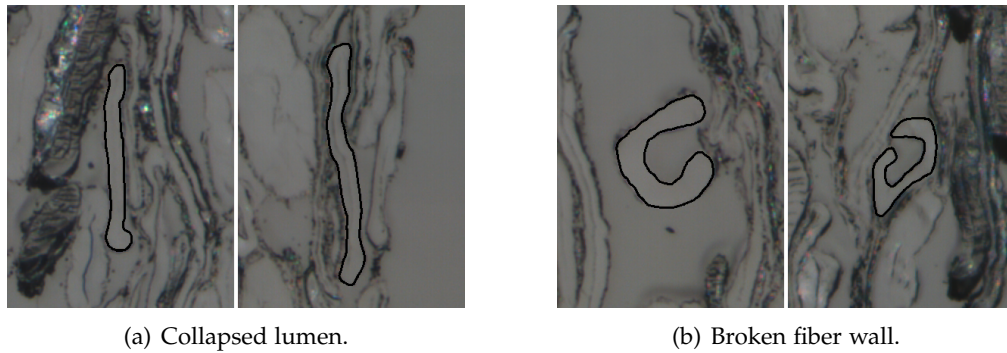


Figure 4.9 Decision either collapsed lumen or broken fiber wall Part II.

The first classification is the decision either the cross section is collapsed or not, see Figure 4.7(a) and (b). This is done with a simple decision criterion: is there a measurable lumen area or not. Manual edition of the cross sections during segmentation ensures that only fibers having a true lumen are considered. Thus the fibers of a first group representing fibers with a visible lumen are separated from the bulk of different fiber classes.

The second classification considers fibers which are collapsed but one part has an intact fiber wall and the other part a broken one, see Figure 4.8 (a) and (b). These two classes can not be distinguished and both will be treated as fibers having a collapsed lumen in later processes.

The third classification differs between fibers having a collapsed lumen with an elongated cross sectional shape and fibers with an intact lumen but a broken fiber wall, see Figure 4.9 (a) and (b). The cross sectional area does not give a measure to differentiate between both cases, also the fiber perimeter can not be used since the lumen surface contributes to the fiber perimeter in the case of a broken fiber wall, indicating a slender cross sectional shape. The major differences between the classes presented in Figure 4.9 appear from the fiber width and the fiber thickness.

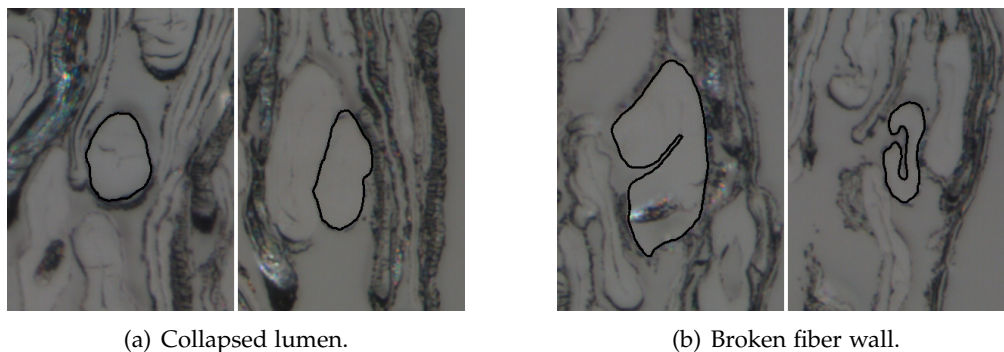


Figure 4.10 Decision either collapsed lumen or broken fiber wall Part III.

The ratio of fiber width to fiber thickness, was found to be a reasonable measure to differ between these cases. Cross sections having a ratio higher than 3 are treated as collapsed fibers. This threshold was chosen intuitively, but seems to be a suitable measure when looking at Figure 4.6, presenting a paper cross section of a commercial kraft paper sample. The collapsed fibers having an elongated cross sectional shape can be separated from the bulk of different fiber classes.

The remaining fibers have an almost roundish shape (ratio of fiber width to fiber thickness below 3) and are either collapsed or have a broken fiber wall, see Figure 4.10 (a) and (b) respectively. The fiber perimeter is the major difference between the two classes and is expected to be lower for the fibers with collapsed lumen. However, this measure cannot be used directly because one can expect a larger perimeter for a larger fiber cross section and therefore it has to be normalized. The fiber width is used to represent the fiber cross section size. This measure was chosen instead of the fiber wall area because of the higher number of true classifications obtained in various trials. The classification itself is based on a ratio between fiber perimeter and fiber width. If this ratio is higher than a defined threshold level, then this cross section is classified as a fiber with a broken fiber wall. The threshold is defined by an expected ratio of fiber perimeter and fiber width calculated from all cross sections available in the data set, multiplied by a factor (1.2) to avoid wrong classifications of fiber cross sections.

The overall process to classify fiber cross sections is rather simple, but sometimes it appears to be crude because of the frequent use of defined thresholds, especially to separate fibers with a broken fiber wall. Nevertheless, a visual inspection of hundreds of fiber cross section reveals that the results obtained are mostly correctly classified fiber cross sections.

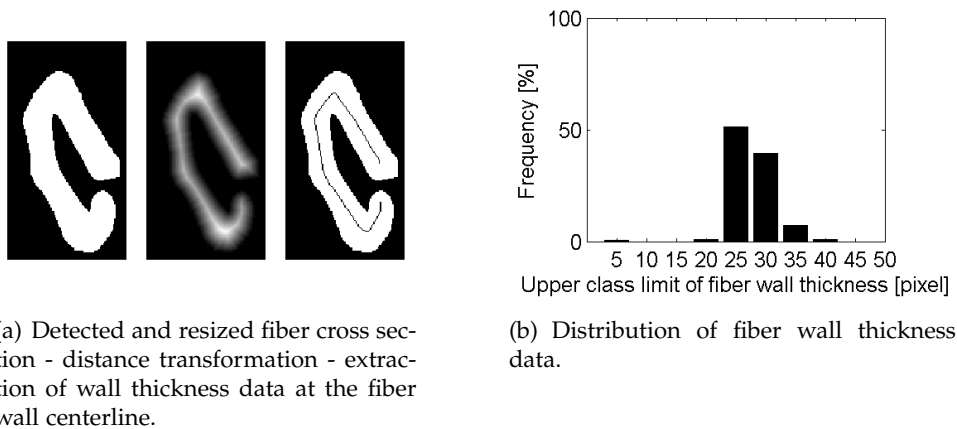


Figure 4.11 Estimation of fiber wall thickness for fibers with a broken fiber wall (a) and distribution of fiber wall thickness data of a single fiber cross section (b).

Calculation of fiber wall thickness

The analysis of fiber wall thickness for fibers with visible lumen and fibers with collapsed lumen has already been introduced by WILTSCHKE [2006]. The calculation of fiber wall thicknesses for the third class of fiber cross sections is similar to the procedure as it is used for the collapsed fibers, see Figure 4.11 (a). Euclidean distance transformation is performed on detected and resized cross section images, giving the shortest distance of a pixel in the fiber wall to the background. The centerline of the fiber wall is calculated with a skeletonisation algorithm. The distance values on the centerline pixels represent the half of the local fiber wall thickness. A resulting wall thickness distribution for an individual fiber cross section is shown in Figure 4.11 (b). A strong variation of wall thickness data is observable. Standard analysis of fiber cross section properties is based on a mean wall thickness for each cross section analyzed. At the moment the distribution of fiber wall thickness data is not used in more detail, but it could be applied in the future to e.g. point out changes of fiber cross section properties along the fiber main axis.

Indices and ratios to characterize fiber cross section properties

Properties of fiber cross sections are expected to have wide variations because of a multitude of reasons, see section 4.1 for more details. To compare fiber cross sections of different sizes, the calculation of indices or ratios is recommended, a summary of several measures is given by WEISE [1993]. The collapse behavior of a fiber cross section is a common example for the use of indices and ratios because only the lumen area does not give an information regarding the degree of collapse. For instance a collapse index defined by the ratio of visible lumen area and theoretically possible lumen area was introduced [JANG ET AL., 1995]. Since a theoretically possible lumen

area is hard to evaluate, a degree of collapse is indicated by two other ratios in this thesis:

- Fill factor:

The fill factor represents the fraction of fiber wall area respectively the lumen area in a fiber cross section. If the value is close to 1, almost no lumen area can be observed in the cross section.

$$\text{fill factor} = \frac{\text{fiber wall area}}{\text{total cross section area}} \quad (4.1)$$

- Collapse factor:

The collapse factor points out the relation between the fraction of fibers with collapsed lumen and fibers with visible lumen. The higher the value, the more fibers are collapsed. This factor is used because it is more sensitive at a higher fraction of collapsed fibers.

$$\text{collapse factor} = \frac{\text{fraction collapsed lumen}}{\text{fraction visible lumen}} \quad (4.2)$$

The flatness of a fiber cross section is another measure which relates to the fiber collapse. An increase of fiber width as well as a decrease of fiber thickness both indicate a higher degree of collapse which again is thought to influence flexibility and conformability of fibers [GREGERSEN AND NISKANEN, 1999]. To avoid influences of different fibers sizes, a ratio of fiber width to fiber thickness is calculated:

- Shape factor:

$$\text{shape factor} = \frac{\text{fiber width}}{\text{fiber thickness}} \quad (4.3)$$

A novel idea to use fiber cross section properties

A completely different and novel way to use fiber cross section properties is to calculate fiber coarseness, for individual fiber sequences in the dry state. The conventional techniques used to measure the fiber coarseness give only a length weighted coarseness, see for instance [HIRN AND BAUER, 2006]. This kind of weighting leads to an underestimation of the fraction of fibers with a thick fiber wall and vice versa for thin walled fibers [JANG AND SETH, 2004]. An approach based on a the definition of fiber volumes enables the calculation of a weight weighted and an average fiber coarseness.

The calculation of the coarseness starts with the calculation of a mean cross sectional fiber wall area for individual fibers (j) from the fiber wall areas obtained

along an analyzed fiber section with (k) frames, see Equation 4.4. This area \bar{A}_j combined with the length l_j of the detected fiber and an assumed fiber wall density of $\rho = 1.44 \text{ g/cm}^3$ gives the mass of the analyzed fiber section, see Equation 4.5. The ratio of mass and fiber length respectively multiplying fiber wall area and density give finally the coarseness for an individual fiber, see Equation 4.6

$$\bar{A}_j = \frac{\sum_{i=1}^k A_i}{k} \quad (4.4)$$

$$m_j = \bar{A}_j l_j \rho \quad (4.5)$$

$$C_j = \frac{m_j}{l_j} = \bar{A}_j \rho \quad (4.6)$$

An arithmetic mean of fiber coarseness, Equation 4.7, as well as a mass weighted mean, Equation 4.8, can be calculated.

$$\bar{C} = \frac{\sum_{j=1}^n C_j}{n} \quad (4.7)$$

$$\bar{C}_w = \frac{\sum_{j=1}^n C_j m_j}{\sum_{j=1}^n m_j} \quad (4.8)$$

4.3.2 Representative number of fiber cross sections

A quantitative analysis of fiber cross section properties in the dry state is a rather novel field of research in the pulp and paper research community. Actually only one publication deals with the number of individual fiber cross sections necessary to obtain statistically meaningful results. REME ET AL. [2002] recommended a number of 1 000 fiber cross sections obtained from different fibers for a representative characterization of TMP fibers with SEM.

This section discusses an approach to determine the required sample size, defined by the number of individual fibers and the number of consecutive fiber cross sections, for a representative analysis of fiber cross section properties with the automated serial sectioning technique. The basic idea to define a required sample size is to look for the smallest sample which represents a large one (representative) with a given accuracy. Therefore, distributions of fiber cross section properties for a large data set containing thousands of measures are compared with smaller ones which are taken from the large one. Each data set is defined by the number of individual fibers and the number

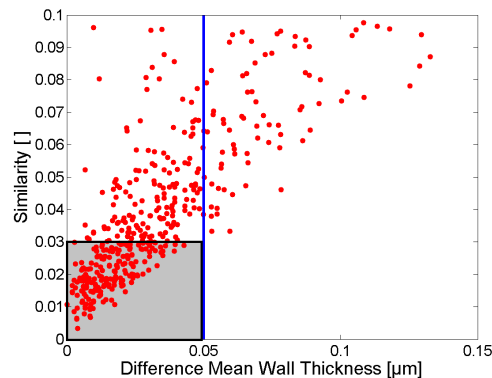


Figure 4.12 Definition of a threshold (similarity measure) for a reasonable difference between the fiber wall thickness of a subsample and the fiber wall thickness of a large population including more than 10 000 fiber cross sections.

of consecutive fiber cross sections. A similarity measure, the Kolmogorow-Smirnow distance, see section 3.3 for more details, is used to compare the distributions.

A commercially available unbeaten eucalypt kraft pulp was used to estimate a representative sample size. A hand sheet formed of this pulp was digitized with a resolution of $0.6 \mu\text{m}$ in the image plane and a distance of $3 \mu\text{m}$ between the cross sections. The data set generated contains 10 800 fiber cross section, resulting from 600 fibers and 18 consecutive cross sections per fiber.

Samples of different sizes, from one to the maximum number of individual fibers as well as from one to the maximum number of cross sections per fiber, were compared with the original data set. Figure 4.13 shows a map of similarity measures, obtained at all possible sample size combinations for the fiber wall thickness. The brighter regions at low numbers of investigated fibers indicate a low similarity between the compared distributions. The dark regions indicate more similar distributions. This plot leads to the expected conclusions that the number of fibers is the decisive parameter for a representative analysis of fiber cross sections using 3D analysis techniques. Property distributions become more similar when more individual fibers are analyzed.

To quantify a reasonable sample size, a threshold indicating acceptable differences between the measured results obtained for the small sample and the entire data set has to be defined. The free chosen aim is a deviation of about $\pm 2.5\%$ from the mean value of the entire data set, which in the case of fiber wall thickness (average $2 \mu\text{m}$) is roughly $\pm 0.05 \mu\text{m}$. Figure 4.12 shows a correlation of similarity measures and the calculated differences of mean fiber wall thickness values between randomly taken small data sets and the entire data set. The line at a wall thickness of $0.05 \mu\text{m}$ indicates the acceptable deviation from the mean value. The plot shows that a similarity measure below 0.03 will always result in the mean fiber wall thickness within the targeted

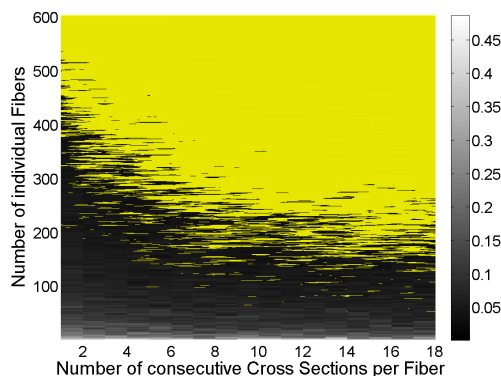


Figure 4.13 Definition of a reasonable number of fiber cross sections. Map of similarity measures for different sample dimensions and the threshold level (light gray area) for the fiber wall thickness.

range of $\pm 2.5\%$ from the mean value; see shaded area in Figure 4.12. Similarity measures below this threshold are shown as a yellow highlighted area in the map of similarity measures for the fiber wall thickness in Figure 4.13. The number of individual fibers is the most important parameter for a representative analysis of the fiber wall thickness with the automated serial sectioning technique, although there is a need for a minimum number of subsequent cross sections if a smaller number of fibers is examined. Having 400 individual fibers, 3 to 4 cross sections per fiber should be considered. A lower number of individual fibers require the analysis of more cross sections per fiber. Nevertheless, the number of individual fibers should not be lower than 200.

These findings are also true for the other properties investigated, like e.g. the fiber wall area, the fiber width or the fiber thickness. For a representative analysis of fiber cross section properties of a hardwood pulp with the serial sectioning method, the analysis of more than 2000 fiber cross sections, resulting from more than 200 individual fibers and 10 consecutive cross sections per fiber, is recommended.

4.3.3 Weaknesses and limitations of the approach

To conclude the section explaining the approach to quantify fiber cross section properties from data obtained with serial sectioning, a discussion of the current weaknesses and limitations also has to be carried out. This is because several process steps are vaguely defined and others use roughly set thresholds. A fundamental research project will be launched in November 2010 (FiberMorph - Cross Sectional Pulp Fiber Morphology) at the Institute for Paper, Pulp and Fiber Technology to tackle these weaknesses and limitations.

Fibers are prepared in hand sheets in order to obtain an unbiased population of fibers. This works out well for chemical pulps, but it cannot be used for most of

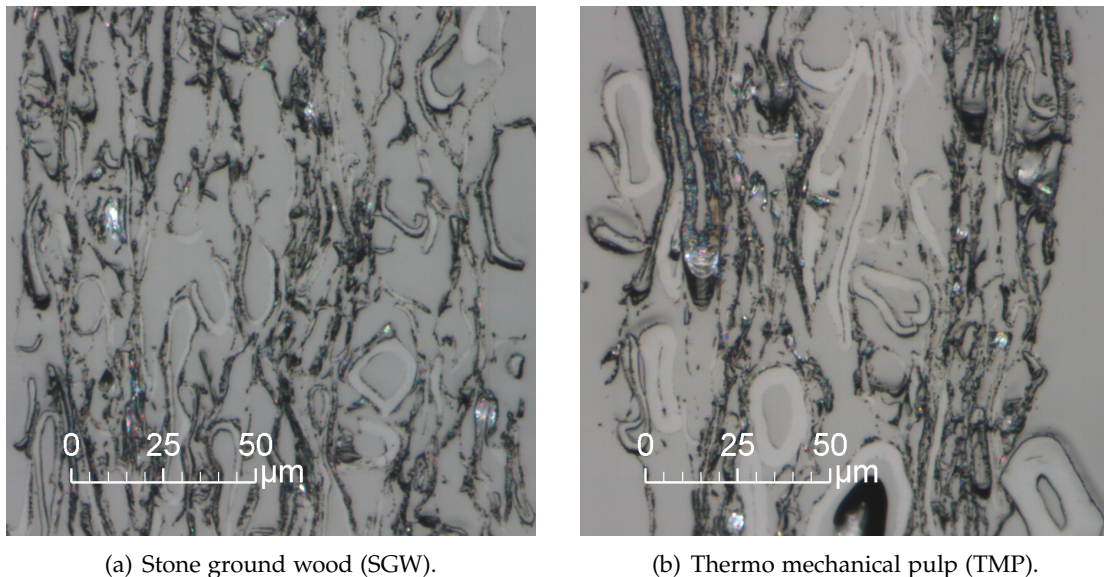


Figure 4.14 Cross sections of hand sheets made from mechanical pulps, stone ground wood (a), pressure ground wood and thermo mechanical pulp (b) reveal only a small number of fiber cross sections. Other preparation techniques will be required.

mechanical pulps, see Figure 4.14 (a) for stone ground wood (SGW) and (b) for thermo mechanical pulp (TMP). Similar images have been obtained for pressure ground wood (PGW). Only a low fraction of fibers can be used for analysis, most of the material visible in this cross section can be defined as fines. To analyze mostly intact fibers, samples have to be prepared more elaborately, see for instance [REME ET AL., 2002].

The extraction of fiber cross sections from cross section images require laborious user interaction. First of all, a user has to identify fibers in a starting image of the image sequence to be analyzed. These fibers are tracked through the image sequence with the presented image analysis routine, but then they have to be edited. Besides

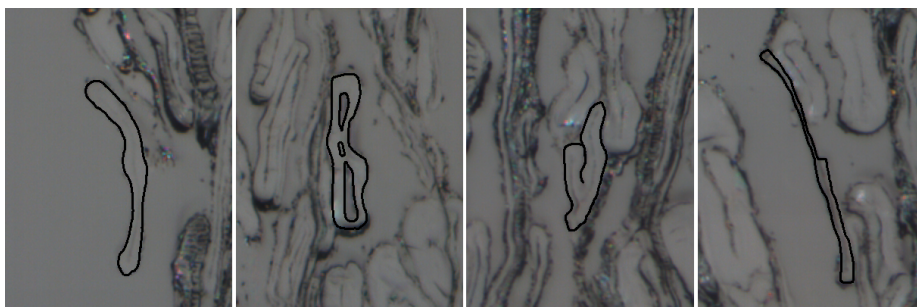


Figure 4.15 Some fiber cross sections cause problems in the classification or do not fit in the classes defined: collapsed fibers having a shape similar to broken fibers with a visible lumen, partly collapsed fibers and folded fibers. There are also fibers which are not detectable with the currently used fiber segmentation routine.

the time needed for the user interaction, also the unbiased population of fibers suffers. Figure 4.15 shows examples of different fibers which are usually not considered for analysis.

The resizing operation of fiber cross sections by removing individual lines and columns from the matrix of the original image is a crude way to transform the cross sections. It would be better to use a more accurate method like affine shape transformation. One possible idea is to rotate the fiber cross section image in the main direction and then compress the cross section only once.

Presently, the way to estimate fiber width and fiber thickness (axis of an ellipse with the same second moments) does not give true dimensions. Other approaches must be found to obtain a true measure for the longest distance in a fiber cross section representing the fiber width and perpendicular to this distance the fiber thickness.

In the classification of fiber cross sections, manually set thresholds are used to differ between fibers with a broken fiber wall and fibers with a collapsed lumen. These are not very accurate and will result in false classifications if slender cross sections are arranged in C-like shapes as it is shown exemplarily in the left image of Figure 4.15. There are also fibers, which do not fit in the current classes, like partly collapsed fibers and folded fibers. These fibers are usually not considered for analysis because e.g. fiber wall thickness cannot be determined correctly for both classes. New classification criteria as well as new approaches in analysis will be necessary to analyze also these cross sectional shapes.

Despite the different limitations, the presented approach outlines the capability to carry out an unbiased measurement of fiber cross section properties of a representative and unbiased population of fibers that is unique in this field of research.

4.4 First results obtained with the presented approach

The capability to analyze fiber cross section properties with automated serial sectioning is shown in this section. Changes induced by beating a fiber in a PFI mill as well as the influence of fiber cross section properties on dewatering and sheet properties were analyzed. Results obtained with automated serial sectioning and flow cells were compared and complete these trials.

4.4.1 Effect of laboratory beating on cross section properties

Beating alters the fiber cross sectional shape and dimensions, see for instance [BRINDLEY AND KIBBLEWHITE, 1996; KANG ET AL., 2008; KIBBLEWHITE AND BAWDEN, 1991]. Detailed knowledge about changes in the cross sectional shapes like the collapse ratio or dimensions like the fiber width are important parameters for paper properties like strength, see for instance [DINWOODIE, 1965].

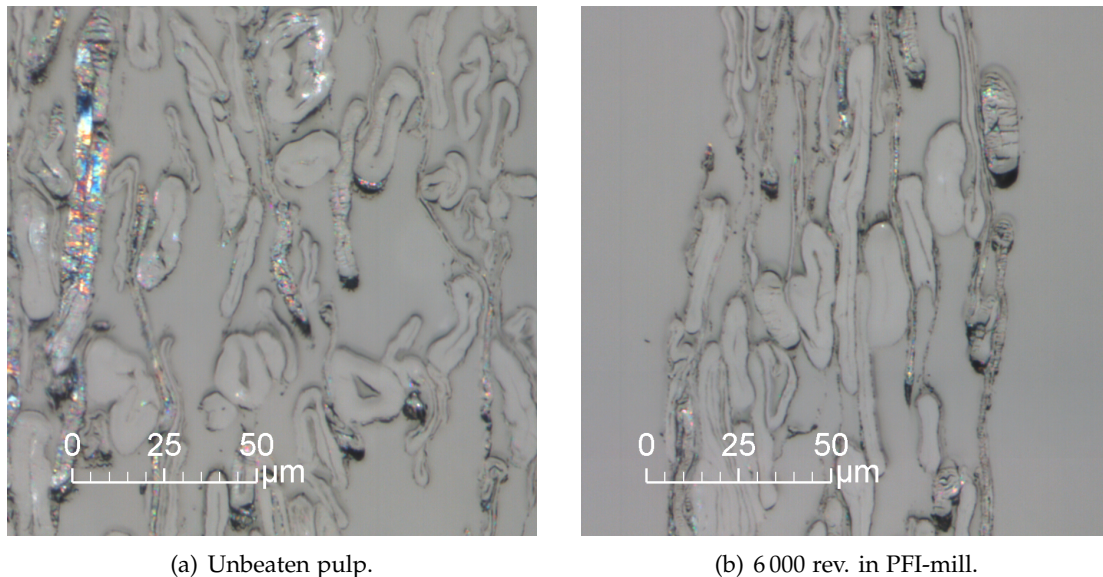


Figure 4.16 Effect of beating on fiber cross sections prepared in hand sheets.

A flash dried bleached softwood (spruce) kraft pulp was used to analyze the effect of laboratory beating in a PFI-mill on fiber cross section properties. Three beating levels were analyzed; unbeaten, 2000 and 6000 revolutions in the PFI-mill. Small cutouts of typical cross sections of standard hand sheets (Rapid Koethen method) made from the pulps are presented in Figure 4.16 (a) for the unbeaten pulp and (b) for the pulp after 6000 revolutions in the PFI-mill.

Several effects of laboratory beating on fiber and paper structures can already be seen in these images. The unbeaten pulp contains a fraction of fibers with visible lumen, but the fibers are strongly deformed in many cases. The paper structure appears very porous. After beating, the fibers are almost fully collapsed. An increased flexibility of fibers is obvious because of a denser network with a lower void volume between individual fibers is observable. The higher network strength achieved in beating can be imagined because of the apparently larger contact areas between the fibers.

Several subsequent cross sections with a length of more than 2 mm were digitized. The distance between the cross sections was set to 1 μm . An average of 2000 fiber cross sections were analyzed in each case. The most important results obtained in fiber cross section analysis are summarized in Table 4.2. Fiber wall area and fiber wall thickness are significantly reduced in the beating process. The actual reasons for this effect have not been found so far, however there might be some peeling of outer layers at the fiber wall or a compression of the fiber wall. The fiber width, the major length of a fiber cross section, is slightly increased, whereas the fiber thickness is decreased significantly. This is an indication for strong fiber collapse during beating.

Cross section property	Unbeaten	2 000 rev.	6 000 rev.
# Fiber cross sections	~1 900	~2 100	~2 100
Fiber wall area [μm^2]	170.2 \pm 3.2	150.1 \pm 3.0	142.8 \pm 2.7
Fiber wall thickness [μm]	3.25 \pm 0.06	2.75 \pm 0.05	2.66 \pm 0.05
Fiber width [μm]	28.58 \pm 0.49	31.26 \pm 0.54	30.84 \pm 0.52
Fiber thickness [μm]	9.01 \pm 0.14	7.28 \pm 0.12	6.97 \pm 0.93
Fiber perimeter [μm]	69.17 \pm 0.99	69.42 \pm 0.98	67.95 \pm 0.93
Shape factor []	3.70 \pm 0.11	5.11 \pm 0.15	5.35 \pm 0.16
Fill factor []	0.990	0.997	0.997
Visible lumen [%]	10.90	4.14	1.83
Collapsed lumen [%]	87.3	93.9	96.2
Broke fiber wall [%]	1.78	1.96	1.97
Collapse factor []	8.01	22.69	52.57
Coarseness (w.w.) [mg/m]	0.276 \pm 0.005	0.253 \pm 0.005	0.235 \pm 0.004

Table 4.2 Effect of beating with a PFI-mill on fiber cross section properties.

The fiber perimeter is not affected by different beating levels. The fill factor confirms the observations made in Figure 4.17. This value is always close to one which indicates strongly collapsed cross sections at all beating levels. The fraction of fibers with a visible lumen is decreased during beating from about 11% in the unbeaten pulp to approximately 2% after 6 000 revolutions in the PFI-mill. To the same extent, the fraction of collapsed fibers increases. The fraction of fibers with a broken fiber wall is hardly affected during beating in a PFI-mill.

A more detailed analysis of fiber wall thickness data is presented in Figure 4.17, showing the wall thickness distribution for (a) the unbeaten pulp and (b) the pulp after 6 000 revolutions in the PFI-mill. The bars are split into fractions of fibers with visible lumen (blue part), fibers with collapsed lumen (green part) and fibers with a broken fiber wall (red part). As has been already discussed, the fraction of fibers with visible lumen is strongly decreased after beating in the PFI-mill. The fiber wall thickness seems to be an influencing parameter on the resistance of fiber collapse. As can be seen from the mean values, collapsed fibers tend to have a thinner fiber wall than the fibers with a visible lumen. The mean values also indicate that the decrease of the fiber wall thickness during beating is more pronounced for fibers with visible lumen and fibers with a broken wall than for already collapsed fibers.

Figure 4.18 shows the correlation between fiber thickness and fiber width, (a) for the unbeaten pulp sample and (b) for the pulp after 6 000 revolutions in the PFI-mill. Values for the fiber width are considerably larger than for the fiber thickness. This indicates a strong deformation from a roundish like to a flattened cross section in general. Beating again shows some effects. The fiber thickness values are more concentrated below 10 μm , whereas the fiber width is hardly affected as was already summarized in Table 4.2.

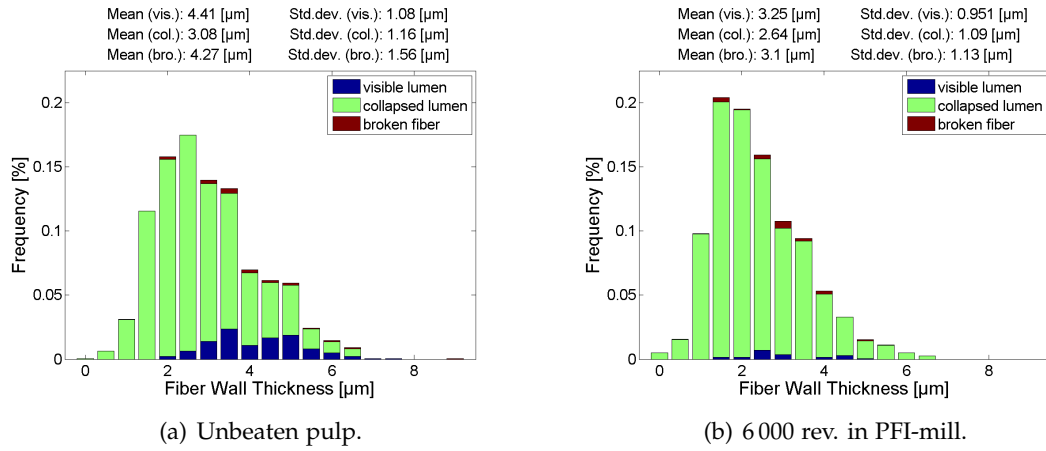


Figure 4.17 Effect of beating on fiber wall thickness distribution and fraction of collapsed fibers. The mean wall thickness and the standard deviation of the corresponding distributions are given for the three different classes of fiber cross sections.

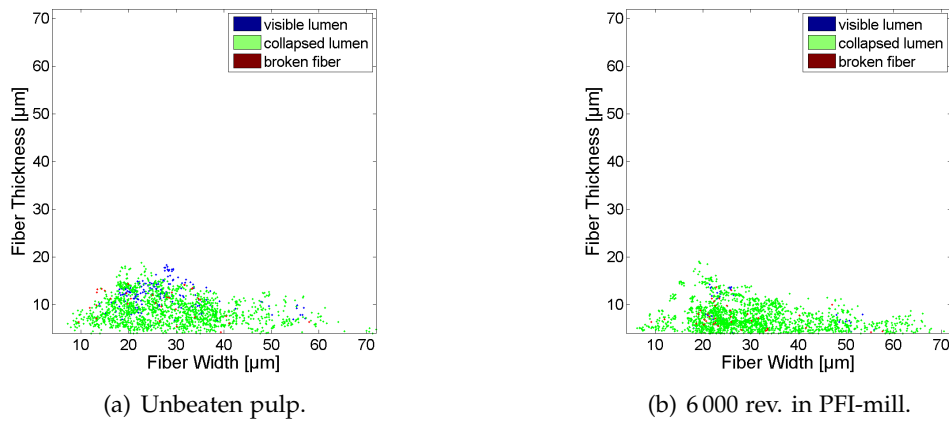


Figure 4.18 Effect of beating on the correlation of fiber thickness and fiber width.

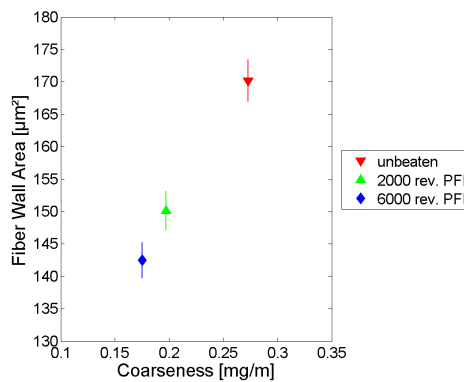


Figure 4.19 Correlation of fiber wall area (serial sectioning) and coarseness (Kajaani FS200). Beating leads to a decrease of fiber wall area and coarseness.

A validation of the results obtained with the novel technique is presented in Figure 4.19, where a correlation of the fiber wall area obtained in the dry state with the serial sectioning technique and the coarseness measured with a Kajaani FS200 in the wet state is shown. The fiber wall area as a measure for the fiber volume is thought to influence the coarseness of a pulp which can be interpreted as another method to measure the fiber volume. The data show a strong correlation, a decrease in the fiber wall area corresponds to a decrease in the coarseness. Two completely different measuring systems show a similar trend of the properties investigated.

4.4.2 Effect of cross section properties on paper properties

Several studies regarding the influence of fiber cross section properties on paper properties were presented during the past decades, see for instance [DINWOODIE, 1965; HORN, 1974, 1978; OLUWAFEMI AND SOTANDE, 2007; TIIKKAJA, 1999]. However, these studies were always limited by the weak reliability of obtained results. This section shows several examples for the influence of fiber cross section properties on dewatering properties of pulps and mechanical properties of the final sheets.

Various pulp samples were examined at different beating levels, see the discussion of the influence of laboratory beating on fiber cross section properties in section 4.4.1:

- Softwood kraft (spruce), unbeaten, 2 000 rev. PFI-mill and 6 000 rev. PFI-mill, see previous section for more details.
- Softwood sulphite (mainly spruce), unbeaten, 2 000 and 6 000 rev. PFI-mill
- Hardwood kraft (eucalyptus), unbeaten, 1 000 and 3 000 rev. PFI-mill
- Hardwood kraft (birch), unbeaten, 1 000 and 3 000 rev. PFI-mill
- Bleached chemi thermo mechanical pulp (BCTMP, aspen), unbeaten
- Additionally unbeaten stone ground wood (SGW), pressure ground wood (PGW) and thermo mechanical pulp (PGW) were analyzed, but there was no way to extract a reasonable number of fiber cross sections for a comparably study, see section 4.3.3 for more details.

Hand sheets of the different pulps were prepared and cross sections were digitized with automated serial sectioning at the highest resolution possible in the image plane and a distance of $1\ \mu\text{m}$ between the image planes. Again about 2 000 fiber cross sections were analyzed for each pulp and beating level, resulting from the analysis of about 10 subsequent cross sections of about 200 individual fibers. The 95% confidence intervals are presented for all results.

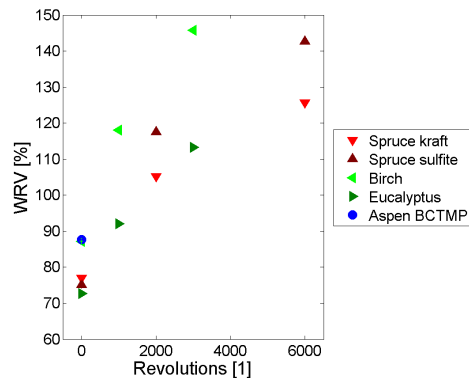


Figure 4.20 The influence of beating exemplarily shown for the water retention value (WRV). Similar results are obtained for the drainability of pulp suspensions ($^{\circ}$ SR).

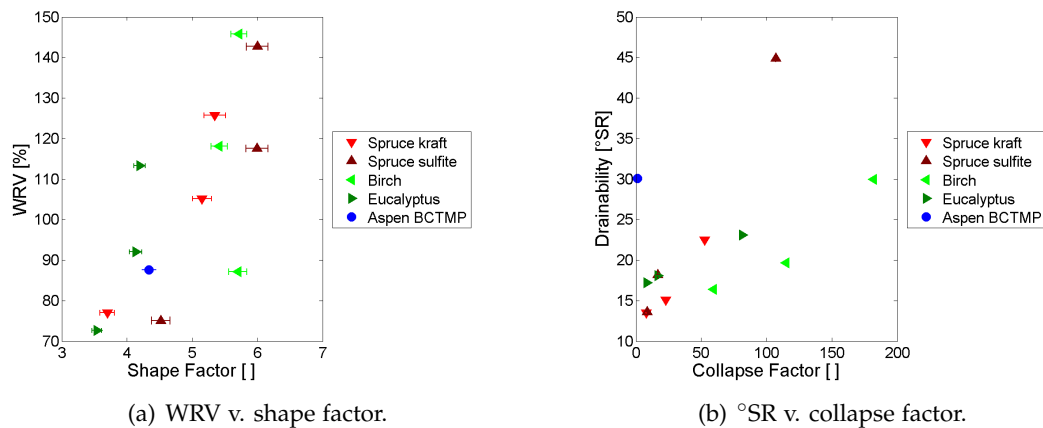


Figure 4.21 Cross section measures show an influence on dewatering properties. A higher shape factor (fiber flatness) leads to a higher water retention value (WRV) (a). A higher collapse factor results in a slower dewatering of the pulp suspension (b).

Effect of pulp fibers on dewatering properties

The dewatering properties of pulp are important during forming and pressing of a paper sheet. Measures like water retention value (WRV) - indicating the amount of water a fiber mat is capable of holding - or drainability of pulp suspensions defined by e.g. Schopper Riegler ($^{\circ}$ SR) are used to characterize pulp samples. The well known effect of beating on dewatering properties is shown in Figure 4.20 for the WRV. An increased beating level leads to an increased water retention value. Similar results are obtained for the drainability of pulp samples. Figure 4.21 shows the influence of fiber cross section properties on these measures; a correlation of WRV and shape factor (fiber flatness) is presented in (a), the influence of fiber collapse (collapse factor) on the drainability of pulp suspensions is shown in (b).

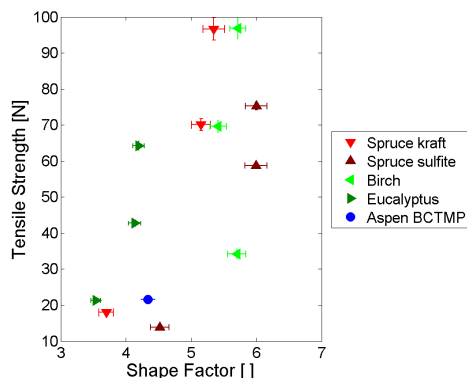


Figure 4.22 Influence of the shape factor on tensile strength. A flatter fiber results in a higher tensile strength.

The WRV increases with increasing shape factor obtained at higher beating levels, see Figure 4.21 (a). This behavior is clearly visible at low beating levels for the softwood samples, the spruce kraft pulp and the spruce sulfite pulp. At higher beating levels, the shape factor keeps almost unchanged whereas the water retention value still increases. Beating of birch fibers hardly influences the shape factor, but the WRV is increased. The eucalypt pulp shows similar characteristics at the higher beating levels, whereas an increase of both, shape factor and WRV, is observed at a low degree of beating. One can conclude that water retention value is clearly influenced by the shape factor at the lower beating levels and this is more pronounced for the softwood pulps.

The drainability of pulp suspensions is influenced by the fiber collapse, represented as collapse factor in Figure 4.21 (b). Softwood and hardwood pulps can be divided into two groups. An increase of the collapse factor of fibers lowers the drainability (higher °SR level) of the softwood pulp suspensions to a larger extent than for the hardwood pulp suspensions.

Effect on the mechanical properties of hand sheets

The influence of fiber cross section properties on tensile strength and tear strength is presented in Figure 4.22 and Figure 4.23 (a) respectively.

A general trend of increased tensile strength of hand sheets at an increased fiber flatness is observed for the softwood pulps, see Figure 4.22. For hardwood pulps, the tensile strength is influenced to a lower degree by the shape factor than for the softwood pulps. In both cases the major influences are observable at low shape factors and a low tensile strength range.

The influence of fiber wall thicknesses of different pulp samples on the tear strength of hand sheets is shown in Figure 4.23 (a). A change of fiber wall thickness by beating (see Table 4.2 for more details) has no clear effect on the tear strength.

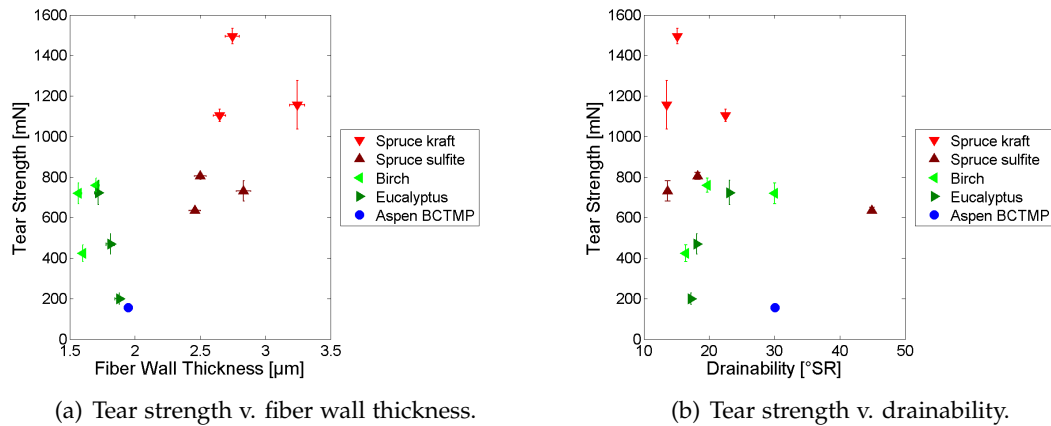


Figure 4.23 The effect of fiber wall thickness on tear strength (a). A similar influence is observed for changes in the drainability of the pulp suspensions (beating level) which also strongly influence the obtained tear strengths (b).

The increase of tear strength gained at lower beating levels is neutralized if the pulp is beaten more extensively. This behavior is similar to the well known effect of beating (expressed by the drainability of pulp suspensions) on tear strength, see Figure 4.23 (b). In order to increase the tear strength of paper, slightly beaten softwood fibers having a thick fiber wall (stiff fibers) should be used.

4.4.3 Comparison to flow cell measurements

The results obtained by serial sectioning of dry fiber samples (see section 4.3.1) were compared to results obtained on fiber suspensions using a FiberLab V3.0 (Metso Automation). The quantification of fiber cross section properties in suspension with flow cells like the FiberLab is widely used, see for instance [HIRN AND BAUER, 2006; PAAVILAINEN, 1993; PULKKINEN ET AL., 2006].

Four different unbeaten pulps (aspen BCTMP, eucalypt pulp, spruce kraft pulp and spruce sulfite pulp) and unbleached spruce kraft pulp samples (unbeaten, 50 and 100 kW/h refining intensity in a laboratory disc refiner) were used. The analysis of fiber cross sections in the dry state was based on about 2000 fiber cross sections per pulp sample, obtained from 200 individual fibers and 10 consecutive cross sections per fiber. In the flow cell a number of about 10 000 fibers was analyzed.

A detailed comparison of fiber cross sections analyzed in dry and wet state is presented in Figure 4.24 (a) for fiber wall thickness and (b) for fiber width. Two different pulps are shown, aspen BCTMP and bleached spruce kraft pulp, both unbeaten. The difference between hardwood and softwood is visible in the obtained fiber wall thickness distributions in dry state analysis. As expected, a wider range of values and thicker fiber walls can be observed for the softwood pulp. In wet state analy-

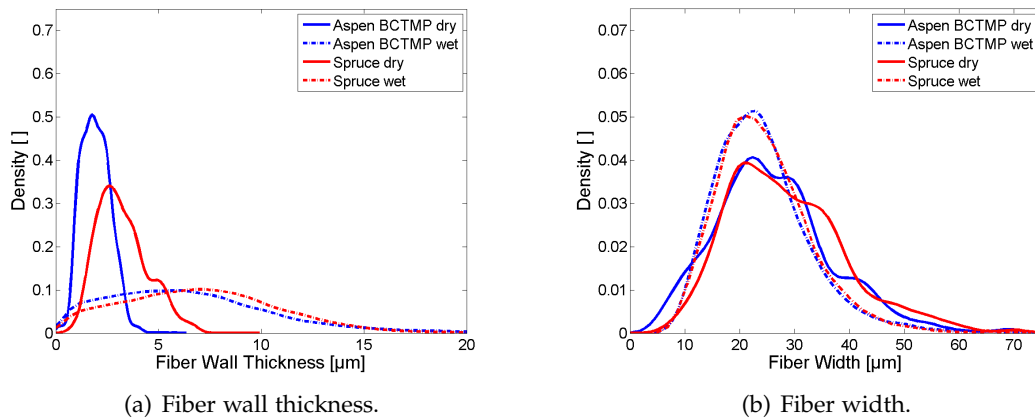


Figure 4.24 Distributions of fiber wall thickness (a) and fiber width (b) obtained in dry and wet state show differences between the measuring systems.

sis, this difference is not obvious anymore. The hardwood pulp gives a similar wall thickness distribution as does the softwood pulp. This behavior probably originates from a different swelling behavior of the fibers in suspension. The distributions of fiber width (Figure 4.24 (b)) are similar for both pulps in the dry and the wet state at slightly different scales. Fiber widths obtained in the wet state seem to be narrower than those measured from dry cross sections. Flow cells usually measure a projected fiber width, being not necessarily the true fiber width at all, whereas a measurement in the dry state indicates the maximum fiber width.

Figure 4.25 shows correlations of (a) fiber wall thickness and (b) fiber width, for the different pulps, analyzed in wet and the dry state. A general trend of an increasing fiber wall thickness in the dry state at an increased fiber wall thickness in the wet state can be observed. The dry state analysis based on data obtained with automated serial sectioning seems to differentiate better between the individual pulp samples. For example, the wall thicknesses obtained in the dry state for the pulps spruce kraft and spruce sulfite differ by about 15%. Measurement in the wet state does not give an obvious difference between the two samples. The measurement of fiber width in the dry and wet state, Figure 4.24 (b), is highly correlated. However, looking at the refining study (gray dots) in both cases, fiber wall thickness and fiber width, a wrong order of the refining levels is observed in the dry state analysis. This could be an indication for an insufficient sample size used in analysis of softwood pulps. But this wrong order is also observed for the fiber wall thickness obtained with the flow cell.

This first validation of methods analyzing fiber cross section properties in the dry and the wet state verifies the capability of both approaches to estimate fiber cross section properties. The results obtained were used by BATCHELOR ET AL. [2010] to characterize changes in the shape of fiber cross sections during drying. But one has also to conclude that both measures are not perfect at the moment. In flow cells only

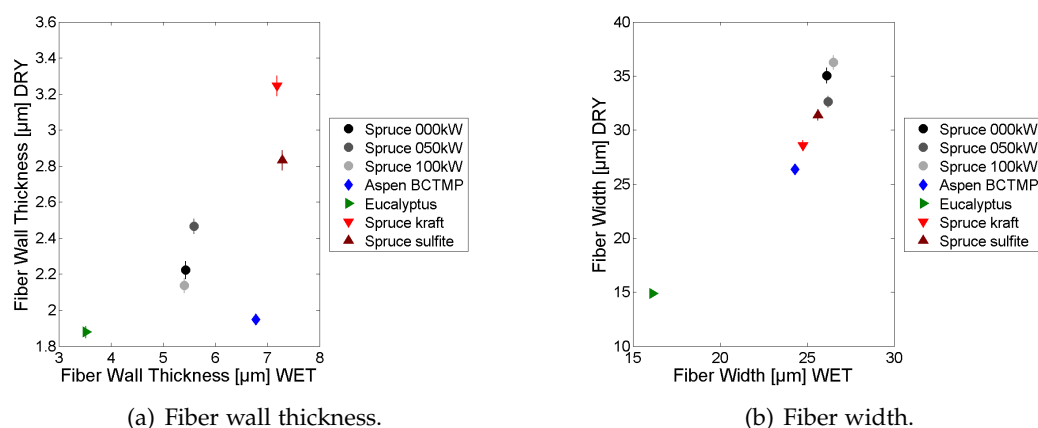


Figure 4.25 Correlation of fiber cross section properties obtained in the wet state and in the dry state, (a) for fiber wall thickness and (b) for fiber width.

a fraction of the fibers is used which results in some classification, probably revealing only a distinct fiber population. A dry state analysis of fiber cross sections from softwood pulps must also be considered as not perfectly reliable. The analysis of an even larger number of fibers is needed in order to support the obtained results.

4.5 Conclusions

Besides coating layer analysis, the evaluation of fiber cross section properties in the dry state from paper cross section images is another important application of the serial sectioning technique. The major benefit is the accessibility of paper cross section sequences without large efforts. In an ideal case, a sequence of subsequent paper cross sections enables an unbiased measurement of fiber cross section properties. In addition, paper cross sections allow a representative analysis of fibers from a more unbiased fiber population, there is no need for manipulation of individual fibers nor laborious sample preparation.

The extraction of fiber cross sections for further analysis is the current limitation of the process. Image analysis routines track individual fibers along the image sequence, after being initiated by a user. Also the segmentation results have to be edited manually.

Image analysis is followed by several other processes. The most important one is to resize the fiber cross section shape. Since the cross sections are usually not digitized perpendicular to the fiber main axis, the visible cross sections are overrated and therefore are mathematically transformed to true sized ones. Having the resized cross sections, several properties are extracted, amongst others the fiber wall area, fiber wall thickness or indices like a shape factor as a ratio of fiber width and fiber thickness indicating the fiber flatness.

First applications clearly demonstrated the applicability of the proposed method. The analysis of different beating levels revealed a clear influence on fiber cross section properties, like a more pronounced fiber collapse at increased beating levels. Also effects of fiber cross section properties on dewatering properties of pulp and mechanical properties of paper were demonstrated. A comparison to a measuring technique analyzing fibers in the wet state in suspensions showed surprisingly good correlations.

The different processes used in this analysis of fiber cross section properties have to be further developed in future work. Besides the image analysis, the transformation of detected fiber cross sections to true sized ones has to be optimized. The classification of fibers into fibers with visible lumen, fibers with collapsed lumen and fibers with a broken fiber wall also has to be improved.

Conclusions and Outlook

A measuring technique is the central theme of this thesis, however two very different fields of research were the main topics discussed; automated serial sectioning used for spatial coating layer analysis and the estimation of fiber cross section properties.

Summary and conclusions

This thesis is a continuation of a previous work focusing on the development of an automated serial sectioning technique for three dimensional analysis of paper structures, WILTSCHKE [2006]. Three dimensional analysis of paper structure became an important field of research in the pulp and paper community. The recent advances in modeling and simulation of paper properties and detailed analysis of interactions between e.g. print quality and coating thickness require in depth knowledge of morphology and spatial distribution of the materials used in paper production.

Automated serial sectioning

The basic concept of the automated serial sectioning technique and a brief review of competing digitization methods in three dimensional paper structure analysis were presented in chapter 2. Technical enhancements, like embedding and cutting of large samples ($>1\text{ cm}^2$ sample area) and an efficiency improvement by adding a blowing device to remove cut off slices from the diamond knife, were implemented.

The final concept enables unsupervised digitization of paper samples and is a powerful digitization technique providing sufficiently high resolution and allowing large sample areas for paper structure analysis. A comparison with the major alternative three dimensional digitization techniques is given in the following:

- 3D SEM: Serial grinding or serial sectioning combined with scanning electron microscopy allows the highest resolution but the smallest sample size. The backscatter mode is usually applied, resulting in high quality gray scale images.
- μ -CT: X-ray microtomography (desktop scanner). The maximum resolution of about $1\ \mu\text{m}$ can only be achieved for small sample areas of approximately $2 \times 2\text{ mm}^2$. The quality of obtained images is a weakness of this method, especially if coating layers are analyzed. This method is non destructive and allows to monitor also dynamic processes.
- CLSM: Confocal laser scanning microscopy. Two different approaches are discussed, scanning through the paper thickness (non destructive), or imaging of paper cross sections. Image quality diminishes rapidly with increasing depth of the focal plane, limiting the 3D applicability.
- μ STRUCSCOP: Automated serial sectioning. A sample area of more than 1 cm^2 can be analyzed. The lens with the highest magnification provides a resolution of $0.6\ \mu\text{m}$ in the image plane. Compared to the other techniques, more sophisticated image analysis tools are needed to extract features from the cross section images.

Coating layer analysis

Chapter 3 presented advances in coating layer analysis which presently is the major application of data obtained with automated serial sectioning.

The validity of results obtained was demonstrated by comparison with other techniques used in coating layer analysis. A paper cross section analyzed with scanning electron microscopy and automated serial sectioning resulted in almost identical coating thicknesses. A comparison of X-ray microtomography to automated serial sectioning gave a similar trend of measured coating thicknesses. Coating layer uniformity determined with serial sectioning was compared to the burnout test revealing a roughly similar trend, a detailed comparison was not possible due to the totally different nature of the two methods. The definition of a recommended sampling procedure completed the work regarding the validity and reliability of obtained results. A large anisotropic sample area ($5 \times 1 \text{ mm}^2$ CD \times MD) was found to be a better choice than single cross sections (5 mm) or squared samples ($1 \times 1 \text{ mm}^2$). In order to allow a representative analysis for a larger sample at least 3 of these $5 \times 1 \text{ mm}^2$ samples have to be evaluated.

The coating layer analysis tool based on automated serial sectioning enables the evaluation of several properties of a coating layer:

- The spatial coating layer formation was analyzed at different length scales to distinguish between void filling effects for structures at the fiber level and the coating layer structure at larger scales like fiber flocs. Differences between application systems as well as influences caused by calendering and coating pigment choice were identified.
- A tool to analyze coating holdout was developed. It was used to discuss the relevance of this property and to evaluate the influence of base paper porosity and pigment variations.
- Coating coverage was determined as a fraction of uncoated area. As expected, coat weight was found to be a decisive factor controlling coating coverage. An analysis of the surroundings of uncoated spots revealed that these were exposed regions on the paper surface, but the paper roughness had no significant effect on coating coverage.

Analysis of fiber cross section properties

A concept to analyze fiber cross section properties and first applications were presented in chapter 4.

The subsequent paper cross sections obtained with automated serial sectioning enable an unbiased measurement of fiber cross section properties as well as a representative analysis of an unbiased fiber population.

5. Conclusions and Outlook

In the current approach, cross sections of individual fibers are detected in paper cross sections. These fiber cross sections have to be resized because the detected cross sections are overrated since they are usually not cut and digitized perpendicular to the fiber main axis. From the true sized cross sections, several properties like e.g. the fiber wall area are calculated. First applications clearly demonstrated the applicability of the proposed method. For example, the analysis of different beating levels revealed a clear influence on fiber cross section properties, like a more pronounced fiber collapse at increased beating levels.

Current limitations of the approach are the reliability of the segmentation of fiber cross sections as well as weaknesses in the estimation of fiber cross section properties which have to be further improved in future work.

Future work and outlook

Coating layer analysis

The results presented in chapter 3 show the focus of ongoing work in the evaluation of coating holdout and the analysis of coating coverage. The initial approaches to evaluate these coating layer properties clearly show further potential in both cases.

The current approach to analyze coating holdout uses the mean coating thicknesses to determine the fraction of penetrated coating color. The next step could be the use of local data (obtained at the individual measuring lines) which will result in a distribution respectively a map of the fractions calculated. A future issue should be the validation of the results with other methods like an analysis of an exposed back side of the coating layer.

A first attempt to analyze the neighboring regions of uncoated spots revealed that these spots are exposed regions on the paper surface. This approach to analyze coating coverage should be discussed in more detail. Besides the base sheet topography also the surrounding coating thickness and surface topography data can be considered. The size and shape of an uncovered area can be determined from data obtained in serial sectioning. Both, size and shape of uncoated spots can also be determined with scanning electron microscopy; a straightforward way to validate the results obtained with serial sectioning.

Fiber cross section properties

As discussed in chapter 4, the concept to estimate fiber cross section properties has to be further developed. The presented approach outlines the capability for a reasonable analysis of fiber cross section properties, but there is still room for further developments.

5. Conclusions and Outlook

Major improvements are necessary in the segmentation of fiber cross sections. In order to minimize the laborious user interactions, three topics are of particular importance: 1) an automated initiation of the detection of fiber cross sections, 2) a detection of a visible fiber lumen and 3) a reliable tracking of fiber cross sections, over a sequence of tens to hundreds of paper cross sections. These tasks are difficult to handle, but already a small improvement in the detection of fiber cross section will contribute to the applicability of automated serial sectioning in fiber cross section analysis.

Besides image analysis, improvements in the individual analysis steps are necessary starting with the transformation of detected fiber cross sections to true sized ones. The current way to calculate fiber width and fiber thickness does not give accurate enough results. The classification of fibers into fibers with visible lumen, fibers with collapsed lumen and fibers with a broken fiber wall has to be reconsidered.

Having a well defined analysis tool, a representative analysis of fiber cross section properties from an unbiased population of fibers prepared in hand sheets or in machine manufactured paper is possible. Another application will be the evaluation of a large number of subsequent paper cross sections. This will allow the analysis of changes in fiber cross section properties along a fiber main axis.

Other approaches to be considered in future

As mentioned in chapter 2 there are some other possibilities to use paper cross sections obtained with serial sectioning which have not been treated in detail so far.

One possibility is the evaluation of paper surface topography respectively the measurement of the "true" paper thickness of uncoated papers. The necessary image analysis algorithms are ready to use. Validations with other measuring techniques providing local thicknesses, e.g. twin laser profilometry [SUNG ET AL., 2005], should be carried out.

Also the estimation of a 3D fiber orientation can be considered as a future field of research. As with fiber cross section analysis, there is a need for further improvements in image analysis. However, this could be the basis for an investigation of fiber tilt in paper and paper board, see for instance [CONSIDINE AND VAHEY, 2008].

Burnout Test

In this appendix, the operating procedure of the burnout test is presented. The basic principle is in accordance to DOBSON [1975]; ENGSTRÖM AND LAFAYE [1992]:

- Dehydration agent: 25 g/l NH₄Cl in 50:50 mixture of ethanol and water.
- Samples to be analyzed were soaked for 10 minutes with the dehydration agent and were then air dried.
- Samples were heated in an oven for 10 minutes at 200 °C.
- Imaging of the carbonized samples (top and bottom side if available) was performed with a commercial scanner (reflectance mode) at a resolution of 1 200 dpi and 8 bit gray scales. The images were saved as uncompressed jpegs.
- The obtained images were analyzed in the following way; An area of $2.1 \times 2.1 \text{ cm}^2$ was used for calculation of a mean gray value as well as a coefficient of variation and a skewness of the gray scale distribution.

Two typical results are shown in Figure A.1 for a film coat (a) and a blade coat (b) applied to the same base paper. The orange peel pattern appearing at higher machine speeds in film coating is clearly visible in the burnout image whereas individual fibers are the predominant structure in the blade coated sample.

A. Burnout Test

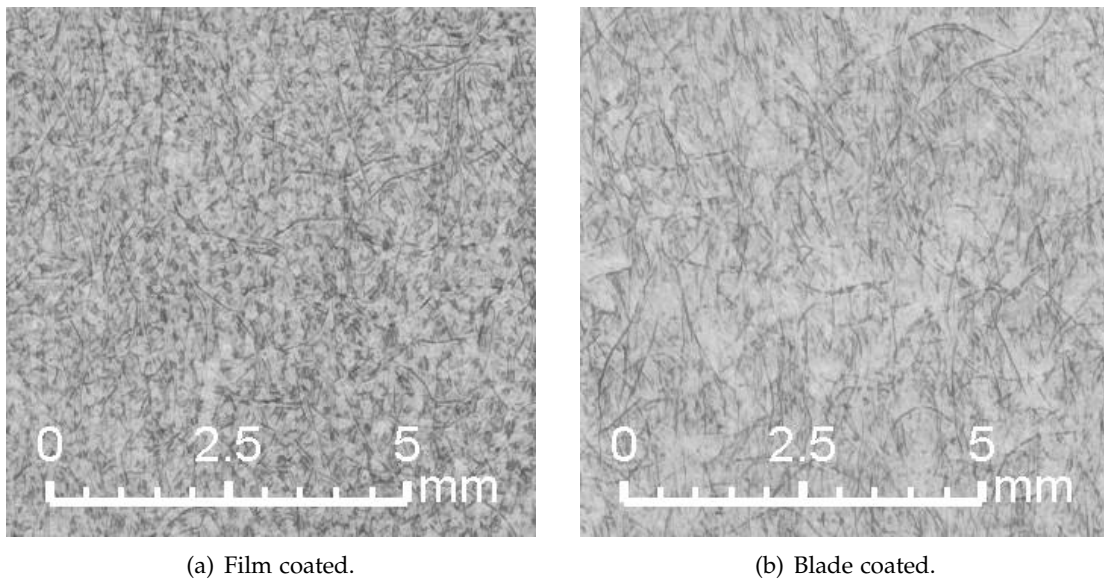


Figure A.1 Typical burnout images obtained from a film coated (a) and a blade coated (b) sample. Coating was applied on a similar base paper.

Samples Analyzed with Coating Layer Analysis Tools

A large quantity of different samples was analyzed with the coating layer analysis tools, see chapter 3. The individual sample series are separated into groups and originate from pilot coating trials as well as from industrial studies.

Group A (red dots)

Group A originates from an extensive pilot coating and calendering trial. Three different wood containing industrially produced base papers were used. Coating was applied with a blade (two different coating formulations) and a film press. The coated papers were calendered in a super calender. Both, uncalendered and calendered samples were analyzed.

Group B (brown dots)

The samples in group B are explained in more detail in section 3.4.2. The samples were coated at the Center of Excellence for Paper and Board Coating of DOW Europe GmbH (now Styron Europe) with blade, film press and slide curtain application systems. In this thesis, those samples were used to study the influence of coating application system on coating layer formation.

Group C (gray dots)

A precoat optimization trial was the origin of this sample group. A woodfree paper was precoated in a film press using different coating formulations. A low coat weight was applied in all cases.

B. Samples Analyzed with Coating Layer Analysis Tools

Group D (green dots)

Pigment variations like the use of a finer clay or a higher carbonate level in the coating color were analyzed in this case.

Group E (blue dots)

This sample group presents a calendering study. Pre-calendered woodfree base papers were curtain coated (coat weight per side: 12 g/m^2) and then post-calendered. Different linear loads have been applied:

- Linear loads used in pre-calendering:
25 kN/m, 50 kN/m, 75 kN/m, 100 kN/m.
- Linear loads used in post-calendering:
0 kN/m, 150 kN/m, 225 kN/m, 350 kN/m.

Section 3.4.3 summarizes the influences of different linear loads on the coating layer formulations.

Group F (black dots)

Group F represents board samples. The samples were two times coated, the application system of the second coating layer was varied - airknife or curtain coater.

Publications

Publications during my research work are listed chronologically below (peer-reviewed publications are printed in bold letters):

- J. Kritzing, M. Wiltsche, M. Donoser and W. Bauer. Characterization of the 3D Structure of Paper by Image Analysis. In *Book of Abstracts - 34th International Meeting of Slovenian papermakers DITP*, Bled (Slovenia), November 2007.
- J. Kritzing, M. Wiltsche, M. Donoser and W. Bauer. Weiterentwicklung einer innovativen Methode zur Untersuchung der 3D Papierstruktur. Österreichische Papierfachtagung 2008, Graz (Austria), May 2008.
- J. Kritzing. 3D-Papierstruktur. *Papier aus Österreich*, 08(6):26-27, 2008.
- J. Kritzing, M. Donoser M. Wiltsche and W. Bauer. Examination of fiber transverse properties based on a serial sectioning technique. In *Progress in Paper Physics Seminar Proceedings 2008*, pages 157-160, Helsinki (Finland), June 2008, TKK.
- **J. Kritzing, U. Hirn, M. Donoser and W. Bauer. Characterization of spatial coating layer formation - Definition of a representative sample size. In 13th TAPPI Advanced Coating Fundamentals Proceedings, pages 340-351, Montreal (Canada), June 2008, TAPPI Press.**
- W. Bauer, U. Hirn, J. Kritzing and C. Voura. Research Activities of the IPZ at TU Graz Targeting at Producing Better Printable Papers. In *Book of Abstracts - 35th International Annual Symposium DITP*. Bled (Slovenia), November 2008.
- **M. Donoser, T. Mauthner, J. Kritzing and H. Bischof. A Probabilistic Approach for Tracking of Fibers. In Proceedings of the 19th International Conference on Pattern Recognition, pages 1-4, Tampa (USA), December 2008, IEEE.**

C. Publications

- J. Kritzinger. Analyse der 3D-Papierstruktur. *APR - Allgemeine Papier-Rundschau*, 2009(2):22-23, 2009
- J. Kritzinger, M. Donoser and W. Bauer. Estimation of fiber cross section properties from image data obtained by a serial sectioning technique. In *Extended Abstracts of the Workshop "New Methods for Paper Fiber Characterization" COST E54*, pages 63-65, Tampere (Finland), May 2009, University of Tampere.
- J. Kritzinger, M. Donoser and W. Bauer. Representation of Fibre Cross Section Properties. Poster Contribution In *Minisymposium Verfahrenstechnik*, pages 80-83, Vienna (Austria), June 2009, Vienna University of Technology.
- J. Kritzinger, M. Wiltsche, M. Donoser and W. Bauer. Application of a Novel Automated Serial Sectioning Technique in the 3D Analysis of Paper Structure. In *Proceedings Microscopy09*, pages 83-84, Graz (Austria), September (2009), felmizfe.
- **U. Hirn, J. Kritzinger, M. Donoser and W. Bauer. Introducing a concept to link 3D paper structure to 2D paper properties. In *Advances in Pulp and Paper Research. Transactions of the 14th Fundamental Research Symposium*, pages 721-748, Oxford (UK), September 2009, The Pulp and Paper Fundamental Research Society.**
- J. Kritzinger, M. Donoser and W. Bauer. Representative analysis of Fibre Cross Section Properties Using Automated Microtomy. In *Reprints Fundamental Research Communications*, pages 28-31, Oxford (UK), September 2009, The Pulp and Paper Fundamental Research Society.
- J. Kritzinger and W. Bauer. Satinage vor oder nach dem Streichfarbenauftrag mit dem Curtain Coater? In *Proceedings of 24th PTS Coating Symposium*, pages 7.1-7.2, Baden-Baden (Germany), September 2009, PTS.
- J. Kritzinger, U. Hirn, H. Schröttner and W. Bauer. New Techniques in Coating Layer Analysis: Light Microscopy and Micro Tomography. In *Proceedings of 24th PTS Coating Symposium*, pages 30.1-30.2, Baden-Baden (Germany), September 2009, PTS.
- U. Hirn, R. Eckhart, J. Kritzinger, L. Kappel And W. Bauer. Fiber Morphology and Bonding, Paper Structure and Printability. SCA Research Seminars SCA R&D Center, Sundsvall (Sweden), October 2009.
- R. Eckhart, J. Kritzinger and W. Bauer. Kenne deine Fasern - Forschung auf dem Gebiet der Faserstoff charakterisierung am IPZ in Graz. Herbsttagung der Österreichischen Papierindustrie. Bruck a.d. Mur (Austria), November 2009.

C. Publications

- P. Salminen, A. Yang, J. Kritzinger, W. Bauer and J. Preston. The Influence of Application System on the Structure of Coating Layer. In *Proceedings of TAPPI Coating & Graphic Arts Conference 2010*, pages 1-11, Atlanta (USA), May 2010, TAPPI Press.
- W. Batchelor, J. Kritzinger, W. Bauer, T. Kuntzsch and G. Meinl. Improved characterization of changes in fibre cross section during sheet forming and drying using optical fibre analyzer data and a serial sectioning technique. In *Progress in Paper Physics Seminar Proceedings 2010*, pages 1-5, Montreal (Canada), June 2010, FP-innovations.
- J. Kritzinger, W. Bauer, P. Salminen and J. Preston. **A Novel Approach to Quantify the Spatial Coating Layer Formation.** In *Proceedings of 14th TAPPI Advanced Coating Fundamentals Symposium*, pages 372-383, Munich (Germany), October 2010, TAPPI Press.
- W. Bauer and J. Kritzinger. Neue Verfahren zur Beurteilung von Strichschichten auf Papier. Herbsttagung der Österreichischen Papierindustrie, Linz (Austria), October 2010.
- J. Kritzinger, W. Bauer, P. Salminen and J. Preston. **A Novel Approach to Quantify the Spatial Coating Layer Formation.** *Tappi Journal*, accepted for publication in a special edition, November 2010.
- J. Kritzinger, M. Donoser, U. Hirn and W. Bauer. Fiber cross section properties estimated with an automated serial sectioning technique. In *COST E54 Book*, accepted for publication.
- M. Wiltsche, M. Donoser, J. Kritzinger and W. Bauer. Automated serial sectioning applied to 3D paper structure analysis. *Journal of Microscopy - Oxford*, accepted for publication.

Bibliography

- A.A. Adams. Effect of size press treatment on coating holdout. *Tappi Journal*, 66(5): 87–91, 1983.
- J. Ahlroos, M. Alexandersson, and J. Grön. Influence of base-paper filler content and precalendering on metered film press coating - paper and print quality. *Tappi Journal*, 85(5):94–100, 1999.
- S. Akinli-Kocak, A. Van Heinigen, and D.W. Bousfield. The influence of fiber swelling on coating penetration. In *Proceedings of the 2002 TAPPI Coating and Graphic Arts Conference and Trade Fair*, pages 275–286, Orlando (USA), May 2002. Tappi Press.
- R. Allem. Characterization of paper coatings by scanning electron microscopy and image analysis. *Journal of Pulp and Paper Science*, 24(10):329 – 336, 1998.
- R. Allem and T. Uesaka. Characterization of paper microstructure: A new tool for assessing the effects of base sheet structure on paper properties. In *Proceedings of Tappi Advanced Coating Fundamentals Symposium*, pages 111–120, Atlanta (USA), May 1999. Tappi Press.
- C. Antoine, R. Holmstad, Ø.W. Gregersen, T. Weitkamp, C. Rau, O. Solheim, and P.J. Houen. Binarisation of 3D images of paper obtained by phasecontrast X-ray microtomography. In *Proceedings of Cost Action E11 Final Workshop*, pages 15–24, Espoo (Finland), October 2001. KCL.
- C. Antoine, P. Nygard, Ø.W. Gregerse, R. Holmstad, T. Weitkamp, and C. Rau. 3D images of paper obtained by phase-contrast X-ray microtomography: image quality and binarisation. *Nuclear Instruments and Methods in Physics Research, Section A: Accelerators, Spectrometers, Detectors and Associated Equipment*, 490(1-2):392 – 402, 2002.
- M. Aronsson, O. Henningsson, and Ö. Sävborg. Slice-based digital volume assembly of a small paper sample. *Nordic Pulp and Paper Research Journal*, 17(1):29 – 33, 2002.
- M. Axelsson. Estimating 3D fibre orientation in volume images. In *Proceedings 19th International Conference on Pattern Recognition*, pages 1762–1765, Tampa (USA), December 2008. IEEE.
- M. Axelsson and S. Svensson. 3D pore structure characterisation of paper. *Pattern Analysis & Applications*, 13(2):159–172, 2009.
- Y. Azimi, M.T. Kortschot, and R. Farnood. A non-destructive method for obtaining a local coat weight map using X-ray imaging. *Journal of Pulp and Paper Science*, 35(1): 11–16, 2009.

C. Bibliography

- W. Batchelor, J. He, and W.W. Sampson. Inter-fibre contacts in random fibrous materials: experimental verification of theoretical dependence on porosity and fibre width. *Journal of Materials Science*, 41(24):8377 – 8381, 2006.
- W. Batchelor, J. Kritzing, W. Bauer, T. Kuntzsch, and G. Meinl. Improved characterization of changes in fibre cross section during sheet forming and drying using optical fibre analyzer data and a serial sectioning technique. In *Proceedings of 2010 Progress in Paper Physics Seminar*, pages 1–5, Montreal (Canada), June 2010. Paprican.
- S. Bhardwaj, M.T. Kortschot, and R.R. Farnood. In-plane movement of coating pigments during hot-soft nip calendering of coated paper. *Journal of Pulp and Paper Science*, 32(4):201 – 204, 2006.
- J.-F. Bloch and S. Rolland du Roscoat. Three-dimensional structural analysis. In S.J. I'Anson, editor, *Transactions of the 14th Fundamental Research Symposium*, volume 2, pages 599–665, Oxford (UK), September 2009. The Pulp & Paper Fundamental Research Society.
- C.L. Brindley and R.P. Kibblewhite. Comparison of refining response of eucalypt and a mixed hardwood pulp and their blends with softwood. *Appita Journal*, 49(1):37–42, 1996.
- M.G. Carvalho, P.J. Ferreira, A.A. Martins, and M.M Figueiredo. A comparative study of two automated techniques for measuring fiber length. *Tappi Journal*, 80(2):137–142, 1997.
- G. Chinga and T. Helle. Three-dimensional reconstruction of a coating layer structure. *Journal of Pulp and Paper Science*, 29(4):119 – 122, 2003.
- G. Chinga, P.O. Johnsen, and O. Diserud. Controlled serial grinding for high-resolution three-dimensional reconstruction. *Journal of Microscopy*, 214(1):13–21, 2004.
- G. Chinga, P.O. Johnsen, H. Kauko, M. Myllys, and J. Timonen. On the three-dimensionality of glossy surfaces. In *Proceedings of 23rd PTS Coating Symposium*, pages 31–1 – 31–12, Baden-Baden (Germany), September 2007a. PTS.
- G. Chinga, O. Solheim, and K. Mörseburg. Cross-sectional dimensions of fiber and pore networks based on euclidean distance maps. *Nordic Pulp and Paper Research Journal*, 22(4):500–507, 2007b.
- G. Chinga-Carrasco. Exploring the multi-scale structure of printing paper - a review of modern technology. *Journal of Microscopy*, 234(3):211–242, 2009.
- G. Chinga-Carrasco, H. Kauko, M. Myllys, J. Timonen, B. Wang, M. Zhou, and O. Fossum. New advances in the 3D characterization of mineral coating layers on paper. *Journal of Microscopy*, 232(2):212–224, 2008.
- G. Chinga-Carrasco, M. Lenes, P.O. Johnsen, and E.-L. Hult. Computer-assisted scanning electron microscopy of wood pulp fibres: Dimensions and spatial distributions in a polypropylene composite. *Micron*, 40(7):761–768, 2009.

C. Bibliography

- J.M. Considine and D.W. Vahey. Investigation of fiber tilt in paperboard. In *Progress in Paper Physics Seminar Proceedings 2008*, pages 153–155, Helsinki (Finland), June 2008. TKK.
- C. Dahlström and T. Uesaka. New insights into coating uniformity and base sheet structures. *Industrial and Engineering Chemical Research*, 48(23):10472–10478, 2009.
- C. Dahlström, T. Uesaka, and M. Norgren. Base sheet structures that control coating uniformity: Effect of length scales. In *Proceedings of 10th TAPPI Advanced Coating Fundamentals Symposium*, pages 124–133, Montreal (Canada), June 2008. Tappi Press.
- S. Di Risio and N. Yan. Characterizing the pore structure of paper coatings with scanning probe microscopy. *Tappi Journal*, 5(3):9 – 14, 2006.
- A.R. Dickson. The quantitative microscopic analysis of paper cross-sections: sample preparation effects. *Appita Journal*, 53(5):362–366, 2000a.
- A.R. Dickson. Quantitative analysis of paper cross-sections. *Appita Journal*, 53(5): 292–295, 2000b.
- A.R. Dickson, S.R. Corson, and N.J. Dooley. Fibre collapse and decollapse determined by cross-sectional geometry. *Journal of Pulp and Paper Science*, 32(4):205–209, 2006.
- R. Dickson, U. Forsström, and J. Grön. Coating coverage of metered size press pre-coated paper. *Nordic Pulp and Paper Research Journal*, 17(4):434–439, 2002.
- R.J. Dickson and P. Lepoutre. Mechanical interlocking in coating adhesion to paper. *Tappi Journal*, 80(11):149–157, 1997.
- J.M. Dinwoodie. The relationship between fiber morphology and paper properties: A review of literature. *Tappi Journal*, 48(8):440–447, 1965.
- R.L. Dobson. Burnout, a coat weight determination test re-examined. In *Proceedings of TAPPI Coating Conference*, pages 123–131, Chicago (USA), 1975. Tappi Press.
- L. Donaldson, S. Bardage, and G. Daniel. Three-dimensional imaging of a sawn surface: a comparison of confocal microscopy, scanning electron microscopy, and light microscopy combined with serial sectioning. *Wood Science and Technology*, 41(7): 551–564, 2007.
- M. Donoser. *Advanced Segmentation and Tracking Algorithms and Their Application to 3D Paper Structure Analysis*. PhD thesis, Institute for Paper, Pulp and Fiber Technology & Institute for Computer Graphics and Vision, Graz University of Technology, 2007.
- M. Donoser and H. Bischof. Efficient maximally stable extremal region (MSER) tracking. In *Proceedings of the IEEE Computer Society Conference on Computer Vision and Pattern Recognition (CVPR 2006)*, pages 553–560, New York (USA), June 2006. IEEE.
- M. Donoser, H. Bischof, and M. Wiltsche. Color blob segmentation by MSER analysis. In *Proceedings of International Conference on Image Processing (ICIP)*, pages 757–760, Atlanta (USA), 2006. IEEE.
- M. Donoser, T. Mauthner, J. Kritzinger, and H. Bischof. A probabilistic approach for tracking fibers. In *Proceedings of 19th International Conference on Pattern Recognition*

C. Bibliography

- (ICPR), pages 1–4, Tampa (USA), December 2008. IEEE.
- R. Eckhart, U. Hirn, and W. Bauer. A method to determine fiber wall damage induced by refining. In *Proceedings of 2006 Progress in Paper Physics Seminar*, pages 30–34, Oxford (USA), September 2006. Miami University.
- R. Eckhart, U. Hirn, and W. Bauer. Refining aggregates. *International Paperworld*, 2007 (6):45–46, 2007.
- R. Eckhart, M. Donoser, and W. Bauer. Single fibre flexibility measurement in a flow cell based device. In S.J. I'Anson, editor, *Transactions of the 14th Fundamental Research Symposium*, volume 1, pages 247–271, Oxford (UK), September 2009. The Pulp & Paper Fundamental Research Society.
- M. Eder, K. Jungnikl, and I. Burgert. A close-up view of wood structure and properties across a growth ring of norway spruce (*picea abies* [L.] karst.). *Trees*, 23(1):79–84, 2009.
- I. Endres and M. Tietz. Blade, film, and curtain coating techniques and their influence on paper surface characteristics. *Tappi Journal*, 6(11):24–31, 2007.
- G. Engström. Formation and consolidation of a coating layer and the effect on offset-print mottle. *Tappi Journal*, 77(4):160–172, 1994.
- G. Engström. Coating coverage - definition and measuring techniques. *Coating*, 32(5):178–185, 1999.
- G. Engström. Interactions between coating colour and base sheet in pigment coating. In S.J. I'Anson, editor, *Transactions of the 13th Fundamental Research Symposium*, volume 2, pages 1011–1073, Cambridge (UK), September 2005. The Pulp & Paper Fundamental Research Society.
- G. Engström and J.F. Lafaye. Precalendering and its effect on paper-coating interaction. *Tappi Journal*, 75(8):117–122, 1992.
- G. Engström and V. Morin. Analysis of the process of forming and consolidation in blade coating. *Tappi Journal*, 79(9):120–128, 1996.
- U. Forsström and H. Pajari. Penetration of coating colour into model substrates: Effect of pore size, wettability and coating method. *Journal of Pulp and Paper Science*, 35 (3-4):155–160, 2009.
- U. Forsström, R. Dickson, and J. Grön. Strichdeckung und Struktur von holzfreien Papieren, die in der Filmpresse vorgestrichen wurden. *Wochenblatt für Papierfabrikation*, (14/15):985–992, 2000.
- U. Forsström, K. Fagerholm, and E. Saharinen. The role of base paper porosity in MSP coating. *Paperi ja Puu - Paper and Timber*, 85(8):454–459, 2003.
- P.A.C. Gane and J.J. Hooper. An evaluation of interactions between coating colour and base paper by coating profile analysis. In C.F. Baker and V.W. Punton, editors, *Transactions of the 9th Fundamental Research Symposium*, volume 2, pages 871–893, Cambridge (UK), September 1989. The Pulp & Paper Fundamental Research Society.

C. Bibliography

- A. Goel, C.H. Arns, R. Holmstad, Ø.W. Gregersen, F. Bauget, H. Averdunk, R.M. Sok, A.P. Sheppard, and M.A. Knackstedt. Analysis of the impact of papermaking variables on the structure and transport properties of paper samples by X-ray microtomography. *Journal of Pulp and Paper Science*, 32(4):111–122, 2006.
- R.C. Gonzalez, R.E. Woods, and S.L. Eddins. *Digital Image Processing using MATLAB*. Pearson Prentice Hall, 2004. ISBN 0-13-008519-7.
- Ø.W. Gregersen and K. Niskanen. Measurement and simulation of paper 3D-structure. In *Characterization methods for fibre and paper - Joint PTS - COST E11 Workshop*, pages 13–1 – 13–6, Munich (Germany), December 1999. PTS.
- J. Grön. The significance of paper machine calendering on coating coverage. *Paperi ja Puu - Paper and Timber*, 82(4):244–249, 2000.
- J. Grön and J. Ahlroos. Influence of base paper filler content and pre-calendering on metered film press coating - Part I: A coating process study. In *TAPPI Proceedings - Coating/Papermaking Conference*, volume 2, pages 52–72, New Orleans (USA), May 1998. Tappi Press.
- J. Grön and J. Ahlroos. Effect of base paper filler content and precalendering on coating colour mist and coverage in MSP coating. *Journal of Pulp and Paper Science*, 27(2):66–73, 2001.
- M. Hagen, R. Holen, R. Holmstad, and R. Blake. Digital identification of connected paper fibres with cracks. In *Proceedings of The 2004 Progress in Paper Physics Seminar*, pages 164–166, Trondheim (N), 2004. PFI.
- N. Hartler and J. Nyren. Transverse compressibility of pulp fibers II. Influence of cooking method, yield, beating, and drying. *Tappi Journal*, 53(5):820 – 823, 1970.
- M. Hasuike, T. Kawasaki, and K. Murakami. Evaluation method of 3-d geometric structure of paper sheet. *Journal of Pulp and Paper Science*, 18(3):114–120, 1992.
- J. He, W.J. Batchelor, and R.E. Johnston. The behavior of fibers in wet pressing. *Tappi Journal*, 2(12):27–31, 2003a.
- J. He, W.J. Batchelor, R. Markowski, and R.E. Johnston. A new approach for quantitative analysis of paper structure at the fibre level. *Appital Journal*, 56(5):366–370, 2003b.
- P.J. Heard, J.S. Preston, D.J. Parsons, and G.C. Allen. Visualisation of the distribution of ink components in printed coated paper using focused ion beam techniques. *Colloids and Surfaces A: Physicochemical and Engineering Aspects*, 244(1-3):67–71, 2004.
- A. Hedman, J. Grön, and M. Rigdahl. Coating layer uniformity as affected by base paper characteristics and coating method. *Nordic Pulp and Paper Research Journal*, 18(3):333–343, 2003.
- K. Hirai and D.W. Bousfield. Characterization of paper coating penetration by laser scanning microscopy. In *Proceedings of 2006 TAPPI Advanced Coating Fundamentals Symposium*, pages 90–105, Turku (Finland), February 2006. Tappi Press.

C. Bibliography

- U. Hirn and W. Bauer. A review of image analysis based methods to evaluate fiber properties. *Lenzinger Berichte*, 86:96–105, 2006.
- U. Hirn, J. Kritzing, M. Donoser, and W. Bauer. Introducing a concept to link 3D paper structure to 2D paper properties. In S.J. I'Anson, editor, *Transactions of the 14th Fundamental Research Symposium*, volume 2, pages 721–748, Oxford (UK), September 2009. The Pulp & Paper Fundamental Research Society.
- R. Holmstad, Ø.W. Gregersen, U. Aaltosalmi, M. Kataja, A. Koponen, A. Goel, and S. Ramaswamy. Comparison of 3D structural characteristics of high and low resolution X-ray microtomographic images of paper. *Nordic Pulp and Paper Research Journal*, 20(3):283–288, 2005.
- R. Holmstad, A. Goel, S. Ramaswamy, and Ø.W. Gregersen. Visualization and characterization of high resolution 3D images of paper samples. *Appita Journal*, 59(5):370–377, 2006.
- R.A. Horn. Morphology of wood pulp fiber from softwoods and influence on paper strength. Technical report, Forest Products Laboratory, Forest Service U.S. Department of Agriculture, 1974.
- R.A. Horn. Morphology of pulp fiber from hardwoods and influence on paper strength. Technical report, Forest Products Laboratory, Forest Service U.S. Department of Agriculture, 1978.
- F. Huang, R. Lanouette, K. Law, and K. Li. Microscopic analysis of early- and latewood in thermomechanical pulp refining. *Appita Journal*, 61(6):445–449, 2008.
- T. Huang and P. Lepoutre. Coating-paper interactions - the effect of basestock roughness, absorbency and formation on coated paper properties. *Paperi ja Puu - Paper and Timber*, 77(8):484–490, 1995.
- T. Huang and P. Lepoutre. Effect of basestock surface structure and chemistry on coating holdout and coated paper properties. *Tappi Journal*, 81(8):145–152, 1998.
- H.F. Jang and R.S. Seth. Using confocal microscopy to characterize the collapse behavior of fibers. *Tappi Journal*, 81(5):167–174, 1998.
- H.F. Jang and R.S. Seth. Determining the mean values for fibre physical properties. *Nordic Pulp and Paper Research Journal*, 19(3):372–378, 2004.
- H.F. Jang, A.G. Robertson, and R.S. Seth. Optical sectioning of pulp fibers using confocal scanning laser microscopy. *Tappi Journal*, 74(10):217–219, 1991.
- H.F. Jang, A.G. Robertson, and R.S. Seth. Transverse dimensions of wood pulp fibres by confocal laser scanning microscopy and image analysis. *Journal of Materials Science*, 27(23):6391–6400, 1992.
- H.F. Jang, R.C. Howard, and R.S. Seth. Fiber characterization using confocal microscopy - the effect of recycling. *Tappi Journal*, 78(12):131–137, 1995.
- H.F. Jang, R. Amiri, R.S. Seth, and A. Karnis. Fiber characterization using confocal microscopy - collapse behavior of mechanical pulp fibers. *Tappi Journal*, 79(4):203–

C. Bibliography

- 210, 1996.
- H.F. Jang, R.S. Seth, C.B. Wu, and B.K. Chan. Determining the transverse dimensions of fibres in wood using confocal microscopy. In *Proceedings of International Paper Physics Conference 2003*, pages 313–322, Victoria (Canada), September 2003. Tappi Press & PAPTAC.
- J. Järnström, L. Sinervo, M. Toivakka, and J. Peltonen. Topography and gloss of precipitated calcium carbonate coating layers on a model substrate. *Tappi Journal*, 6(5):23 – 31, 2007.
- T. Kang, A. Dickson, and H. Paullapuro. The response of the various tmp fractions to refining. *Nordic Pulp and Paper Research Journal*, 23(2):224–230, 2008.
- L. Kappel, U. Hirn, W. Bauer, and R. Schennach. A novel method for the determination of bonded area of individual fiber-fiber bonds. *Nordic Pulp and Paper Research Journal*, 24(2):199–205, 2009.
- I. Kartovaara. Coatweight distribution and coating coverage in blade coating. *Paperi ja Puu - Paper and Timber*, 71(9):1033–1042, 1989.
- H.J. Kent, N.A. Climpson, L. Coggon, J.J. Hooper, and P.A.C. Gane. Novel technique for quantitative characterization of coating structure. *Tappi Journal*, 69(5):78–83, 1986.
- R. Kerschmann. A fully automated three-dimensional microscopy system. In *In-Vitro Diagnostic Instrumentation*, volume 1, pages 86–92, San Jose (USA), January 2000. SPIE - The International Society of Optical Engineering.
- R.P. Kibblewhite and D.G. Bailey. Measurement of fibre cross-section dimensions using image processing. *Appita Journal*, 41(4):297–303, 1988.
- R.P. Kibblewhite and A.D. Bawden. Fibre and fibre wall response to refining in softwood and hardwood kraft pulps. In *Proceedings of PIRA Conference - Current and Future Technologies of Refining*, pages 1–35, Birmingham (UK), December 1991. PIRA.
- B.Y. Kim and D.W. Bousfield. Characterization of base paper properties on coating penetration. *Journal of Korea TAPPI*, 35(5):17–25, 2003.
- R. Klein and U. Schulze. Metrology-related evaluation of graphic paper and board cross sections by digital image analysis. *ipw*, 2006(4):48 – 58, 2006.
- M.T. Kortschot. The role of the fibre in the structural hierarchy of paper. In C.F. Baker, editor, *Transactions of the 11th Fundamental Research Symposium*, volume 1, pages 351–399, Cambridge (UK), September 1997. Pira International.
- H. Koyamoto and K. Okomori. Effect of surface properties of base paper on print quality. In *Proceedings of 2006 TAPPI Advanced Coating Fundamentals Symposium*, pages 217–227, Turku (Finland), February 2006. Tappi Press.
- G. Larsson, M. Engström, D. Vidal, and X. Zou. Impact of calendering on coating structures. *Nordic Pulp and Paper Research Journal*, 22(2):267–274, 2007.
- P. Lepoutre and G. de Silveira. Examination of cross-sections of blade- and roll-coated LWC paper. *Journal of Pulp and Paper Science*, 17(5):J184–J186, 1991.

C. Bibliography

- P. Lepoutre and G. Means. Supercalendering and coating properties. *Tappi Journal*, 61(11):85–87, 1978.
- P. Lepoutre, W. Bichard, and J. Skowronski. Effect of pretreatment of LWC basestock on coated paper properties. *Tappi Journal*, 69(12):66–70, 1986.
- M. Lloyd, S.-A. Stuart, G. Bristow, and M.Reich. Characterisation of coated paper structure. *Appita Journal*, 56(6):421–425, 2003.
- C. Lundgren. Cell wall thickness and tangential and radial cell diameter of fertilized and irrigated norway spruce. *Silva Fennica*, 38(1):95–106, 2004.
- J. Lux, C. Delisee, and X. Thibault. 3D characterization of wood based fibrous materials: an application. *Image Anal Stereol*, 25(25):25–35, 2006.
- I. Miranda and H. Pereira. Variation of pulpwood quality with provenances and site in eucalyptus globulus. *Annals of Forest Science*, 59(3):283–291, 2002.
- H. Mäkinen, P. Saranpää, and S. Linder. Effect of growth rate on fibre characteristics in Norway spruce (*Picea abies* (L.) Karst.). *Holzforschung*, 56(5):449–460, 2002.
- P.A. Moss, E. Retulainen, H. Paulapuro, and P. Aaltonen. Taking a new look at pulp and paper: Applications of confocal laser scanning microscopy (CLSM) top pulp and paper research. *Paperi ja Puu - Paper and Timber*, 75(1-2):74–79, 1993.
- T. Nesbakk and T. Helle. The influence on the pulp fibre properties on supercalendered mechanical pulp handsheets. *Journal of Pulp and Paper Science*, 28(12):406–409, 2002.
- T. Nesbakk, K. Mörseburg, and T. Helle. Relationship between fibre properties and cross-sectional paper characteristics of mechanical pulp handsheets. In *Proceedings of The 3rd biennial Johan Gullichsen colloquium*, pages 63–72, Espoo (Finland), September 2001. The Finnish Paper Engineers Association.
- O.A. Oluwafemi and O.A. Sotande. The relationship between fibre characteristics and pulp-sheet properties of *leucaena leucocphala* (Lam.) De Wit. *Middle-East Journal of Scientific Research*, 2(2):63–68, 2007.
- M. O’Neil and B. Jordan. The burnout test revisited. *Journal of Pulp and Paper Science*, 26(4):131–134, 2000.
- Y. Ozaki, D.W. Bousfield, and S.M. Shaler. Three-dimensional observation of coated paper by confocal laser scanning microscope. *Tappi Journal*, 5(2):3–8, 2006.
- Y. Ozaki, D.W. Bousfield, and S.M. Shaler. Characterization of coating layer structural and chemical uniformity for samples with backtrap mottle. *Nordic Pulp and Paper Research Journal*, 23(1):8–13, 2008.
- L. Paavilainen. Importance of cross-dimensional fibre properties and coarseness for the characterisation of softwood sulphate pulp. *Paperi ja Puu - Paper and Timber*, 75(3):343 – 351, 1993.
- R.A. Peterson and C.L. Williams. Determining paper-coating thickness with electron-microscopy and image analysis. *Tappi Journal*, 75(10):122–126, 1992.

C. Bibliography

- J. Preston. The surface analysis of paper. In S.J. I'Anson, editor, *Transactions of the 14th Fundamental Research Symposium*, volume 2, pages 749–838, Oxford (UK), September 2009. The Pulp & Paper Fundamental Research Society.
- J. Preston, A.G. Hiorns, N. Elton, and G. Ström. Application of imaging reflectometry to studies of print mottle on commercially printed coated papers. *Tappi Journal*, 7(1):11–18, 2008.
- J. Preston, M. Toivakka, P. Heard, and G. Chinga-Carrasco. Coated paper microstructure: Particle shape-microstructure interrelations. In *Proceedings of TAPPI 2nd Annual PaperCon'09 Conference*, pages 1–17, St. Louis (USA), June 2009. Tappi Press.
- I. Pulkkinen, K. Ala-Kaila, and J. Aittamaa. Characterization of wood fibers using fiber property distributions. *Chemical Engineering and Processing*, 45:546–554, 2006.
- P.A. Reme and T. Helle. Quantitative assessment of mechanical fibre dimensions during defibrating and fibre development. *Journal of Pulp and Paper Science*, 27(1):1–7, 2001.
- P.A. Reme, P.O. Johnson, and T. Helle. Assessment of fibre transverse dimensions using sem and image analysis. *Journal of Pulp and Paper Science*, 28(4):122–128, 2002.
- P. Resch, W. Bauer, and U. Hirn. Calendering effects on coating pore structure and ink setting behavior. *Tappi Journal*, 9(1):27–35, 2010.
- G. Robertson, J. Olson, and P. Allen. Measurement of fiber length, coarseness and shape with the fiber quality analyzer. *Tappi Journal*, 82(10):93–98, 1999.
- S. Rolland du Roscoat, J.-F. Bloch, and X. Thibault. Synchrotron radiation microtomography applied to investigation of paper. *Journal of Physics D: Applied Physics*, 38(10A):A78–A84, 2005.
- S. Rolland du Roscoat, M. Decain, C. Geindreau, X. Thibault, and J.-F. Bloch. Microstructural analysis of paper using synchrotron X-ray microtomography: numerical estimation of the permeability and effective thermal conductivity. *Appita Journal*, 61(4):286–290+301, 2008.
- L. Sachs. *Angewandte Statistik. Anwendung statistischer Methoden*, volume 11. Springer-Verlag Berlin Heidelberg New York, 2004. ISBN 3-540-40555-0 11.
- P. Salminen, A. Yang, J. Kritzinger, W. Bauer, and J. Preston. The influence of application system on the structure of coating layer. In *Proceedings of Tappi Coating & Graphic Arts*, pages 1–11, Atlanta (USA), May 2010. Tappi Press.
- E.J. Samuelsen, Ø.W. Gregersen, P.J. Houen, C. Raven, and A. Snigirev. Three-dimensional imaging of paper by use of synchrotron X-ray microtomography. *Journal of Pulp and Paper Science*, 27(2):50–53, 2001.
- R.S. Seth, H.F. Jang, B.K. Chan, and C.B. Wu. Transverse dimensions of wood pulp fibers and their implications for end use. In C.F. Baker, editor, *Transactions of the 11th Fundamental Research Symposium*, volume 1, pages 473–500, Cambridge (UK), September 1997. Pira International.

C. Bibliography

- P. Shallhorn and N. Gurnagul. A simple model of the air permeability of paper. In S.J. I'Anson, editor, *Transaction of the 14th Fundamental Research Symposium*, volume 1, pages 475–490, Oxford (UK), September 2009. The Pulp & Paper Fundamental Research Society.
- I.A. Sintorn, S. Svensson, M. Axelsson, and G. Borgefors. Segmentation of individual pores in 3D paper images. *Nordic Pulp and Paper Research Journal*, 20(3):316 – 319, 2005.
- O. Steffner and M. Nylund, T. Rigdahl. Influence of precalendering on the properties of a coated woodfree paper and the covering ability of the coating. In *Proceedings of TAPPI Coating Conference*, pages 335–342, Atlanta (USA), 1995. Tappi Press.
- Y.J. Sung, C.H. Ham, O. Kwon, H.L. Lee, and D.S. Keller. Applications of thickness and apparent density mapping by laser profilometry. In S.J. I'Anson, editor, *Transactions of the 13th Fundamental Research Symposium*, volume 2, pages 961–1007, Cambridge (UK), September 2005. The Pulp & Paper Fundamental Research Society. ISBN 0 9545272 3 2.
- S. Svensson and M. Aronsson. Using distance transform based algorithms for extracting measures of the fiber network in volume images of paper. *IEEE Transactions on systems, Man and Cybernetics - Part B: Cybernetics*, 33(4):562–571, 2003.
- E. Tiikkaja. Fiber dimensions: their effect on paper properties and required measuring accuracy. *Pulp & Paper Canada*, 100(12):114–116, 1999.
- H. Tomimasu, K. Suzuki, T. Ogura, and P. Luner. The effect of basestock structure on coating weight distribution. *Tappi Journal*, 73(5):179–187, 1990.
- M. Trefz. Theoretical aspects and preactical experiences for film coated offset grades. *Tappi Journal*, 79(1):223–230, 1996.
- R.J. Trepanier. Automatic fiber length and shape measurement by image analysis. *Tappi Journal*, 81(6):152–154, 1998.
- T. Turpeinen, M. Myllys, M. Kataja, and J. Timonen. Computerized tomographic imaging of paper coating layers. In *Proceedings of 22nd PTS Coating Symposium*, pages 36–1 – 36–14, Baden-Baden (G), September 2005. PTS.
- M. Turunen, C. LeNy, T. Tienvieri, and J. Niinimäki. Comparison of fibre morphology analysers. *Appita Journal*, 58(1):28–32, 2005.
- J. Vyörykkä, A. Fogden, J. Daicic, M. Ernstsson, and A.-S. Jääskeläinen. Characterization of paper coatings - review and future possibilities. In *Proceedings of 9th Tappi Advanced Coating Fundamentals Symposium*, pages 41–66, Turku (Finland), February 2006. Tappi Press.
- T. Walther, K. Terzic, T. Donatz, H. Meine, F. Beckmann, and H. Thoemen. Microstructural analysis of lignocellulosic fiber networks. In *Progress in Biomedical Optics and Imaging - Proceedings of SPIE; Developments in X-Ray Tomography V*, volume 6318, pages 631812.1 – 631812.10, San Diego (USA), August 2006. SPIE - The International

C. Bibliography

- Society of Optical Engineering.
- U.W.H. Weise. Image analysis applied to images gained by confocal laser scanning microscopy: Fibre cross-sectional measurements. In *Proceedings of 2nd European Research Symposium: Image Analysis for Pulp and Paper Research and Production*, pages 51–62, Darmstadt (Germany), September 1993. IfP, TU Darmstadt.
- M. Wikström and J. Grön. Formation of patterns on paper coated with a metering size press. *Journal of Pulp and Paper Science*, 29(1):11–16, 2003.
- M. Wiltsche. *Three Dimensional Analysis of Paper Structure Using Automated Microtomy*. PhD thesis, Institute for Paper, Pulp and Fiber Technology, Graz University of Technology, 2006.
- M. Wiltsche, M. Donoser, W. Bauer, and H. Bischof. A new slice-based concept for 3D paper structure analysis applied to spatial coating layer formation. In S. J. I’Anson, editor, *Transactions of the 13th Fundamental Research Symposium*, volume 2, pages 853–899, Cambridge (UK), September 2005. The Pulp & Paper Fundamental Research Society.
- M. Wiltsche, W. Bauer, and M. Donsoer. Coating application method and calendering influence on the spatial coating layer formation obtained by an automated serial sectioning method. In *Proceedings of 9th Tappi Advanced Coating Fundamentals Symposium*, pages 413–415, Turku (Finland), February 2006. Tappi Press.
- M. Wiltsche, M. Donoser, J. Kritzing, and W. Bauer. Automated serial sectioning applied to 3D paper structure analysis. *Journal of Microscopy*, accepted for Publication, 2010.
- I. Xu, I. Parker, and C. Osborne. Technique for determining the fibre distribution in the z-direction using confocal microscopy and image analysis. *Appita Journal*, 50(4): 325 – 328, 1997.
- D. Yan and K. Li. Measurement of wet fiber flexibility by confocal laser scanning microscopy. *Journal of Material Science*, 43(8):2869–2878, 2008.
- J.Y. Zhu, D.W. Vahey, C.T. Scott, and G.C. Myers. Effect of tree-growth rate on paper-making fiber properties. *Appita Journal*, 61(2):141–147 + 155, 2008.
- X. Zou. Main factors affecting roughening of paper in coating and printing - a review of recent literature. *Nordic Pulp and Paper Research Journal*, 22(3):314–324, 2007.
- X. Zou, R. Allem, and T. Uesaka. Relationship between coating uniformity and base-stock structures. Part I: Lightweight coated papers. *Paper Technology*, 42(5):27–37, 2001.
- A. Zubizarreta Gerendiain, H. Peltola, P. Pulkkinen, V.P. Ikonen, and R. Jaatinen. Differences in growth and wood properties between narrow and normal crowned types of norway spruce grown at narrow spacing in southern finland. *Silva Fennica*, 42(3):423–437, 2008.